DISSERTATION

submitted to the
Combined Faculty of Natural Sciences and Mathematics
of the Ruperto Carola University Heidelberg, Germany
for the degree of
Doctor of Natural Sciences

Presented by
Dipl. Ing. Kristin Oberländer

Born in: Rudolstadt, Germany
Oral examination: 20.02.2019

Neuronal activity-dependent gene expression in learning and excitotoxicity

Referees: Prof. Dr. Hilmar Bading
Prof. Dr. Christoph Schuster

Summary

Genes regulated by neuronal activity are the focal point of plasticity-related brain functions, thereby providing the basis for behavioural adaptations such as memory. Cellular functions of activity-regulated genes are diverse; several genes encode transcription factors thus regulating a wide range of downstream processes. Pro-survival genes such as *Bdnf* rendering neurons more resistant against cellular stress and degeneration are another important class of activity regulated genes. Due to those crucial functions, it is essential to understand the regulation and relevance of activity-induced genes under physiological conditions, but also their response to pathological signals like glutamate mediated excitotoxicity. To examine neuronal activity-dependent gene regulation in physiological as well as pathological environments, this thesis was divided into two parts.

The first part investigated whether activity-regulated gene expression is correlated with memory ability by comparing two inbred mouse strains, C57BL/6 and DBA/2. Robust spatial memory impairments were observed for DBA/2. However, the cognitive deficits in DBA/2 were not exclusive for this type of memory. Analysis of basic characteristics such as morphology and electrophysiological properties of CA1 pyramidal neurons, which are crucial for spatial memory formation, revealed no strain difference. Also, activity-dependent gene induction was mostly similar between the strains in cell culture and *in vivo* after a learning paradigm. Yet, two genes, *Inhba* and *Npas4*, showed significantly increased basal expression and increased induction in DBA/2 hippocampal regions, respectively. Since both genes are implicated in excitation/inhibition regulation, inhibitory neuronal input for CA1 neurons via mIPSC electrophysiological recordings was analysed and revealed decreased inhibition in DBA/2. Attenuated inhibition may underlie the DBA/2 learning impairment. Yet, dysregulation of single activity-regulated genes, in particular *Inhba* and *Npas4*, correlates with differences in memory ability and might be involved in dysfunction processes.

The second part of this thesis analysed activity-dependent gene expression during the pathological condition of excitotoxicity. Intriguingly, differential response pattern of activity-dependent genes towards toxic NMDA stimuli were observed. Single genes like *Inhba* and *Bdnf* were intensely downregulated by NMDA-induced active deactivation processes, in contrast, rapid immediate early genes like *Arc*, *Npas4* or *Nr4a1* displayed no transcriptional shut-off during excitotoxicity. By analysing the activity of upstream kinases and transcription factors the mechanism underlying the differential regulation was investigated. Fast signalling kinases like ERK1/2 seem to depend predominantly on synaptic activity, transcription factors, however, were broadly dephosphorylated after NMDA application. Furthermore, additional experiments indicate that excitotoxicity-induced mitochondrial depolarization does not act as initiator of active transcriptional downregulation.

Together, the presented data illustrate that dysregulation of single activity-dependent genes occurs in a physiological model of memory impairment, but also under the pathological condition of excitotoxicity. *Inhba* might play an important role in both processes and for memory formation in general since it was dysregulated in both models which are implicated in memory attenuation.

Zusammenfassung

Gene, die durch neuronale Aktivität reguliert werden, sind essentiell für die Funktionalität und Plastizität des Gehirns und bilden dadurch die Grundlage für alle Adaptions- und Lernprozesse im Menschen. Die zelluläre Funktion dieser Gene ist divers, jedoch kodiert ein Großteil von ihnen selbst Transkriptionsfaktoren, die wiederum weitreichend Einfluss auf Signalwege haben. Eine weitere wichtige Gruppe aktivitäts-regulierter Gene sind Viabilitätsfaktoren, die die Resistenz von Neurone gegen zellulären Stress und Degeneration erhöhen. Da aktivitäts-regulierte Gene solch entscheidende Funktionen übernehmen, ist es wichtig Regulation und Relevanz einzelner Gene während physiologischer als auch pathologischer Prozesse zu verstehen. Zu diesem Zweck wurde diese These in zwei Abschnitte aufgeteilt.

Zunächst wurde untersucht, ob eine Korrelation zwischen aktivitäts-abhängiger Genexpression und Lernvermögen besteht, indem zwei murine Inzuchtstämme, C57BL/6 und DBA/2, verglichen wurden. Zusätzlich zu einer eher allgemeinen Lernbeeinträchtigung, wurde in DBA/2 vermindertes räumliches Lernvermögen eindeutig festgestellt. Die Analyse grundlegender neuronaler Eigenschaften wie Morphologie und elektrophysiologische Charakteristika zeigten keine Unterschiede zwischen CA1 Pyramidalzellen der jeweiligen Stämme auf. Desweiteren konnte kein genereller Unterschied der Geninduktion in Zellkultur als auch nach einem Lernparadigma festgestellt werden. Einzig *Inhba* und *Npas4* bildeten eine Ausnahme, da im DBA/2 Hippocampus jeweils basale Expression und Induktion erhöht sind. Für beide Gene wird eine Beteiligung in der Inhibitions- und Aktivierungsregulation berichtet. Aus diesem Grund wurde das eingehende inhibitorische Signal in CA1 Pyramidalzellen mittels mIPSC Messung ermittelt und festgestellt, dass DBA/2 verminderte Inhibition in dieser Region ausweisen. Es wird vermutet, dass diese verminderte Inhibition die eigentliche Ursache für das DBA/2 Lerndefizit ist, jedoch kann eine Beteiligung der *Inhba* und *Npas4* Dysregulation nicht ausgeschlossen werden.

Die Feststellung, dass geringe Fehlregulation einzelner aktivitäts-regulierter Gene eventuell relevant für die Gehirnfunktion ist, gibt den folgenden Ergebnissen noch mehr Bedeutung. Unter pathologischer Exzitotoxität, welche im zweiten Abschnitt der These untersucht wurde, konnte eine differentielle Dysregulation der Gene beobachtet werden. Einzelne Gene wie *Inhba* und *Bdnf* wurden stark durch aktive Deaktivierungsprozesse während NMDA-Toxizität runter reguliert, hingegen zeigten *Npas4* und *Nr4a1* keine aktive Expressionsminderung. Um diese differentielle Regulation zu erklären, wurde der Aktivitätszustand von vorausgehenden Signalmolekülen untersucht. Es zeigte sich, dass cytoplasmatische Kinasen wie ERK1/2 eher auf synaptische Aktivität reagieren und Transkriptionsfaktoren generell währen NMDA-Toxizität dephosphoryliert werden. Zusätzliche Experimente weisen außerdem darauf hin, dass die Depolarisierung von Mitochondrien, die ebenfalls durch Exzitotoxität ausgelöst wird, nicht Auslöser der aktiven Runterregulation ist.

Zusammengefasst zeigen die präsentierten Daten, dass eine differentielle Dysregulation einzelner Aktivitäts-regulierter Gene in einem physiologischen Modell verminderter Gedächtnisbildung auftritt, als auch während pathologischen NMDA Signalen. Insbesondere

Inhba scheint eine wichtige Rolle in der Gedächtnisbildung zu spielen, da es in beiden gedächtnismindernden Modellen dereguliert ist.

Acknowledgement

I want to thank all those who supported me during my PhD and who gave me the opportunity to start and complete this thesis.

First of all, I would like to thank Prof. Hilmar Bading for his great supervision, support and stimulating discussions during the whole PhD process. I also want to thank Prof. Christoph Schuster for accepting to become my second supervisor of this thesis and member of my thesis advisory committee (TAC). Furthermore, I am thankful to Prof. Peter Gass who accepted to be my third TAC advisor and supported me with his constructive advice and helpful collaboration.

I also thank Dr. Anne Mallien for her fantastic contribution to this thesis and the DBA/2 project in general. Furthermore, I am grateful that Dr. Peter Bengtson and Victoria Witte supported the DBA/2 project with essential electrophysiology data.

I want to thank following institutions for funding my PhD position and research: the Deutsche Forschungsgemeinschaft (DFG), the Heidelberg Biosciences International Graduate School (HBIGS) and the European Research Council (ERC).

Most importantly, I thank all the friends and colleagues in the Neurobiology department for their support, advice and the great work atmosphere in general. In particular, I want to thank Dr. David Lau for his constant aid and advice for all experimental problems. Thanks to Dr. Thekla J. Hemstedt for teaching me the basics of behavioural research and to Dr. Ana M. M. Oliveira, David Brito and Kübra Gülmez for sharing their experience on several behavioural methods with me. I also want to thank Dr. Priit Pruunsild, Dr. Daniela Mauceri, Dr. Anna M.H. Hertle, Dr. Carlos Bas-Orth and Dr. Bettina Buchthal for their constant help and teaching me all kinds of methods.

Thanks to Otto Bräunling for organizing the daily life in the lab and to Irmela Meng for her great lab administration. In particular, thanks to Iris Bünzli-Ehret for providing great neuronal cultures and for keeping the cell culture running perfectly. Thanks to Ursula Weiss, Andrea Hellwig, Monika Keusch, Oliver Teubner and Alan Summerfield for their excellent job and making my life in the lab much easier.

Last but not least, I thank my family and my boyfriend for their understanding and endless support.

Heidelberg, November 2018
Kristin Oberländer

Content

List of Figures

List of Tables

List of Abbreviations

β-ME	β-mercarptoethanol
aCSF	artificial Cerebrospinal Fluid
AD	Alzheimer's Disease
AMPA	α-amino-3-hydroxy-5-methyl-4-isoxazolepropionic acid
AP-1	Activator Protein 1
APV	(2R)-amino-5phosphonovaleric acid
ATP	Adenosine Triphosphate
BIC	Bicuculline
BSA	Bovine Serum Albumin
Ca2+/CaM	Calcium/Calmodulin complex
CaM	Calmodulin
CaMKIV	Calcium/calmodulin-dependent protein kinase type IV
cAMP	cyclic Adenosine Monophosphate
CBP	CREB Binding Protein
ChIP	Chromatin Immunoprecipitation
CMKII	Ca2+/CaM dependent protein kinase II
CMKIV	Ca2+/CaM dependent protein kinase IV
ConG	Conantokin G
CRE	Cyclic-AMP Response Element
CREB	Cyclic-AMP Response Element Binding protein
DEG	Delayed Early Genes
DIV	Day *in vitro*
DNA	Deoxyribonucleic Acid

DRE	DNA Replication-related Element
DREAM	DRE-anatagonist Modulator
ELK1	ETS domain-containing Protein
ER	Endoplasmic Reticulum
ERK	Extra-cellular signal Regulated Kinase
EtOH	Ethanol
fMRI	functional Magnetic Resonance Imaging
GABA	γ-aminobutyric acid
GAD	Glutamate Decarboxylase
GMP	Guanosine Monophosphate
GTP	Guanosine Triphosphate
IEG	Immediately Early Gene
IEI	Inter Event Interval
IP3	Inositol 1,4,5-triphosphate
LTM	Long-Term Memory
LTP	Long-Term Potentiation
MAPK	Mitogen-activated Protein Kinase
MEF2A	Myocyte Enhancer Factor 2A
mEPSC	miniature Excitatory Postsynaptic Current
mIPSC	miniature Inhibitory Postsynaptic Current
M.W.	Molecular Weight
NGS	Normal Goat Serum
NMDA	N-methyl-D-aspartate
OA	Okadaic Acid
PBS	Phosphate Buffered Saline

PBST	Phosphate Buffered Saline with Tween 20
PCR	Polymerase Chain Reaction
pCREB	phosphorylated CREB at Ser133 site
pELK1	phosphorylated ELK1 at
pERK	phosphorylated ERK1/2, dually phosphorylated at Thr202 and Tyr204
pMEF2A	phosphorylated MEF2A at
PKC	Phosphokinase C
PTEN	Phosphatase and Tensin Homolog
PP	Protein Phosphatase
RNA	Ribonucleic Acid
rpm	round per minute
RT qPCR	Real Time Quantitative Polymerase Chain Reaction
SCC	Saline-Sodium Citrate buffer
SDS-PAGE	Sodium Dodecyl Sulfate Polyacrylamide Gel Electrophoresis
SRE	SRF Element
SRF	Serum Response Factor
STEP	Striatal Enriched Tyrosine Phosphatase
TCF	Ternary Factor Complex
Tm	Melting temperature
TTX	Tetrodotoxin
VDCC	Voltage-Dependent Calcium Channel

Chapter 1

Introduction

1.1 Neuronal activity-dependent gene expression

Adaptation processes are fundamental for higher cellular and organismal function. The brain with its complex cellular organisation and complicated circuit operations relies on remarkable adaptation capacities. Those adaptations are driven by sensory experience-evoked neuronal activity and rely on synaptic, neuronal and circuit plasticity. Plasticity processes can be short-lasting through transcription-independent cellular alterations like post-translational modifications of channels and scaffolding proteins, protein trafficking and sensitization as well as local protein translation [1-3]. Long-lasting plasticity requires activation of gene transcription generating new proteins involved in long-term modulation of synaptic efficacy, synaptic and cellular morphology and network connectivity [4, 5]. The majority of synaptic activity-induced gene transcription depends on cytoplasmic and nuclear calcium signalling mediated by L-type voltage-gated calcium channels (VGCC-L) and/or N-methyl-D-aspartate (NMDA) receptors [6, 7]. A complex cascade of calcium-dependent signalling pathways activates a diverse set of transcription factors and regulators culminating in a specific transcriptional program [8]. The mode of activity, temporal progression and route of calcium entry can determine particular signalling routes leading to transcriptional activation of a specific subset of genes [9-11].

The aim of this thesis is to investigate the regulation and expression pattern of specific activity-regulated genes in a physiological model of memory impairment as well as during toxic glutamate/NMDA signalling (excitotoxicity) which occurs in several neuronal pathologies. Therefore, every chapter of this thesis except chapter 2 is divided into two parts. The first part refers to activity-dependent gene expression in learning and memory and the second part examines expression and regulation patterns of those genes during excitototoxicity *in vitro*.

1.1.1. Characterization of activity-induced genes

Neurons induce hundreds of activity-dependent genes [12]. They can be classified according to their induction kinetics (Figure 1). The first wave of genes activated after synaptic activity are called rapid early response genes or immediate early genes (IEGs) [13]. By definition IEG transcription induction is independent from novel protein translation and relies on activation of already expressed second-messengers, transcription factors and regulators alone. Most

IEGs are transcription factors themselves, responsible for the expression of numerous downstream targets [14]. The accumulation of transcripts from the second wave of early response genes, the delayed early genes (DEGs), is not as rapid as for IEGs, but does also not require novel translated factors. In contrast, most of the delayed response genes (DRG) require *de novo* transcription and translation. Most transcription induction of delayed response genes is caused by newly translated factors and regulators of the IEG and DEG group [15]. This strict temporal classification does not account for all activity-induced genes but provides an overview of the different gene modules activated after synaptic activity. Transcriptome data shows that there are various exceptions to the general classification [8].

Not only temporal properties can determine the induction of a specific gene module, also different firing patterns, firing duration and neurotransmitters can activate the expression of several specific gene sets. For example, transcription of the well characterized IEG *cFos* which encodes for an activator protein 1 (AP-1) complex transcription factor is firing frequency dependent and can also be induced by acetylcholine receptor mediated calcium signalling [11]. Additionally, calcium influx through different calcium channels activates distinct gene programs which can be traced back to differentially activated upstream signalling pathways [11].

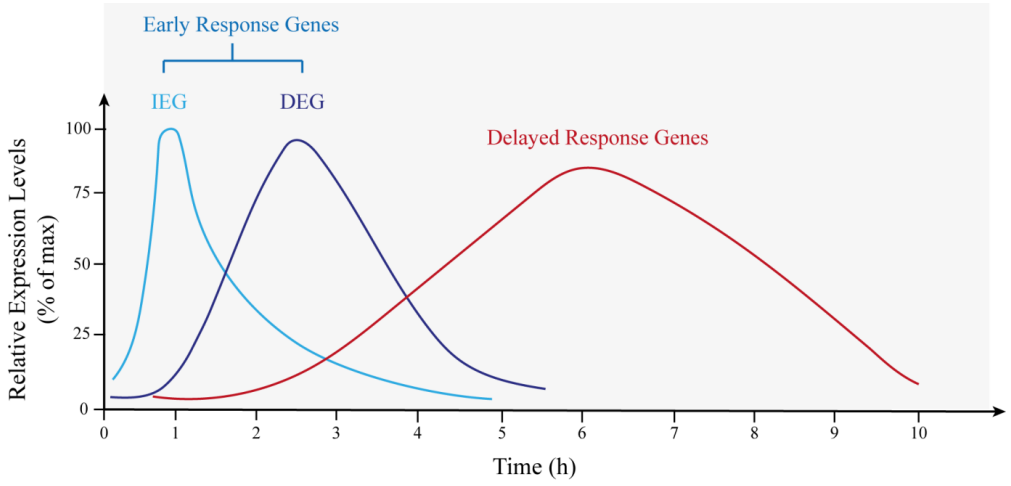

Figure 1: Schematic presentation of neuronal activity-induced gene classes. Theoretical kinetic course of transcript accumulation presented as relative gene expression in percent of maximal expression over time is plotted. Immediate early genes (IEGs) are depicted as bright blue curve, delayed early genes (DEGs) are plotted in dark blue and delayed response genes in red.

1.1.2. Activity-transcription coupling mechanism

A complex cascade of distinct receptor and second-messenger signalling is responsible for differential gene module activation. The type of neurotransmitter released into the synaptic cleft already determines specific gene induction by activating a distinct set of receptors and thereby distinct secondary messengers. The main route of transcription activation by excitatory glutamatergic signalling which activates NMDA-type glutamate receptors

(NMDARs), α-amino-3-hydroxy-5-methyl-4-isoxazolepropionic acid (AMPA)- and kainate-type glutamate receptors involves calcium dependent signal transduction [16]. Activation of synaptic NMDARs via the release of the magnesium block results in a strong cytoplasmatic calcium influx [17]. Additionally, the induced membrane depolarization activates somatically and perisomatically localized VGCC, in particular L-type channels, which have a slow deactivation rate. The route of calcium entry through these two channels already initiates distinct kinase and gene activation (Figure 2) [18].

Upon calcium entry a set of kinase cascades is activated. The two main signalling routes leading to activity-dependent gene induction are the mitogen-activated protein kinase (MAPK) cascade and signal transduction via calmodulin (CaM) kinases (CaMK) [19, 20]. The MAPK cascade is initially activated by calcium-dependent increase in GTP bound Ras, activating Raf. Signalling is now transmitted in a cascade via tyrosine phopsphorylation of MAPK/ERK kinase (MEK), extracellular signal–regulated kinase (ERK) 1/2 and ribosomal s6 kinase (RSK). ERK1/2 and RSK are shuttled in the nucleus to activate transcription factors [21].

CaM-dependent kinases are serine/threonine kinases. CaMKII gets activated at the synapse and is involved in transcription-independent synaptic plasticity. CaM also activates CaMK kinase (CaMKK) in the cytoplasm leading to CaMKK nuclear translocation and CaMKIV activation. CaMKIV which is predominantly located in the nucleus can also be directly activated by nuclear calcium/CaM. CaMKIV is the main CaMK responsible for direct transcription factor activation (Figure 2) [22].

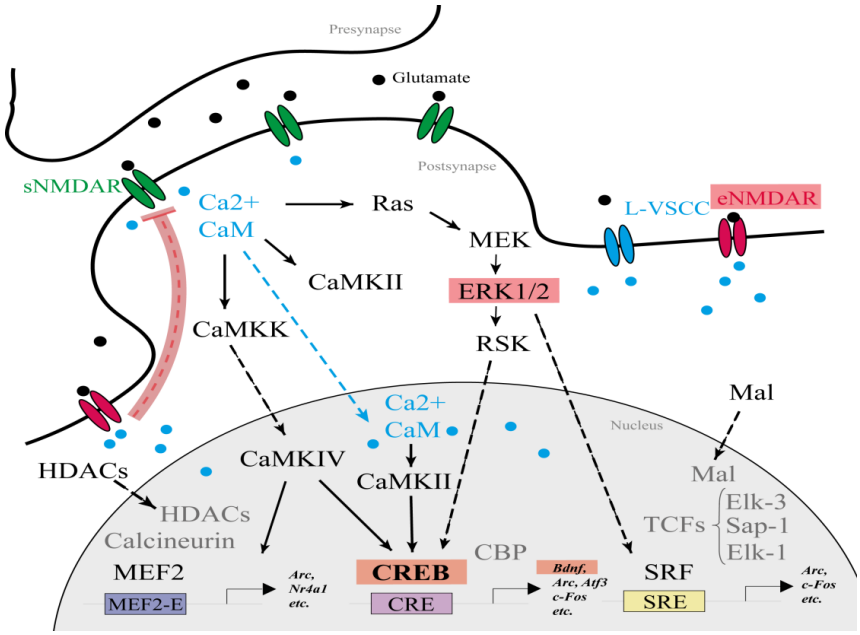

Figure 2: Schematic overview of calcium-dependent gene induction pathways after synaptic activity in glutamatergic neurons. Calcium influx occurs via N-Methyl-D-aspartic acid (NMDA) receptors and voltage gated calcium channels (VGCC). Two main cytoplasmic signalling pathways are activated by calcium: calmodulin (CaM) kinases (CaMKs) and mitogen-activated protein kinases (MAPKs). Kinase signalling results in nuclear transcription factor activation. CREB, MEF2 and SRF are predominantly responsible for neuronal activity dependent gene induction. Arrows indicate activation, dotted lines translocation and names highlighted in red deactivation/downregulation of proteins by excitotoxicity (see chapter 1.3.1).

Besides calcium, other second-messengers like cyclic adenosine monophosphate (cAMP), cyclic guanosine monophosphate (cGMP), arachidonic acid metabolites, diacylglycerol and inositol phosphates are implicated in activity-dependent gene expression [23]. Among those, cAMP signal transduction via protein kinase A (PKA) activation is also an important pathway in glutamatergic neurons, influencing activity-dependent gene induction by activating MAPK and transcription factors. cAMP signalling is often initiated by G-protein-coupled ATP receptors; however, G-protein-coupled receptors binding ligands like dopamine or acetylcholine are important for gene induction in other neuronal cell types [24, 25].

The main transcription factors implicated in activity-dependent gene induction are calcium/cyclic AMP response element-binding protein (CREB), serum response factor (SRF) and myocyte enhancer factor-2 (MEF2) [26] (Table 1). The DNA regulatory elements that they bind are distributed in promotor regions of numerous activity-inducible genes. Chromatin immunoprecipitation (ChIP)-sequencing data from ENCODE, analysing binding near transcription start sites, predicted approximately 13251 cAMP-response elements [27], 7718 serum response elements (SREs) and 954/2987 MEF2 (MEF2C/MEF2A, respectively) response elements (MREs,) distributed in the human genome [28]. All three elements together are located in the promotor region of the IEG *Arc* forming the synaptic activity-responsive element (SARE) [29].

Regulatory events for those main transcription factors are different. CREB is activated by phosphorylation at Ser^{133}. This phosphorylation site is target of several activity-induced signal cascades and the best described mechanism for transcription factor activation in neuronal activity-dependent gene induction. CREB binding protein (CBP) binds phosphorylated CREB and recruits the RNA polymerase II-containing transcription initiation complex while loosening chromatin structure via histone acetylation [30]. CREB activation is implicated in positive regulation of neuronal survival, plasticity processes and memory.

SRF activation in neurons occurs predominantly by binding the ternary factor complex (TCF) protein ELK1 or megakaryoblasic acute leukemia-1 (MAL/MKL1). Since ELK1 and MAL share the same binding region in SRF their coactivator function is mutually exclusive. Synaptic activity activates ELK1 via MAPK/ERK signalling and MAL via ERK and nuclear shuttling [31]. SRF-dependent gene activation is important for plasticity processes and in particular maintenance of long-term potentiation (LTP).

Regulation of MEF2, which can be found in four isoforms (MEF2 A-D), is more complex. Besides phosphorylation, sumoylation and dimerization can regulate MEF2 activity [32]. Phosphorylated MEF2 shows weaker DNA binding and phosphorylation of MEF2D at Ser^{444} inhibits transcription. MEF2-dependent transcription negatively regulates memory and spine density [33-35].

Besides those transcription factors, also transcription regulators like the transcriptional repressor downstream regulatory element antagonist modulator (DREAM, Table 1) are important for neuronal activity-regulated gene induction. DREAM is directly activated by calcium, upon calcium binding by its four EF-hand motifs, DREAM unbinds from its DNA binding site [36] and stops inhibiting transcription [37].

Table 1: Parameters of important transcription factors and cofactors in neuronal activity-dependent gene induction. Listed transcription factors and cofactors play a major role in activity-dependent gene induction.

Transcription Factor/Cofactors	*Binding Element*	*Binding Sequence*	*Co-Regulators*	*Activators*	*Mechanism of Activation*	*Function*
CREB	CRE	-TGACGTCA-	CBP, TORC	cAMP, CaMKIV, Ras	Phosphorylation at Ser^{133}	Survival, Plasticity, Memory
SRF	SRE	-CC(A/T)$_6$GG-	TCF: Elk1 SAP-1, SAP-2, MAL	MAPK/ERK	Phosphorylation of Elk1 at $Ser^{383,389}$, MAL Shuttling	LTP and LTD maintenance
MEF2	MRE	-TGTTACT(A/t) (a/t)AAATAGA(A/t)-	P300, $MeCP_2$, NFkB	Calcineurin, CaMK, HDACs	Hypophosphorylation MEF2D: Dephosphorylation of Ser^{444}	Suppresses memory and spine formation
DREAM	DRE	-GTCA- or -TGAC-	-	Calcium	Nuclear translocation	Downregulates induced genes

1.1.3. Functions of activity-induced genes

Approximately 200 genes are induced by synaptic activity [8, 12], since not all genes can be discussed, this thesis will concentrate on relevant and well characterized genes. In general, neuronal activity-induced genes can be divided into two functional categories: transcription factors and effectors. IEGs belong mainly to the first category with the exceptions of *Arc*, being responsible for tagging activated synapses and homeostatic scaling of AMPA receptors [38, 39] and *Homer*, a PDZ protein that binds metabotropic glutamate receptors [40]. Among the induced transcription factors, *cFos* is one of the fastest and most strongly induced IEGs. It can function as transcriptional repressor or activator depending on its Jun binding partner. cFos and Jun heterodimers bind AP-1 sites, whereas cFos/cJun activates gene transcription and cFos/Jun-B represses it [41]. *cFos* and *Arc* expression/induction is also used as a marker for activated neurons and neuronal ensembles, however, the expression overlap of those highly induced IEGs has not been well investigated, yet [42]. Another well characterized IEG is *Zif268/Egr1*, it is required for LTP and crucial for long-term memory (LTM) formation [43]. Nuclear receptor subfamily 4, group A, member 1 (*Nr4a1*) encoding orphan nuclear receptor 1 is also involved in memory formation by regulating synapse distribution and function [44]. Another well characterized transcription factor involved in synaptic scaling is neuronal PAS domain protein 4 (*Npas4*). It was shown that *Npas4* is responsible for formation of inhibitory synapses on excitatory neurons and thereby regulating excitation/inhibition signalling balance. *Npas4* expression is also required for spatial memory formation especially in the CA3 hippocampal region [45, 46].

Brain-derived neurotrophic factor (*Bdnf*) belongs to the group of delayed early response effector genes. As a nerve growth factor BDNF is relevant for autocrine and endocrine survival and growth signalling. BDNF interaction with its predominant receptor TrkB is also involved in plasticity processes and LTM formation [47]. In psychological and neurodegenerative diseases BDNF and pro-BDNF levels are dysregulated which has a detrimental effect on disease progression [48]. *Bdnf* transcription is regulated in a complex

manner, the *Bdnf* gene has nine alternative promoters, among them promotor IV is activated by activity-induced calcium signals via CREB binding. In contrast to *Bdnf* which is one of the most studied activity induced gene, not much information about inhibin subunit beta A (*Inhba*) function in neurons is available. *Inhba* encodes a subunit which can be found in activin A, AB and inhibin A dimers. Inhibin and activin both belong to the TGF-β protein superfamily and often have opposing effects. Their functions in organs other than the brain are well characterized, for example activin is involved in wound healing, immune response and menstrual cycle regulation [49]. Only a few studies analysed *Inhba*/activin A for their neuronal and brain function. The data available however indicates diverse and crucial function of *Inhba*/activin in neuronal regulation, development and survival [50]. For example, activin A is involved in downregulation of extrasynaptic NMDA receptors and spine plasticity by modulating actin dynamics [51]. Also neuronal and network development is influenced by activin A signals [36], and it was shown that activin A application downregulates GAD-positive interneurons in developing primary neuronal cultures [52].

Whereas IEGs are often short transcripts with similar promotor binding sites, activity-induced genes belonging to the group of delayed/secondary response genes are more frequently complex transcripts. In many cases delayed response genes express extracellular and extracellular matrix proteins like the matrix metalloproteinase-3 (*Mmp3*) [53].

In summary, activity-induced genes encode diverse sets of proteins linked to transcription regulation, cytoskeletal formation, growth factor signalling, metabolism and signal transduction. Most genes are responsible for neuronal adaptation processes and a subset of genes directly influence plasticity processes. One of the most remarkable aspects of neuronal adaptation and plasticity is its function in learning and memory processes.

1.2. Learning and memory

Learning is the ability of an animal to adapt its behaviour by retention of already experienced situations and information. The acquisition of new ideas especially in humans relies on memorized experience and to retain these ideas over time a functional memory system is necessary. However, there is no single brain structure or molecular mechanism that accounts for all learning processes. Therefore, memory is categorized according to its type, its duration and the involved brain regions. In general, it is distinguished between the memory of facts, declarative memory, and the memory of skills/behaviour, non-declarative or procedural memory. Declarative memory can be further divided in short-term (STM), long-term (LTM) and working memory [54]. STM is short lasting with low capacity, whereas LTM can be long lasting and even permanent with a much greater capacity, but permanent consolidation is necessary. In contrast to STM where only a single memory system is involved, working memory which is often defined as a special form of STM engages several sites in the brain for temporary information storage and processing. Working memory is also heavily dependent on attention [55]. The memory trace, or engram, can be stored in different brain regions depending on the type and age of the stored information. One crucial region for declarative memory formation and consolidation is the temporal lobe with its hippocampal

formation [56]. It is also the most studied region on anatomical and molecular level. In rodents, which are standardly used in memory research, the hippocampus is especially important for spatial memory formation.

1.2.1. Hippocampus-dependent spatial memory

The relevance of the hippocampus for the formation of new memories was discovered due to temporal lobe lesions of epileptic patients. Most famously, reports about patient H.M. started the field of hippocampus-dependent memory research around six decades ago [57]. In rodents lesion studies showed that the dorsal hippocampus is especially relevant for memory formation of spatial information. Information first processed in sensory brain regions is sent via the perforant path of the enthorinal cortex (EC) to the hippocampus (Figure 3). Here, the dentate gyrus (DG) is first activated and processes the information [58]. Since the DG is one of the few regions with adult neurogenesis it is theorized that DG processing is important for pattern separation, the ability to differentiate between two similar sensory information [59]. The DG then transmits the information via its mossy fiber axon bundles to the heavily interconnected *cornu ammonis* (CA) region 3, which again passes the signal on to the CA1 with its Schaffer collateral bundles. After CA1 processing the hippocampal output is again send to the EC and from there to other higher processing cortical regions.

Due to implementation of electrophysiological activity recordings from hippocampal neurons in awake and freely moving animals, it was discovered that a subset of hippocampal cells responded specifically to the current location of the animal. These cells were named place cells and they are located in the CA3 and predominantly in the CA1 subregion [60]. The combination of cells activated at one location was unique. This led to the suggestion that the hippocampus contains a cognitive map of the spatial environment.

Testing hippocampal function *in vivo* employs tasks where the test subject has to show correct spatial orientation in a previously exposed environment. Thereby, it is tested whether the test subject was able to build and recall the cognitive map of the spatial environment. In rodents the best established tests for analysing spatial memory ability are contextual fear conditioning (CFC), Morris water maze (MWM) and spatial object relocalization (SOR) tasks [61]. CFC assesses the association of a specific environment with Pavlovian conditioning mediated by a foot shock as unpleasant stimulus. Correct recall of the unpleasant stimulus in the specific context results in freezing behaviour. However, since fear and anxiety are also heavily involved in this task, CFC is influenced by amygdala signalling and function.

The MWM task is often seen as gold standard for spatial memory assessment. The rodent is trained in a water filled pool to find a visible platform. Spatial cues are given around the pool to enable formation of a cognitive map. During the test phase the platform is removed and the swimming path of the test subject is tracked. In case of accurate memory, a higher percentage of the path lies in the quadrant where the platform was located during training [62].

A low anxiety influence can be achieved by spatial object recognition (SOR) training. In SOR the test subject has to remember the localization of two different objects. During test session one object is relocated. In case of correct memory formation and recall the relocated object will be explored more than the non-relocated one.

Those spatial memory tasks are not exclusively reliant on the hippocampal regions. Other structures are needed for successful memory formation and expression. It is well established that the prefrontal cortex (PFC) is also involved in spatial working memory [63]. The parietal lobe is needed for spatial attention [64] and lesion studies showed that the retrosplenial cortex (RSC) is needed for allocentric spatial memory and navigation [65]. Although different memory tasks rely on different brain regions, the cellular and molecular mechanisms for neuronal plasticity share several similarities between regions.

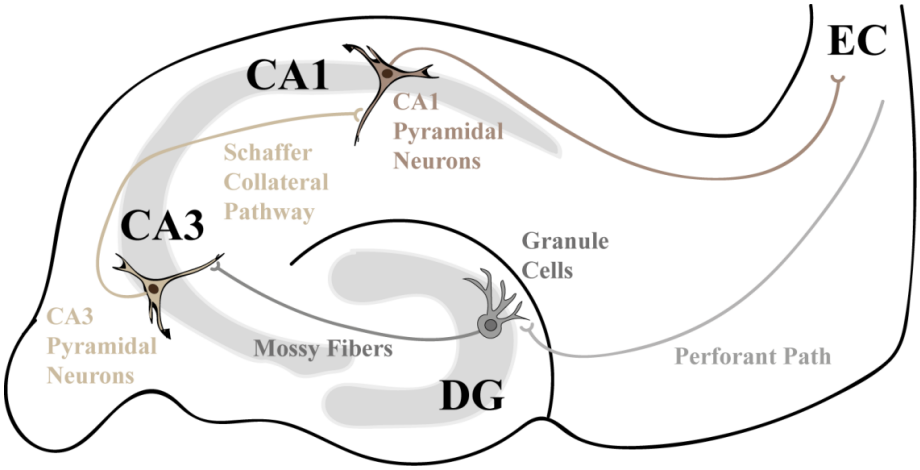

Figure 3: Anatomical illustration of rodent hippocampal microcircuits. Hippocampal signals are received from the enthorinal cortex (EC) and transmitted to the dentate gyrus (DG) via performant path axons. The receiving DG granule cells pass the signal via their mossy fibers to the heavily interconnected *cornu ammonis* (CA) region 3 pyramidal neurons. After processing, CA1 pyramidal neurons are activated by Schaffer collateral path axons. The processed signal is sent again to the EC, followed by other cortical regions. Besides the depicted circuits, every hippocampal region also receives input and sends output to other cortical regions.

1.2.2. Plasticity processes in memory formation

The molecular basis for long-lasting plasticity and memory always depends on activity-induced gene transcription and *de novo* protein synthesis. Analysing the gill- and siphon-withdrawal reflex of *Aplysia*, Eric Kandel and his group discovered that protein synthesis inhibitor (anisomycin) application during training impaired long-term but not short-term sensitization [4]. In search for the responsible mechanism activity-induced genes were discovered. Many genes showed a direct participation in plasticity processes as mentioned in 1.1.3. Neuronal plasticity processes are manifold and span from metabolic adaptations, synaptic scaling, increased myelination and receptor trafficking to long-lasting actin alterations.

The best described long-lasting plasticity mechanism is the increase of synaptic strength in form of LTP. LTP facilitates synaptic transmission and can last several hours. In different brain regions different LTP induction mechanism were observed. In the hippocampal Schaffer collateral pathway the early unstable form of LTP relies upon NMDA receptor activated AMPA receptor recruitment to the postsynaptic site, whereas LTP maintenance is

attributed to CaMKII and protein kinase A (PKA) activity [66]. For late persistent LTP activity induced gene expression is mandatory. Several early response genes like *Arc*, *c-Fos* and *Bdnf* are associated with lasting LTP formation and facilitation [27]. For memory formation and in particular a balanced signal/noise ratio, the LTP counter mechanism long-term depression (LTD) is equally important. In contrast to hippocampal CA1 LTP which is induced by NMDA receptor dependent high and fast rises of intracellular calcium levels, CA1 LTD is induced by NMDA receptor dependent slow and low calcium rises. If the calcium rise stays under a certain threshold, which depends on the activity history of each synapse, calcium increases lead to internalization of synaptic AMPA receptors. Furthermore, sub-threshold calcium concentration activates calcium-dependent phosphatases like calcineurin which results in deactivation of kinase signalling. Altogether those mechanism result in depressed excitatory postsynaptic potentials [67].

Another important hippocampal plasticity mechanism is the elevation of adult neurogenesis after neuronal activity in the DG region for example after environmental enrichment. Inhibiting neurogenesis by inhibiting WNT-signalling results in impaired spatial and object recognition memory. It was shown that immature DG granule cells show increased intrinsic excitability and plasticity compared to mature granule cells. Therefore, immature cells are more likely to be included in novel engrams, thus encoding significant features of novel spatial environments and playing a key part in pattern separation [59].

All long-lasting plasticity mechanisms rely on activity-induced genes. Knockout or knockdown of several early response genes like *Nr4a1*, *Npas4* or *Bdnf* result in impaired LTP and/or memory formation [45, 68, 69]. Cases of cognitive disorders including autism, schizophrenia, and dementia are related to mutations in genes associated with activity-dependent gene expression dysregulation [70, 71]. However, it is not known whether slight gene and the resulting mild plasticity dysregulation also occurs in inter-individual learning variability in healthy adults which is not defined as pathological condition.

1.2.3. DBA/2 as model for inter-individual learning impairment

Crucial information about the neural basis of human cognition and memory can be obtained by specifically studying inter-individual variability. So far, only inter-individual structural differences assessed by structural functional magnetic resonance imaging (fMRI) and their correlation with performance capacity were investigated. Most studies found a positive correlation between grey matter volume and performance, for example, increased hippocampal and prefrontal cortex grey matter was found in individuals with improved context-dependent navigation ability [72]. Investigating whether cellular and/or molecular mechanisms like activity-dependent gene induction contribute to human inter-individual learning variability is complicated and for some cases impossible to achieve. Similar to neurological disease research, a murine model would be beneficial for answering this question. The search for a mouse model simulating inter-individual learning differences was focused on hippocampus dependent learning and memory since the underlying molecular mechanisms are well characterized.

In comparison to the murine inbred strain C57BL/6 the inbred strain DBA/2 is described in the literature to be impaired in hippocampus dependent spatial learning tasks such as CFC [73] and MWM [74]. Since DBA/2 spatial memory performance decreases only slightly with hippocampal lesions it was concluded that their hippocampus is dysfunctional [75]. This conclusion is supported by evidence of attenuated hippocampal LTP in DBA/2 for high frequency stimulation of the perforant path but not for theta burst stimulations [76]. Since DBA/2 as an inbred strain show a naturally occurring phenotype not generated by artificial gene modifications, we theorized that their impairment could serve as a suitable model of human cases of inter-individual differences in memory performance. Findings about the cellular and molecular cause of the DBA/2 learning impairment could indicate target pathways or mechanism relevant for human learning variability.
As described, hippocampal connectivity, morphology and ability for signal transduction, in particular of CA1 pyramidal neurons, play a major role in spatial memory acquisition (1.2.2) [77] [78]. Yet, it was shown by ultrastructural analysis that DBA/2 CA1 stratum radiatum synapses do not differ from C57BL/6 in their size of postsynaptic density and active zone [78]. No morphological or functional analyses of DBA/2 CA1 pyramidal neurons are reported so far. However, one publication demonstrates a reduced size of CA3 intra- and infrapyramidal mossy fiber terminal field in DBA/2 [79].
Few studies investigated strain differences at a molecular level which tried to explain the spatial memory dysfunction. In comparison to C57BL/6, DBA/2 display lower hippocampal protein kinase C (PKC) activity and impaired learning induced phosphorylation of the PKC target GAP-43 [76, 80, 81] as well as reduced expression of presynaptic vesicle release proteins Rab3c, Rasal1 and a lower number of reserve vesicles in CA1 synapses [78]. In regard to activity-induced genes, one study showed reduced basal expression of the IEG *Egr1/Zif268* in the DBA/2 hippocampus by *in-situ* hybridisation [82]. However, DBA/2 and C57BL/6 showed similar *Egr1/Zif268* expression after physical activity. The reduced basal expression of one IEG in DBA/2 is particularly interesting since, as described in chapter 1.1.3 and 1.2.2, NMDA receptor dependent signalling culminating in the induction of activity-induced genes is a well characterized and essential pathway involved in learning and memory. Although IEGs have important physiological functions in long-term memory formation no study investigated IEG expression or induction in DBA/2 in respect to their claimed hippocampal dysfunction so far.

1.3. Toxic glutamate signalling

Activity-dependent gene induction and other neuronal plasticity mechanisms rely on NMDA receptor activation (1.1.2). However, NMDA receptors control not only neuronal physiology but also pathological processes. In contrast to healthy physiological NMDA receptor/calcium signalling, neuronal depolarization caused by excessive excitatory signals leads to neurotoxic events [83]. This detrimental process is named excitotoxicity. The initial step of excitotoxicity is excessive presynaptic glutamate release generating a synaptic glutamate spill and hereby

activating synaptic as well as extrasynaptic NMDA receptors (sNMDAR, eNMDAR respectively) intensely or chronically. Hereupon calcium reaches critical intracellular concentrations due to extracellular calcium influx as well as intracellular release of calcium stores, like the endoplasmic reticulum, disturbing neuronal calcium homeostasis [84]. Excitotoxic events lead to neuronal degeneration and cell death, the occurrence of excitotoxicity is reported for diverse neurodegenerative and neurological diseases like Huntington´s disease (HD) or stroke.

1.3.1. eNMDAR mediated excitotoxicity

Intriguingly, not the intracellular calcium concentration per se determines the toxicity, but the route of extracellular calcium entry decides whether glutamate signals are toxic. This was shown by boosting sNMDAR activation with the potassium channel inhibitor 4-Aminopyridine (4AP) which results in similar intracellular calcium levels as excitotoxic insults induced by bath glutamate application, but without cell death increase [85, 86]. It was concluded that specifically eNMDAR activation triggers toxicity. Further indication for specific eNMDAR initiated toxicity came from NMDA receptor inhibition with ifenprodil which prevented neuronal cell death. Ifenprodil specifically binds and inhibits NMDA receptors containing the NR2B subunit (Figure 4) and it is reported that NR2B-receptors are predominantly localized extrasynaptically, whereas NR2A containing receptors are found at the synapse [87, 88]. Furthermore, at low concentrations the slow binding NMDA receptor open-channel blocker memantine is specific for eNMDAR binding due to their slower opening kinetics compared to sNMDARs (Figure .4). Memantine treatment protects neurons *in vitro* and *in vivo* from cell death [89]. A detailed explanation about NMDA receptor inhibition is given in figure 4.

The sustained increase of intracellular calcium levels via eNMDAR activation blocks synaptic signalling in a glutamate dose dependent manner since complete neuronal depolarization after excitotoxic stimulation does not allow further action potential firing [86]. Therefore, eNMDAR stimulation is dominant over sNMDAR signalling (Figure 2). Further detrimental effects caused by excitotoxicity in the postsynaptic neuron are for example mitochondrial damage through mitochondrial depolarization, production of nitric oxide (NO) and free radicals, cell membrane disruption, cytoskeletal breakdown, DNA fragmentation and acidosis [90]. Mitochondrial depolarization, initiated by heavy calcium influx in the mitochondrial matrix, results in the loss of mitochondrial membrane potential, thereby impairing the proton transport and ATPase function. The following energy loss and other death signals induced during this process explain why mitochondria have an essential role in excitotoxicity-induced necrotic cell death [91]. Strong mitochondrial depolarization is seen as point of no return for cell death induction.

The neuron can be intrinsically protected against death and degeneration by the induction of activity-regulated inhibitor of death (AID) genes like *Bdnf, Atf3, Btg2, Gadd45β, Gadd45γ* or *Inhba*. AID genes are a group of activity-induced genes which support cell survival, for example by maintaining mitochondrial integrity or eNMDAR downregulation via BDNF

signalling [92, 93]. Yet, another early mechanism following an excitotoxic insult is the deactivation of CREB also named CREB shut-off, causing a decrease in transcription of the CREB target gene *Bdnf* (Figure 2) and therefore acting against neuronal self-protection [86].

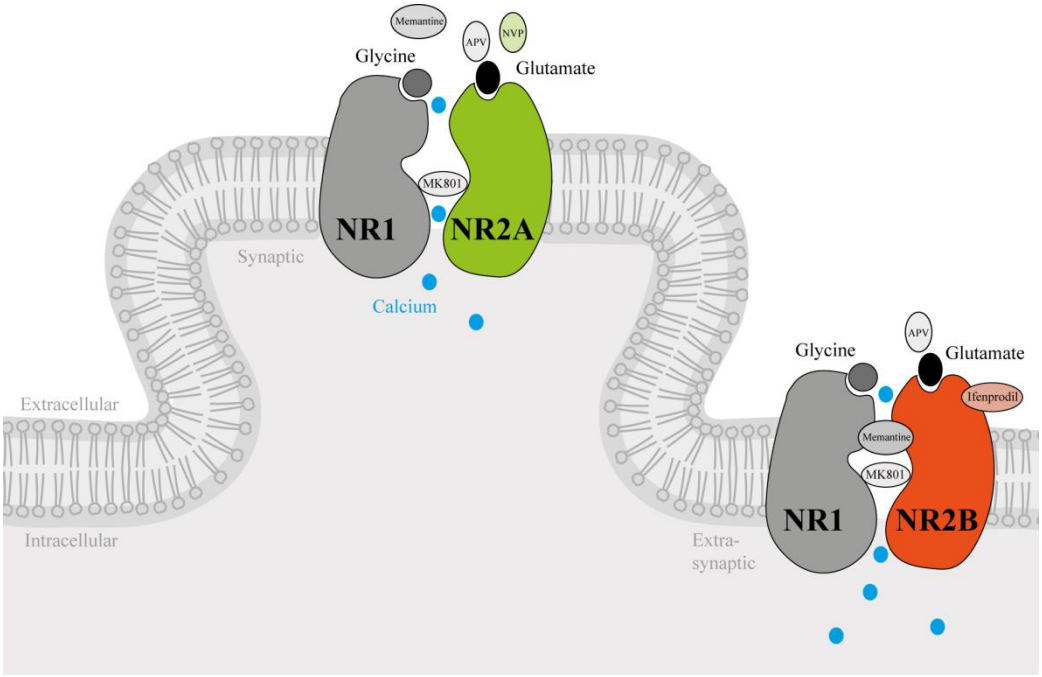

Figure 4: Overview of NMDA receptor inhibitors and their site of function. NMDA receptors are heterotetrameric complexes mainly composed of two NR1 and two NR2 subunits, whereas the subunits bind glycine and glutamate, respectively. At mature synapses the predominant NR2 isoform is NR2A, extrasynaptically NR2B is more frequently expressed. Ifenprodil is specifically antagonizing NR2B allosterically and NVP-AAM077 (NVP) inhibits NR2A glutamate binding competitively. Contanokin G (ConG) competetivly blocks glutamate binding specifically for NR2B containing receptors. APV competes for glutamate binding in NR2A and NR2B. MK801 is an uncompetitive open-channel blocker with high affinity and fast binding kinetics, in contrast, memantine has low open channel binding affinity and a fast off-binding rate. In low concentrations memantine predominantly binds extrasynaptic NMDA receptors.

1.3.2. CREB shut-off

Activation of eNMDARs results in dephosphorylation and thereby deactivation of CREB at Ser^{133} within 2-5 minutes. A second step of the CREB shut-off is the degredation of CREB occurring after 10-30 minutes [93]. Besides *Bdnf*, no other activity-induced gene is reported to be affected by the CREB shut-off. In addition to CREB deactivation also the deactivation of ERK1/2 by dephosphorylation of Thr^{202}/Tyr^{204} takes place during excitotoxicity (Figure 2) [94]. During synaptic firing, the duration of ERK1/2 activity is determined by the striatal enriched phosphatase (STEP) which is activated by NMDA mediated calcium influx [95]. However, for both eNMDAR dependent deactivation events the initiation mechanism is not known. One study reports that the very broad acting protein phosphatase 1 (PP1) is involved in nuclear CREB dephosphorylation [96], but how PP1 gets activated and if PP1 is the only

phosphatase involved in the shut-off process is not known. Other candidate proteins which are activated during the excitotoxicity-induced necrotic cascade are calpain proteases which cleave CaMKs, calcineurin (PP2-B) and caspases [97-99]. It was also observed that the phosphatase and tensin homolog (PTEN), which is capable of CREB dephosphorylation [100], shuttles to the nucleus upon excitotoxicity [101].

Furthermore, Kreutz *et al.* report about the shuttling protein Jacob as an important mediator of synapse-nucleus signalling during synaptic activity and excitotoxicity. They show the involvement of Jacob in CREB activation via Ser^{180} phosphorylation by ERK1/2 shuttling and Jacob´s participation in the CREB shut-off [102]. According to their data, eNMDAR signals result in the nuclear import of unphosphorylated Jacob, which does not support CREB phosphorylation, via NR2B/CaMKII and not NR2A or RasGRF2 signalling [103]. Although Jacob could explain the CREB shut-off mechanism, this model still depends on ERK1/2 activity and to date there is no explanation about the initiation of excitotoxicity dependent ERK1/2 dephosphorylation.

It was shown that the CREB shut-off can be prevented by NMDAR inhibition and in particular by the eNMDAR inhibitor memantine (Figure 4) [104]. Memantine is a drug approved for the treatment of moderate to severe Alzheimer´s disease (AD). Since heightened eNMDAR signalling is implicated in several neurodegenerative and neuroinflammatory diseases like AD, HD, amyotrophic lateral sclerosis (ALS) and Multiple Sclerosis [105], it is reasonable to assume the involvement of CREB and ERK1/2 shut-off and their downstream effect on activity-induced genes in the pathology of neurodegenerative diseases as well.

1.3.3. Excitotoxicity in neurodegenerative diseases

The involvement of eNMDAR activity in neurodegenerative disease pathogenesis is best documented in HD. HD is a rare monogenetic neuropsychiatric disorder caused by increased number of 3´CAG repetitions of the huntingtin (HTT) gene, resulting in huntingtin protein with an elongated polyglutamine tract. Symptoms of HD include motor and coordination disturbances and the decline of mental abilities into dementia. In a standard mouse model of HD, YAC128, an elevated eNMDAR current was observed, as well as an increase of NR2B-NMDA receptor surface expression [106]. Moreover, NMDA receptors localized to a greater extent to extrasynaptic sites in YAC128 compared to the wild type YAC18. Interestingly, reduced basal CREB phosphorylation was detected in the striatum of YAC128 which was rescued by memantine treatment. This strongly supports the theory of the involvement of eNMDAR-dependent CREB shut-off in HD pathogenesis [107]. Furthermore, BDNF depletion can be detected in the striatum of HD mouse models and in patients [108].

The most common neurodegenerative disease with implications of excitotoxic signalling during disease pathology is AD. AD is characterized by a dysfunction of the episodic memory, leading to severe dementia. The decrease of mental ability is accompanied by a loss of cortical and hippocampal neurons in later stages of the disease [109]. Most forms of AD occur sporadically, however, some cases of AD are autosomally dominantly inherited due to a mutation in amyloid precursor protein (APP) or presinilin 1 or 2 [110]. Both proteins are

involved in Aβ42 accumulation, which led to the amyloid hypothesis as cause of AD [111]. In AD, extracellular glutamate builds up slowly as a result of amyloid beta promoted glutamate release from neurons and glia cells [112]. An analysis of activated CREB in AD is not yet reported, however, *Bdnf* mRNA and mature protein downregulation was observed in the parietal cortex and the hippocampus of AD patients even in pre-clinical AD stages [113, 114]. This is especially harmful since it was also shown that BDNF protects neurons from Aβ42 toxicity [115].

Another neurodegenerative disease with excitotoxic implications is ALS. ALS patients show elevated glutamate levels in the cerebral spinal fluid, which may result from decreased glutamate uptake of neurons and glia cells [116]. Although, there is not much evidence for excitotoxicity in Parkinson´s disease (PD), a PD mouse model showed elevated glutamate concentrations in the substantia nigra as well and in parkinsonian dyskinesia a shift in NMDAR distribution towards extrasynaptic sites was observed [117]. Even in the neuroinflammatory disease MS excessive glutamate is released at the sites of demyelination and axonal degeneration [118]. Acute excitotoxic events occur during brain ischemia and traumatic brain injury due to a massive glutamate release after the insult and excitotoxicity contributes greatly to the rapid tissue degeneration [119].

All in all, excitotoxicity accompanied by the CREB shut-off is implicated in several neurological disorders, yet, there is only little information about the shut-off available. Affected genes besides *Bdnf* are not described and it is unknown whether other transcription factors and/or signalling kinases are deactivated after eNMDAR stimulation or whether CREB and ERK1/2 are exclusive. Furthermore, it is unknown how and why the shut-off occurs after eNMDAR and not after sNMDAR activation. Discovering the initiation mechanism of the shut-off would be very valuable, especially in regards of disease treatment. Since excitotoxicity is associated with many neurological diseases, findings about the shut-off could benefit therapeutic drug development for a broad spectrum of diseases.

1.4. Aim of this thesis

The overall aim of this thesis was to investigate neuronal activity-regulated gene expression in a healthy physiological system and, in contrast, during the pathological process of excitotoxicity. Therefore, the thesis was divided into two parts with specific aims for each part (Figure 5).

1.4.1. Neuronal activity-induced gene expression in a murine model of impaired spatial memory

Lasting neuronal adaptation processes resulting in the ability of persistent memory formation are driven by activity-dependent gene transcription and *de novo* protein syntheses (1.1.3). Until now, genetic manipulation studies showed the importance of single activity-regulated-

genes for plasticity and/or learning processes, especially for spatial memory in the well characterized hippocampal region. Also in neurodevelopmental and neurodegenerative pathologies differences in gene expression were observed. However, expression of activity-induced genes under non-pathological naturally occurring *in vivo* conditions is not well characterized. Therefore, the aim of the first part of this thesis was to examine expression and potential dysregulation of neuronal activity-induced genes in a less-artificial, unpathological model of variability in memory capacity, by comparatively analysing healthy adult DBA/2 and C57BL/6 inbred mice. DBA/2 as inbred strain carry a diverse spectrum of genetic differences compared to C57BL/6 that is corresponding to differences between two human individuals. The main goal of the first part of the thesis was to investigate whether the reduced performance of DBA/2 in spatial memory tasks is correlated with differences in activity-dependent gene expression.

To answer this question, the initial experiments of the first part aimed to examine the DBA/2 spatial memory impairment in comparison with C57BL/6 (Figure 5). In addition to proving literature findings, further parameters about the impairment and general DBA/2 behaviour were investigated. These information are necessary for evaluating the DBA/2 phenotype. To interpret gene expression results correctly, basic cellular and electrophysiological properties important for hippocampal function were also investigated. Basal gene expression and neuronal activity-dependent induction of classical IEGs was analysed. First *in vitro* without the physiological circuitry to examine cell intrinsic gene induction and signalling functionality, later *in vivo* to analyse a possible involvement of extrinsic factors like network and microcircuit function. Findings about the DBA/2 impairment, particularly in respect to their gene expression, could give indications about the significance of neuronal activity-regulated genes for inter-individual differences in human learning abilities.

1.4.2. Activity-dependent gene regulation during excitotoxicity

The second part of this thesis aims to investigate neuronal activity-regulated gene expression under the pathological condition of excitotoxicity. Excitotoxic processes are implicated in several neurodegenerative pathologies. For single activity-controlled genes like *Bdnf* a downregulation in the disease state was found and explained by the activity shut-off of CREB and ERK1/2. However, a comprehensive overview of expression dysregulation and the activity status of other kinases and transcription factors involved in activity-dependent gene induction in an excitotoxic paradigm are missing. This thesis intends to shed light on the differential aspect of excitotoxicity-induced protein deactivation, gene downregulation and their initiation mechanism.

To accomplish those aims, the second part of this thesis characterized the differential expression of several IEGs during strong and mild excitotoxic insults *in vitro* (Figure 5). In addition, the possibility of a rescue of excitotoxicity-induced expression dysregulation with diverse NMDA receptor inhibitors was tested. This was followed by the characterization of dephosphorylation/deactivation of crucial kinases, transcription factors and transcription regulators for activity-dependent gene induction. Also protein degradation processes were

assessed with a longer protocol. Finally, the initiation mechanism of the transcription downregulation was investigated by phosphatase inhibitor application and artificial mitochondrial depolarization.

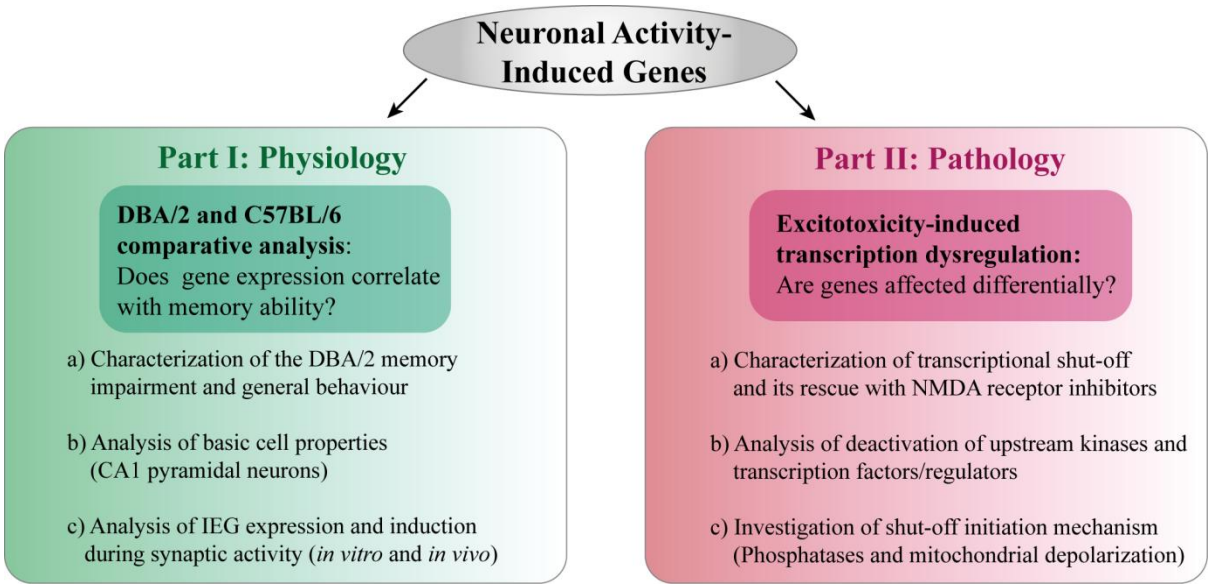

Figure 5: Schematic overview of main aims of the thesis. Left side of the diagram depicts aims affiliated with the first part of the project, the expression and induction of activity-induced genes in DBA/2 and C57BL/6 as model of naturally occurring differences in learning ability. The right side is listing aims affiliated with the second project part, the transcription shut-off of neuronal activity-induced genes during excitotoxicity.

Chapter 2

Material and Methods

1.2 Behaviour

2.1.1. Mice

8-week-old male DBA/2J (Janvier, Le Genest-Saint-Isle, France) and C57BL/6N (Charles River, Sulzfeld, Germany) mice were initially ordered and housed for at least one more week in the housing rooms of the neurobiology department (University Heidelberg, Germany) before behavioural experiments started. The mice were group-housed on a 12-h light/dark cycle and had *ad libidum* access to water and food. Experiments assessing spatial memory and anxiety took place during the light phase. First at age of 9 weeks learning ability in the spatial object recognition task (SOR) and in parallel open field behaviour was tested, followed by one week rest. At an age of 11 weeks mice were trained and tested in contextual fear conditioning (CFC) and at 12 weeks nesting performance was assessed. Mice that were sick and/or injured from cage-mate fighting were excluded from the study. For the assessment of the visuo-motor conditional learning task mice were single-housed under reversed dark/light cycle in the housing rooms of the group psychiatric animal models (Center Institute of Mental Health, Mannheim, Germany). During the operant conditioning, food supply was restricted to maintain 85-90% of the individual free-feeding body weight as described in [120-122]. For the VMCL task, housing started at 8 weeks and lasted until the age of 13 weeks. Mice tested in VMCL were used for visible water maze performance at 16 weeks. All procedures were carried out in accordance with German guidelines for the care and use of laboratory animals (Regierungspräsidium Karlsruhe) and with the European Community Council Directive 86/609/EEC.

2.1.2. Contextual fear conditioning

Mice were habituated for three days 0.5 h per day prior training to the experiment room and handled 2 min per day by the experimenter. During the training day, mice were placed into the conditioning chamber (23cm × 23cm × 35 cm) and received a 2-s foot shock (0.7 mA) 148 s after placement into the chamber. Mice were removed from the chamber 30 s after the shock terminated. Testing occurred 1 h (short-term memory) or 24 h (long-term memory) after conditioning. During testing, mice received one 5-min exposure to the same context in the absence of foot shock. Freezing, defined as absence of movement except for respiration, was scored manually and continuously during training and testing sessions. Mean velocity

was scored automatically by TSE Fear Conditioning System software (TSE Systems GmbH, Bad Homburg, Germany) and shown in cm/s. Depicted freezing data is shown as percentage of total interval duration: pre-shock: (time freezing [s]/148 [s]) × 100 [%], post-shock: (time freezing [s]/30 [s]) × 100 [%], test: (time freezing [s]/300 [s]) × 100 [%].

2.1.3. Spatial object recognition

Spatial memory acquisition

Mice were habituated for three days 0.5 h per day prior training to the experiment room and handled 2 min per day by the experimenter. The experimental apparatus consisted of a black, square open field (50 cm × 50 cm × 50 cm) with a visual cue placed on one arena wall. During the training day, mice received one habituation and three training sessions consisting of 6 min each. Between sessions, mice were returned to their home cage for 3 min. At the beginning of every session mice were placed at the right bottom corner of the box and after every session ground and walls were cleaned with 70% ethanol. Habituation to the open field was conducted in the absence of objects and recorded for open field analysis. During the three training sessions, two distinct objects (a glass bottle and a metal box) were present. After 24 h or 1h (long-term memory and short-term memory assessment, respectively), mice were returned to the open field, and one of the objects was displaced to a novel spatial location. For half of the two groups (DBA/2 and C57BL/6) the glass bottle was relocated, for the other half the metal box to avoid bias due to differences in object preference. Time spent exploring the displaced and non-displaced objects was manually scored. Exploration was analysed during the training and testing phases. The response to spatial change was measured by dividing the mean time exploring the displaced object by the mean of the total time exploring the displaced and non-displaced objects during the test session. This value was multiplied by 100 to obtain a percentage of preference for the displaced object: ($t_{displaced}$ [s]/($t_{nondisplaced}$ [s]+ $t_{displaced}$ [s]) × 100 [%]).

Expression analysis after spatial object recognition

For gene induction analysis, mice were trained as described and brains were collected 30min after training. The control group (home cage animals) was handled and placed in the behaviour room at the training day, but was not subjected to training. All control brains were collected after the trained animals within 1h. Half of the animals per cage were control the other half trained animals to avoid cage bias. All brains were coronally sliced in a brain matrix and stored in RNAlater (Sigma Life Science, St. Louis, USA) for one week upon brain area dissection. Dissection was performed with a binocular microscope (Stemi SV6, Zeiss, Oberkochen, Germany) under a flow hood. Areas were dissected from both hemispheres according to Allen brain reference atlas (coronal slices, adult mouse). Every area was stored in a separate tube at -80 °C upon total RNA extraction.

2.1.4. Visuo-motor conditional learning

Apparatus

Visuo-motor conditional learning (VMCL) was assessed in operant touchscreen chambers (Model 80614-20, Campden Instruments Ltd., Longborough, UK). The trapezoid chambers (h 19 cm, w 24 respectively 6 cm, d 17 cm) consisted of black Perspex walls and a metal grid floor and were equipped with a liquid dispenser tray with illumination on the short end and a screen on the opposing wall. The liquid dispenser delivered the palatable reward solution (sweet condensed milk (SCM) 1:4 diluted with tap water, Milchmädchen, Nestle). A black Perspex mask separated the screen into three touch sensitive fields (7 x 7 cm), which could display visual cues and detect responses. Additionally, the chamber environment was equipped with a house light, which was mounted above the chamber, and a tone generator. Software (ABET II Touch software, Campden, UK) controlled the functions of chamber components and detected the behavioral output.

Pokey training

Pokey training procedure has been published frequently [121, 123, 124]. After a habituation session (20 min with accessible SCM), the mice were familiarized with the functions of the box in successional training programs. This included the association of the reward delivery with a tone in the Initial Touch phase, the touch of the screen on the indicated touch field (display of a white square) in the Must Touch phase, the obligatory initiation of the next trial by entering the food tray in the Must Initiate phase and the indication of incorrect responses by a 5-seconds time-out with illumination of the chamber. Lastly, the mice were trained to touch a white square on the central touch field in order to trigger the choice phase, in which squares appeared on both marginal fields. This sequence directly corresponds to the procedure of the VMCL, where the central field is used to display the side-indicating visual cue.

VMCL

The VMCL was assessed as previously described by Delotterie, Mathis [125] with slight variation. Briefly, the task is to identify visual stimuli presented on the central screen and hence decide to touch either the left of the right touch field in order to receive a reward, following the rule “If stimulus A, then go left; if stimulus B, then go right”. After initiation of the trial, one of two discriminative visual stimuli (white icicle or white equal) appeared in a pseudorandom frequency. Here, only one of those fields led to the delivery of a reward, tray illumination and tone generation and were counted as correct responses, while the other triggered the 5-second timeout and illumination and were considered incorrect. Incorrect responses caused a correction trial to be initiated, in which the previous stimulus receiving an incorrect response was presented repeatedly until the correct response was given. Correction trials were independent and not counted into the measure of accuracy. In a 5-second inter-trial interval, after ‘reward’ or ‘punishment’ the mouse could initiate the next trial. Subjects were tested for 15 days with 1 session per day and 30 trials per session with a maximum duration of 60 min. The direction of the reward indicating visual stimuli between the groups

was counterbalanced: half the mice learned to touch the left field when presented with the white icicle and touch the right field when the white equal appeared, while the other half learned the opposite rule.

2.1.5. Open field task

The open field test was carried out within the habituation session (6 min) of the object recognition task. Characterization of anxiety-like behaviour in the open field was conducted using Smart Video Tracking Software (version 3.0.05, Panlab Harvard Apparatus, Holliston, USA). The central 32 % of the open field arena was assigned as the central zone and the rest defined to be periphery. Anxiety-like behaviour of the mice was quantified as the percentage of the time spent in the central zone ((t_{center}/560 [s]) × 100 [%]), the latency to the first entrance to the central zone [s], number of entries in central zone [n] and distance travelled in central zone ($distance_{center}$ [cm]/$distance_{center+periphery}$ [cm]) × 100 [%]).

2.1.6. Nesting behaviour

Nest building ability was assessed as described by Deacon [126] one week after contextual fear conditioning. In short, mice were separated at the evening overnight and placed with one cotton square nestlet (Plexx B.V., Netherlands) per cage. 12 h after separation, nest quality was scored according to the Deacon scoring system and the untorn nesting material was weighted. The mass of the untorn nestlet was calculated as followed: weight of nestlet $_{after\ separation}$ [g]/weight of fresh nestlet $_{before\ separation}$ [g]) × 100 [%].

2.1.7. Visible water maze

The visual version of the water maze was performed as described previously [127] with modifications. The setup consisted of a water-filled (24°C) circular pool (150 cm in diameter), a black platform (14 x 14 cm²) and an orange and black coloured 15-ml centrifuge tube, which was placed on the platform and served to indicate the position of the platform from afar. Mice habituated to the experimental room 0.5h before the experiment started. We assessed the latency to reach the platform for each mouse in four trials. The platform position changed between the trials to circumvent orientation with other cues. We adapted the start position in each trial, keeping the distance from entry point to platform identical. The direction of the quickest path was counterbalanced, thereby having the shortest distance twice to the left and twice to the right side in a random manner. Each trial ended when the mouse reached the platform or after 2 min. Mice were placed in front of warming light for 5 min and remained in their home cage for additional 40 min during the inter-trial interval.

2.1.8. Kainic acid induced gene expression

Young adult DBA/2 and C57BL/6 were weighted and injected *intraperitoneally* (i.p.) with 15mg kainic acid (Sigma-Aldrich, St. Louis, USA) in PBS per kg bodyweight. Control mice from each strain received i.p. injection of PBS only. Injected mice were put in a black bin (25cm × 30cm × 60cm) separately to avoid self-injury due to seizures. Mice were observed during the following 30min and severity of seizures was scored according to the following *status epilepticus* scoring system: 0: no reaction; 1: immobility; 2: sudden shaking, chewing movements; 3: clonus of front extremities; 4: erecting of the body; 5: continuous body erection, seizures; 6: death. After 30min mice were sacrificed via cervical dislocation and the brain was removed and stored as described in 2.1.3.

2.2. Primary neuronal culture

2.2.1. Culture preparation

Dissociated hippocampal and cortical neuronal cultures were prepared from new-born (P0) wild type C57BL/6 (Chares River, Sulzfeld, Germany) or DBA/2J (Janvier, Le Genest-Saint-Isle, France) pups. Total hippocampus and total cortex was dissected in a 1:9 volume ratio sterile filtrated mixture of Ky/Mg solution (Table 2) and dissociation medium (DM, Table 3). Mixture is referred to as Ky/Mg/DM. Hippocampal and cortical tissue was then dissociated by enzyme solution (Papain latex 10 Units/ml and 3.7mML-Cysteine in Ky/My/DM) for 20 min at 37 °C in a water bath separately. During enzyme incubation, the tube was stirred continuously at 15 mot/min, every 5 min the tube was shaken to homogenize the solution and to avoid local acidification. Enzyme incubation was repeated once with a total enzyme solution change in between. Enzyme activity was stopped by addition of the trypsin inhibitor solution (1%, w/v trypsin inhibitor in Ky/My/DM) 3 times with a complete inhibitor solution change in between. Each time tissue was incubated at 37 °C for 5 min in a water bath and stirred continuously at 15 mot/min. After enzyme inhibition, tissue was washed 3 times with growth medium (GM, Table 4) and triturated by pipetting to get a single cell suspension.

Cell suspension was diluted in Opti-MEM supplemented with 20 mM glucose to a concentration of 0.7×10^6 cells/ml (experiments in 3.1) or about 0.8 hippocampi/2 ml (experiments in 3.2). Cells were counted in a Thoma chamber at a 1:2 dilution with tryptophan blue (experiments in 3.1). Cells were plated on poly-D-lysine/laminin (BD Biosciences, Franklin Lakes, USA) coated 12-well plates (Falcon™; polysterol; 3.8 cm^2/well, 1ml medium/well, used for gene expression experiments), 4-well plates (Nunc, Nuncton Delta, 1.9 cm^2/well, 1ml medium/well, used for cell death experiments), dishes (Falcon™; 9.6 cm^2/dish, 2ml medium/dish, used for Western blot experiments) or dishes containing 4 12-mm diameter glass coverslips (2ml medium/dish, used for imaging experiments), according to experiment design. 2.5 h after plating, medium was replaced with Neurobasal-A growth medium (GM, Table 4) and put back to a 37 °C incubator supplied with 5% CO2.

Table 2: **Ky/Mg solution.**

[a]Component	Final concentration	Stock concentration	For 80 ml
Kynurenic acid	10 mM	Powder	158.56 g
$MgCl_2$	100 mM	2 M	4 ml
HEPES	5 mM	1 M	0.4 ml
Phenol red	0.5% v/v	100%	0.4 ml
NaOH	12.5 mM	1 N	1 ml
H_2O			up to 80 ml

[a]All chemicals are from Sigma-Aldrich Chemie GmbH, München, Germany.

Table 3: **Dissociation Medium (DM).**

[a]Component	Final concentration	Stock concentration	For 250 ml
Na_2SO_4	81.8 mM	1 M	20.45 ml
K_2SO_4	30 mM	0.25 M	30 ml
$MgCl_2$	5.85 mM	1.9 M	0.77 ml
$CaCl_2$	0.25 mM	1 M	0.063 ml
HEPES	1 mM	1 M	0.25 ml
Glucose	20 mM	2.5 M	2 ml
Phenole red	0.2% v/v	100%	0.5 ml
H_2O			up to 250

[a]All chemicals are from Sigma-Aldrich Chemie GmbH, München, Germany.

Table 4: **NB-A/Growth Medium (GM).**

[a]Component	For 100 ml
Neurobasal A-medium	97 ml
B27	2 ml
Rat serum	1 ml
Glutamin (200 mM)	0.25 ml
Penicillin/Strepomycin	0.5 ml
H_2O	up to 100

[a]All chemicals are from Sigma-Aldrich Chemie GmbH, München, Germany.
Sterile filtered through 0.22 m Millipore filter and stored at + 4 °C.

2.2.2. Culture maintenance

On day-*in vitro* (DIV) 3 the mitosis inhibitor AraC (cytosine-D-arabinofuranoside; Sigma-Aldrich, St. Luis, USA; C1768) was added at a final concentration of 2.8 M to inhibit the proliferation of non-neuronal cells, in particular astrocytes. On DIV 8, GM was replaced by transfection medium (TM; Table 6; 10% v/v MEM; ITS containing: 7.5 g/ml Insulin, 7.5 g/ml, Transferrin, 7.5 ng/ml Sodium selenite; 50 Units/ml Penicillin; 50 mg/ml Streptomycin; dissolved in SGG: Table 5). All *in vitro* experiments were conducted on DIV 10 or 11.

Table 5: **Salt Glucose Glycine Solution (SGG).**

[a]Component	Final concentration	Stock concentration	For 500 ml
NaCl	114 mM	5 M	11.4 ml
$NaHCO_3$	0.22% v/v	7.5% m/v	14.6 ml
KCl	5.29 mM	3 M	0.882 ml
$MgCl_2$	1 mM	1.9 M	0.264 ml
$CaCl_2$	2 mM	1 M	1 ml
HEPES	10 mM	1 M	5 ml
Glycine	1 mM	1 M	0.5 ml
Glucose	0.54% v/v	45% m/v	6 ml
Sodium pyruvate	0.5 mM	0.1 M	2.5 ml
Phenole red	0.2% v/v	100%	0.5 ml
H_2O			up to 500 ml

[a]All chemicals are from Sigma-Aldrich Chemie GmbH, München, Germany.
Sterile filtered through 0.22 m Millipore filter and stored at + 4 °C.

Table 6: **Transfection Medium (TM).**

[a]Component	For 100 ml
SGG	88 ml
MEM (without glutamine)	10 ml
ITS	1.5 ml
Penicillin/Strepomycin	0.5 ml
H_2O	up to 100 ml

[a]All chemicals are from Sigma-Aldrich Chemie GmbH, München, Germany.
Sterile filtered through 0.22 m Millipore filter and stored at + 4 °C.

2.2.3. Stimulation protocols

All stimulation experiments were performed on DIV 10 or 11. For $GABA_A$ receptor inhibition and activation of synaptic firing, bicuculline (BIC) was applied. C57BL/6 and DBA/2 cultures (Results 3.1.3) were stimulated by BIC for 0h (unstimulated control), 0.5h, 1h and 2h. Stimulation protocols for active and passive shut-off analysis (Results 3.2) are shown in table 8. Gene expression analysis was always performed for cells plated on a 12-well plate containing 1ml medium. Therefore, drug dilution was calculated for 1ml final volume. Drugs were pipetted in a reaction tube according to the given final concentration (Table 7) and diluted with 500µl of the 1ml culture medium. After thoroughly mixing, the 500µl drug containing medium was distributed equally over the well. Western blot analysis was always performed in dishes with 2ml final volume; drugs were applied the same way except that 1ml medium was removed from the dish and used for the initial dilution.

Table 7: **List of drugs applied in primary neuronal cultures.**

[a]Drug	Stock Concentration	Final Concentration
Bicuculline (BIC)	50 mM	50 µM
Tetrodotoxin (TTX)	1 mM	1 µM
DL-threo-β-Benzyloxyaspartic acid (TBOA)	50 mM	50 µM
N-Methyl-D-aspartate (NMDA)	100 mM	10 µM, 30 µM
Carbonyl cyanide-4 (trifluoromethoxy)phenylhydrazone (FCCP)	5 mM	0.1, 0.5, 1 µM
Actinomycin D (Act.D)	20 mg/ml	10 µg/µl
Phosphatase Inhibitors:		
Ocadaic acid (OA) (Protein phosphatase 1 inhibitor)	100 µM	2 µM
Cyclosporin A (Protein phosphatase 2B inhibitor)	10 mM	250 µM
FK506 (Protein phosphatase 2B inhibitor)	1 mM	1 µM
TC-2153 (STEP inhibitor)	14 mM	1 µM
Phosphatase and tensin homolog (PTEN) inhibitors:		
SF1670	30 mM	30 µM
bbV(phen)	100 mM	100 µM
VO-OHpic trihydrate	30 mM	30 µM
NMDA receptor inhibitors:		
Memantine	10 mM	10 µM, 100 µM
Ifenprodil	10 mM	3 µM
MK801	20 mM	10 µM
APV	50 mM	50 µM
ConantokinG (ConG)	400 µM	0.2 µM, 1 µM

[a]All drugs were purchased from Sigma-Aldrich/Merck (St. Louis, USA).

Table 8: **Overview shut-off protocols.**

Protocol	[a]Drug application
Short protocol	0.5h BIC + 0.5h (TTX or TTX/NMDA or NMDA or Act.D)
Intermediate protocol	1h BIC + 1h (TTX or TTX/NMDA or NMDA or Act.D)
Long protocol	2h BIC + 2h (TTX or TTX/NMDA or NMDA or Act.D)
Phosphatase inhibitors	1h (BIC + Inhibitor) + 1h (TTX or TTX/NMDA or NMDA or Act.D)
NMDA receptor inhibitors	1h Inhibitor + 1h BIC + 1h (TTX or TTX/NMDA or NMDA or Act.D)

[a] Drugs were applied in addition and not washed out.
For each experiment one well was added as untreated control.

2.3. Gene expression analysis

2.3.1. Total RNA Extraction

In vitro material

All RNA related work was conducted under RNase-free condition. Total RNA was extracted using RNeasy Plus Mini Kit (Qiagen, Venlo, Netherlands) with additional on-column DNaseI digestion (RNase-Free DNase Set, Qiagen) during RNA purification. Briefly, cell samples were lysed with lysis buffer (RLT) which was supplemented with 1% β-Mercaptoethanol (ME). In each well of a 3.8 cm^2 12-well plate 300 µl freshly prepared RLT/ME mix was added and cells were scraped off. Cell lysis suspension was transferred in a new RNase-free tube, 300 µl of 70% Ethanol (dissolved in diethylpyrocarbonat treated H_2O) was added and mixture was homogenized thoroughly by pipetting. Each sample was transferred to an RNeasy spin column placed in a 2 ml collection tube. After 1 min the tube was spun for 15 sec at 13,000 rpm in a Fresco17 centrifuge (Heraeus, Hanau, Germany). The flow through was discarded and the column membrane was washed with 350 µl wash buffer (RW1) once, spun down and the flow-through was discarded again. This was followed by the on-column DNaseI digestion which was performed at room temperature for 15 min with 80 µl DNase solution (10 µl DNaseI stock in H2O plus 70 µl RDD buffer for each column, final DNaseI concentration: 340 Kunitz units/ml). After digestion, the column was washed again once with 350 µl RW1 and twice with 500 µl wash buffer RPE. The last RPE centrifugation lasted 2min to get rid of all ethanol from the column, since ethanol inhibits polymerases. The column was then placed into a new RNase free 1.5 ml tube and 40µl RNase-free H_2O (Ambion, USA) was directly added to the column membrane, incubated for 5min and centrifuged for 1 min at 13,000 rpm. Concentration of eluted RNA was measured with a DS-11 spectrophotometer (DeNovix Inc., Wilmington, USA) and RNA was stored at -80 °C for later use.

In vivo material

Brain tissue was homogenized in 300 µl RLT/ME mix on ice by high speed vortexing (Pellet Pestle^R Motor, Kontes). 300 µl of 70% ethanol was added; solution was mixed thoroughly and centrifuged for 1 min at 13.000 rpm. The remaining protocol was carried out as described for *in vitro* material.

2.3.2. cDNA synthesis

1.0 µg of total RNA was used for cDNA synthesis with the High Capacity cDNA Reverse Transcription Kit (Applied Biosystems, Waltham, USA). Reverse transcription was carried out with 40 µl total volume. First RNA was diluted to a concentration of 1.0 µg in RNase-free H_2O (Ambion, USA) to a volume of 20 µl. Reverse transcription solution was mixed according to table 9 to a volume of 20 µl per sample, whereupon a master mix was made for all samples. Then 20 µl of the RNA dilution was mixed with 20 µl reverse transcription solution in a 0.2 ml RNase-free PCR reaction tube (Sarstedt, Nümbrecht, Germany). PCR program for cDNA synthesis is shown in table 10. cDNA products were stored at -20 °C.

Table 9: **cDNA synthesis mixture.**

[a]Solution	Volume for total 20 µl
RT buffer (10x)	2 µl
dNTP (100 mM, 10x)	0.8 µl
Random primers (10x)	2 µl
Reverse transcriptase (50 U/µl)	1 µl
RNase inhibitor (40 U/µl)	0.5 µl
RNase-free H2O	3.7 µl

[a]All chemicals are from Applied Biosystems[R], Waltham, USA.
+ 20 µl diluted RNA (1,0 µg) for each reaction

Table 10: **cDNA synthesis program.**

Step	Temperature	Duration
1 Annealing	25 °C	5 min
2 Annealing/Elongation	37 °C	120 min
3 Denaturation	85 °C	5 s
4 Storage	4 °C	for ever

PCR reaction was performed in thermal cycler C1000[TM] (Bio-Rad, Hercules, USA)

2.3.3. Real-time quantitative PCR

For real-time (RT) quantitative (q) PCR analyses, cDNA was diluted 1:3 – 1:5 with RNAase-free H_2O (Ambion, USA) after thawing on ice. TaqMan[R] Universal PCR Master Mix (Applied Biosystems[R], Waltham, USA), ready to use probe sets designed by TaqMan[R] Gene Expression (Table 11) and cDNA were mixed together according to table 12 in a 96-well plate from Applied Biosystems[R] (Micro Amp[R] Fast 96-Well). RT-qPCR was performed in a StepOnePlus[R] real time PCR system (Applied Biosystems[R]) with the temperature program presented in table 13. Signal acquisition occurred in the 4th step at 60 °C. Each sample was assayed as duplicate and the mean cycle time value was calculated by the software StepOne[TM] (version 2.3). Target mRNA expression level was normalized to the relative ratio of the expression of *Gusb* mRNA.

Table 11: **RT-qPCR taqman probes.**

Acronym	Gene name	Assay ID
Arc	Activity regulated cytoskeletal-associated protein	Mm00479619_g1
Atf3	Activating transcription factor 3	Mm00476032_m1
Bdnf	Brain derived neurotrophic factor	Mm00432069_m1
cFos	FBJ osteosarcoma oncogene	Mm00487425_m1
Egr1	Early growth response 1	Mm00656724_m1
Gusb	Glucuronidase, beta	Mm00446953_m1
Inhba	Inhibin beta-A	Mm00434338_m1
Npas4	Neuronal PAS domain protein 4 (Nfx)	Mm00463644_m1
Nr4a1	Nuclear receptor subfamily 4, group A, member 1	Mm00439358_m1

All probes are designed by Applied Biosystems^{R} (Waltham, USA).

Table 12: **RT-qPCR reaction mix per well.**

Solution	For 20 µl
Master mix, 2x	10 µl
Probe, 20x	1 µl
cDNA (diluted)	9 µl

Table 13: **RT-qPCR temperature program.**

Step	Temperature	Duration
1	50 °C	2 min
2	95 °C	10 min
3	95 °C	15 sec
4	60 °C	1 min
5	Go to step 3	50 cycles
6	Stop	For ever

2.4. Western blot

200 µl of 1x sample buffer (3x sample buffer: 9%SDS, 187.5 mM Tris, pH 6.8 and 30% glycerol w/v. + 10% ME and bromophenol blue) were added to each dish containing primary hippocampal cultures. Cell extracts in 1x sample buffer were incubated for 5 min at 95 °C and stored at -80°C or directly loaded to SDS-PAGE. In case of storage 95 °C incubation was always repeated directly prior loading. Proteins were separated with 10% SDS-PAGE (Table 14) with constant current at 30 mA per gel (Running buffer: 190 mM glycine, 25 mM Tris, 0.1% SDS and pH 8.8) and transferred to nitrocellulose membrane (Waterman) with constant

voltage of 20 V for 1.5 h (Transferring buffer: 150 mM glycine, 20 mM Tris, 0.1% SDS and 20% Methanol). After the transfer, total protein on the membrane was stained for 5 min by Ponceau S (SERVA Electrophoresis, Heidelberg, Germany) and washed twice with Millipore H_2O. This allowed the detection of unsuccessful transfer (bubbles) and the cutting of the membrane. Nitrocellulose membrane was then blocked in 5% milk (m/v, Reform instant skimmed milk powder, Frema, Radolfzell, Germany) in PBST (0.1%Tween-20 in PBS: 137 mM NaCl, 2.7 mM KCl, 10 mM Na_2HPO_4 $2H_2O$, 2 mM KH_2PO_4, pH 7.4) at room temperature for 1 h. The membrane was then incubated with the primary antibodies at 4 °C overnight (Table 15: List of primary antibodies). On the next day, the membrane was washed 3 times with PBST for 10 min and the secondary antibody was incubated at room temperature for 30 min (Table 16: List of secondary antibodies). The membrane was washed again 3 times for 10 min using PBST. All incubation and washing steps were carried out under continuous shaking. ECL detection was performed according to the manual (Amersham or Bio-Rad). The film was developed with a Kodak developing machine or by the ChemiDoc™ imaging system (Bio-Rad, Hercules, USA). Alpha Tubulin signal was used as loading control for every blot. In case of P-CREB, CREB, P-ERK1/2 and ERK1/2 membrane was cut after Ponceau staining and Tubulin was analysed in parallel. In case of P-ELK1, ELK1, MEF2A and P-MEF2A, Tubulin was stained in a second blotting round after membrane stripping (0.1 % NaN3 in PBS, 1h, room temperature). Signal quantification was done with Fiji image analysis software (version 2.0.0).

Table 14: **SDS-PAGE.**

Solution	Upper/Stacking gel 10 ml, 3.7%	Lower/Resolving gel 20ml, 10%
H2O	6.25 ml	8.2 ml
[a]4x Buffer	2.5 ml	5 ml
[b]Rotiphorese[R] Gel 30	1.25 ml	6.7 ml
[c]10% APSc	100 µl	100 µl
[d]TEMED	10 µl	10 µl

[a] 4x upper gel buffer: 0.5 M Tris-HCl, pH 6.8 and 0.4% (w/v) SDS;
4x lower gel buffer: 1.5 M Tris-HCl, pH 8.8 and 0.4% (w/v) SDS.
[b] 30% Acrylamid solution with 0.8% Bisarcrylamid from Carl Roth (Karlsruhe, Germany).
[c] 10% (w/v) ammonium persulfate (APS) in H2O.
[d] N,N,N',N'-Tetramethyl-ethylenediamine from SERVA Electrophoresis (Heidelberg, Germany).

Table 15: **List of primary antibodies.**

Name	Host species	Company	Dilution	Size
Phospho-CREB (Ser133)	rabbit polyclonal	Millipore, 06-519	1:1000 in 5% BSA/PBST	43 kDA
CREB	rabbit monoclonal	Cell Signaling, 9197	1:1000 in 5% BSA/PBST	43 kDA
phospho-ERK1/2 (Thr 202/ Tyr 204)	mouse monoclonal	Cell Signaling, 9106	1:2000 in 5% BSA/PBST	42 kDa/ 44 kDa
ERK1/2	rabbit polyclonal	Cell Signaling, 9102	1:4000 in 5% BSA/PBST	42 kDa/ 44 kDa
Phosphor-MEF2A (Ser408)	rabbit polyclonal	LS BIO, LS C381453	1:1000 in 5% BSA/PBST	55 kDa
MEF2A	rabbit polyclonal	Enogene E021039	1:1000 in 5% BSA/PBST	55 kDa
Phospho-ELK1 (Ser383)	mouse monoclonal	Santa Cruz Sc-8406	1:500 in 5% BSA/PBST	47 kDa
ELK1	rabbit polyclonal	Cell Signaling 9182	1:500 in 5% BSA/PBST	47 kDa
Alpha Tubulin	mouse monoclonal	Sigma, T9026	1:400000 in 5% milk/PBST	50 kDa

All primary antibody dilutions were stored with 0.05% NaN_3 at 4 °C.

Table 16: **List of secondary antibodies.**

Name	Host species	Conjugate	Company	Dilution
Mouse	goat IgG (H+L)	[a]HRP	Jackson Immuno Research 115-035-003	1:5000 in 5% milk/PBST
Rabbit	goat IgG (H+L)	[a]HRP	Jackson Immuno Research 115-035-144	1:5000 in 5% milk/PBST

[a]Peroxidase-conjugated affinity-pure goat IgG.
All secondary antibody solutions were freshly prepared before use.

2.5. Cell death analysis

Cultures plated on 4-well plates (1ml medium) were treated according to the shut-off protocol, or 1h inhibitor treatment was followed by 15min 30µM NMDA application. For both protocols cells were washed twice with TM after treatment and fixed with RotiR-Histofix 4% (Carl Roth GmbH & Co. KG, Karlsruhe, Germany) after a 24-h recovery period. Cell death was assessed by the analysis of morphological abnormalities of the nuclei. The percentage of neurons with condensed nuclei or large chromatin clumps was determined by counting Hoechst 33258-stained (1:5000 of 10 mg/ml stock solution, SERVA

Electrophoresis, Heidelberg, Germany) nuclei in 20 visual fields for every condition in each experiment with a light microscope (Leica DM IRBE) with 40× magnification. Counting and classification was performed automatically after manual program training by CellProfiler^{TM} and CellProfiler Analyst^{TM} software (Carpenter Lab at Broad Institute, Harvard, USA, version 2.0).

2.6. Morphological analysis

2.6.1. Nissl staining

For Nissl staining, brains from adult C57BL/6 and DBA/2 were imbedded in tissue freezing medium (Leica Biosystems, Wetzlar, Germany), cut in 20 µm thick slices with a Leica CM1950 cryostat at -18 °C and stained according to Mulisch and Welsch [128]. First, imbedding medium was removed from slices by decreasing ethanol concentrations (100%, 90%, 70%, 50%) and slices were treated with 50% $K_2S_2O_5$ (m/v, in H_2O) for 5 min. This was followed by 10 min cresyl violet solution (1.5% cresyl violet m/v, 1% 1M $C_2H_3NaO_2$, 1% 1M acetic acid) incubation. Acetate buffer (0.1M $C_2H_3NaO_2$, 0.1 M acetic acid, pH 4.6) treatment lasted for 30 min. Slices were imbedded in Xylol. The whole procedure was carried out at room temperature. Pictures were taken with the upright widefield Ni-E microscope (Nikon GmbH, Düsseldorf, Germany) with a 10x objective.

2.6.2. Golgi staining

For assessing dendritic morphology, 100 µm thick brain slices were stained with Golgi-Cox using the FD Rapid GolgiStainTM Kit (FD NeuroTechnologies Inc., Ellicott City, USA) according to their protocol. Images were acquired with a Nikon Ni-E microscope (Nikon GmbH, Düsseldorf, Germany) with a 20x objective. Total dendritic length of CA1 pyramidal neurons was calculated by using the freeware software Fiji (version 2.0.0) with a specific set of macros (written by E. Ruthazer, McGill University). Briefly, a z-stack acquisition was imported, calibrated and manually traced. For each strain, a minimum of four neurons per mouse from four different mice was analysed.

2.7. Rhodamine-123 imaging

Mitochondrial membrane potential was analysed by Rhodamine-123 (Rh123, Thermo Fisher Scientific, #R302) fluorescence imaging. Neurons were loaded with Rh123 (10 µg/ml) in SGG medium (without phenol red) for 10 min at 37 °C. This was followed by SGG washing. Rh123 incorporates into polarized mitochondria where it self-quenches at the used concentration. During mitochondrial depolarization, Rh123 leaks out of the mitochondria into the cytoplasm, it dequenches and a strong fluorescent signal is measurable. Rh123 signal (excitation wavelength: 480±20, emission wavelength: 527±15) was measured in the mitochondria-free nuclear region. Around 10 regions of interest were analysed per cover slip.

Maximum Rh123 signal was obtained by exposing the culture to the mitochondrial uncoupler FCCP at high concentration (5 µM; Sigma-Aldrich/Merck, St. Louis, USA) which results in complete elimination of the mitochondrial membrane potential. For comparing bath NMDA (30 µM) induced depolarization with low FCCP concentrations, hippocampal neurons were treated after 2 min baseline assessment for 10 min with the respective drug, followed by maximal 5 µM FCCP depolarization for 5 min. Images were analysed by open-source imaging software Fiji (version 2.0.0) and fluorescence signal was quantified with Igor Pro (WaveMetrics Inc., Nimbus, USA; version 6.3).

2.8. Electrophysiological analysis

Slice preparation

Acute slices were obtained from 10-week old C57BL/6 or DBA/2 mice. Mice were anaesthetized with isoflurane (2%) and perfused with slicing solution (NMDG-recovery solution in mM: NMDG, 93; 37%HCl, 93; KCl, 2.5; NaH_2PO_4, 1.2; L(+)ascorbic acid, 5; thiourea, 2; sodium pyruvate, 3; $MgCl_2$, 10; $CaCl_2$, 0.5; HEPES, 20; $NaHCO_3$, 30; glucose, 25; N-acetyl-l-cysteine, 10). Coronal slices 300 µm thick were incubated in the slicing solution gassed with 95% O_2 and 5% CO_2 for 10 minutes and then transferred to a chamber containing the recording solution.

Electrophysiology

Whole-cell patch clamp recordings were made from acute hippocampal slices. Slices were secured with a platinum ring in the recording chamber and were submerged in continuously flowing (3 ml/min) artificial cerebrospinal fluid (aCSF; in mM: NaCl, 125; KCl, 3.5; $CaCl_2$, 2.4; $MgCl_2$, 1.3; NaH_2PO_4, 1.2; glucose, 25; $NaHCO_3$, 26) gassed with 95% O_2 and 5% CO_2. Patch electrodes (3-5MΩ) were made from 1.5mm borosilicate glass and filled with the appropriate internal solution. The following intracellular solution was used for action potential, paired pulse, and current recordings (in mM): $KMeSO_4$, 127; EGTA, 0.2; HEPES, 10; K_2Phosphocreatine, 10; KCl, 12; NaCl, 8; Mg-ATP, 4; Na_3-GTP, 0.5. For seven recordings (B6 N=4, D2 N=3), the intracellular solution contained 30% Neurobiotin tracer. Spontaneous IPSCs were recorded in the voltage-clamp configuration at -70mV in symmetric chloride conditions using the following intracellular solution (in mM): CsCl, 130; HEPES, 10; EGTA, 5; CsOH, 20; $CaCl_2$, 0.5; Mg-ATP, 4; Na_3-GTP, 0.5. IPSCs were recorded in the presence of 10 µM of the AMPAR inhibitor NBQX and 0.5 µM TTX, after 6 min of recording, 5 µM of the $GABA_A$ receptor antagonist gabazine was applied to ensure that recorded currents were mediated by $GABA_A$ receptors. Recordings were made with a Multiclamp 700A amplifier, digitized through a Digidata 1322A A/D converter and acquired and analysed using pClamp 10 software (Molecular Devices).Voltage-clamp recordings were made at 5x gain, with a lowpass filter of 1 kHz and a sampling rate of 20 kHz. Current-clamp recordings were made at 10x gain with a lowpass filter of 10 kHz and 20 kHz sampling rate.

Analysis

Passive properties were monitored throughout the recording of a cell. Pipette access resistance was maintained below 25 MΩ, range: 5-25 MΩ. Spike threshold, action potential amplitude, half width, after hyperpolarization amplitude and delay were calculated using the first action potential elicited by a cell that fell within the duration of the stimulating current injection (i.e. not spontaneously elicited APs – present in 2 cells - or those coinciding with stimulation onset). AP threshold was taken as the point where the first derivative exceeds 20mV/ms. AP amplitude and AHP were calculated in relation to this threshold. Accommodation index was calculated as the ratio of the time interval between the first and last pairs of action potentials in response to a 1sec current injection evoking at least six action potentials. In 9 cases (B6: 3 cells, D2: 5 cells), fewer than 6 spikes were elicited before showing total accommodation and thus, these were the traces used to calculate accommodation index (maximum 4 or 5 spikes). For the IPSC data, 120-second sections of recordings occurring after 3 min of 10 µM NBQX + 0.5 µM TTX wash-in were analysed.

2.9. Data analysis

All graphs were made with Prism™ (GraphPad Software, La Jolla, USA, version 6.0). Images and graphs were then processed and organized in Adobe Illustrator (Adobe Systems Inc., San Jose, USA, version 2015). References were managed through Endnote (Clarivate Analytics, Philadelphia, USA, version X8). Statistical analysis was also performed with Prism™. Each figure description in chapter 3 indicates the used statistical test. In general, Gaussian distribution was tested for every data set with the Shapiro-Wilk normality test first. Normally distributed data was tested with two-tailed parametric Student's t-test in case of comparing two groups and one-way ANOVA with multiple comparison in case of multiple group comparison. For *in vitro* shut-off experiments one-way ANOVA with repeated measures was used, since all samples stem from one culture preparation and were only treated differently. For every analysis alpha was set to 0.05, therefore: not significant (n.s.): $p > 0.05$; *: $p < 0:05$; **: $p < 0:01$; ***: $p < 0:001$.

Chapter 3

Results

3.1. Neuronal activity-induced gene expression in a murine model of impaired spatial memory

The inbred strain DBA/2 was analysed for their performance in hippocampus-dependent and independent memory tasks to verify extent and specificity of the memory impairment. In addition, further behavioural parameters were investigated to evaluate the overall DBA/2 behavioural phenotype. The main aim of this section was to analyse whether a correlation between activity-induced gene induction and the potential DBA/2 memory impairment exists. Therefore, basic cellular properties were examined first, since impairments on this level would obscure dysfunctions on a signalling level. Potential impairments of basic cellular properties might also be caused by activity-induced genes, though. The following section analyses the induction of activity-dependent genes, in particular IEGs, after neuronal activity *in vitro* and *in vivo*. Thus, cell intrinsic function in DBA/2 can be distinguished from extrinsic network function under physiological conditions.

3.1.1. DBA/2 as model for spatial memory impairment

Protocols assessing memory performance vary between labs; every minor change can influence the mouse behaviour. Therefore, the first aim of this part was to confirm the described DBA/2 spatial memory impairment with the CFC and SOR task protocols used in our lab. Most publications report about DBA/2 LTM but not STM performance; therefore, spatial memory tasks for both types of memory were conducted. DBA/2 performance was always compared with the performance of the inbred strain C57BL/6 which served as "normal performance" control.

As previously reported [129], DBA/2 display a severe impairment in CFC as shown by reduced freezing time compared to C57BL/6 mice during the test phase, however for both STM and LTM, assessed 1 h and 24 h post training, respectively (Figure 6A). The initial response to the shock during the training differed between the strains. In particular, DBA/2 mice displayed stronger response to the shock, shown by an elevated mean velocity during shock phase (Figure 6B right; DBA/2: 54.16 ± 16.01 [cm/s], C57BL/6: 38.54 ± 10.07 [cm/s]) followed by increased freezing during the post-shock phase (Figure 6B left; DBA/2: 32.60 ± 22.46 [%], C57BL/6: 14.33 ± 8.75 [%]). This is in line with a previous report showing elevated DBA/2 freezing immediately after shock application compared to C57BL/6 [130] and

indicates that the reduced freezing time during the test phase is not caused by reduced pain perception in DBA/2 during training or an inability of DBA/2 to freeze. Although CFC is considered to be a hippocampus-dependent memory paradigm, amygdala-dependent anxiety and fear also influence CFC performance [131]. Therefore, strain-dependent differences in anxiety-like behaviour were tested with the open field protocol. Increased anxiety-like behaviour in DBA/2 compared to C57BL/6 was observed for several parameters (Figure 6C) such as total time spent in the central zone, latency of first entry in the central zone, number of entries in the central zone and distance travelled in central zone. Increased avoidance of the bright, unprotected central zone is thought to reflect an elevated anxiety-like behaviour. DBA/2 display significantly greater avoidance of the central zone for all parameters; which suggests increased anxiety-like behaviour in DBA/2 mice. This increased anxiety could potentially interfere with learning in the CFC task and may be partly responsible for their reduced performance. Therefore, a task with reduced anxiety influence compared to CFC is required.

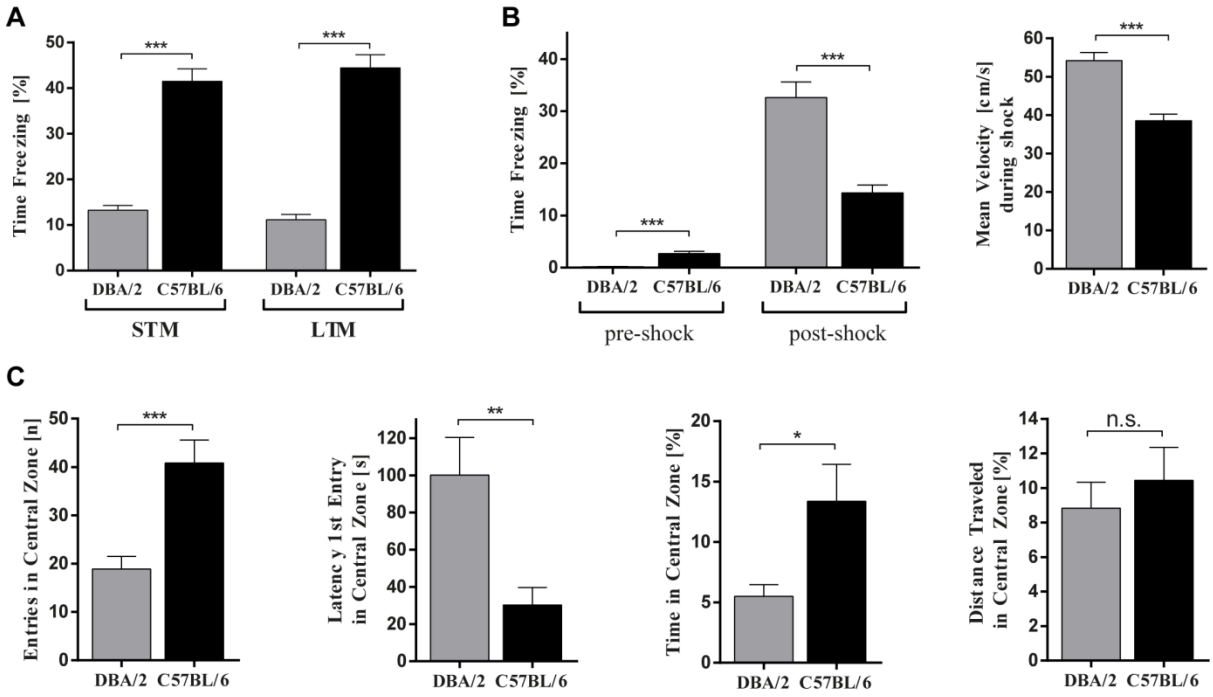

Figure 6: Comparative analysis of DBA/2 and C57BL/6 contextual fear conditioning learning and open field behaviour. (A) CFC memory performance depicted in time freezing in percent of total time during test session for STM and LTM. Unpleasant stimulus during training = 0.7mA shock intensity for 2s. N (DBA/2, STM) = 29; n (C57BL/6, STM) = 17; n (DBA/2, LTM) = 27; n (C57BL/6, LTM) = 16. **(B)** Left: Time freezing in percent of total time duration during CFC training. Duration of pre-shock period = 148s, duration of post-shock period = 30s. Right: Mean velocity of mouse movement within the arena during the 2s 0.7mA shock interval during CFC training. N (DBA/2) = 50; n (C57BL/6) = 30. **(C)** Anxiety-like behaviour parameters during open field test. From left to right: total number of entries in central zone, latency of the first entry in the central zone, time spend in central zone as percent of total trial time, distance travelled in central zone as percent of total distance travelled. N (DBA/2) = 25; n (C57BL/6) = 21. All graphs are plotted as mean + SEM. Statistical significance was determined by unpaired, two-tailed t-test; n.s. = not significant, *$p < 0.05$, **$p < 0.01$, ***$p < 0.001$.

To verify a spatial memory deficit, DBA/2 were additionally analysed in the SOR task, a hippocampus-dependent memory task that is minimally influenced by anxiety. SOR assesses the exploration time of a relocated object during the test phase and evokes only mild anxiety and no fear. In this task, DBA/2 showed significant LTM impairment but only a trend toward STM impairment, indicating a deficit in hippocampus-dependent long-term memory formation (Figure 7A). Two further parameters indicative of a hippocampal dysfunction were observed in DBA/2 mice. Specifically, DBA/2 mice exhibited increased exploration in a novel environment (Figure 7B) and impaired nesting behaviour (Figure 7C). Similar alterations have been reported to occur in hippocampus lesioned mice and rats [132, 133].

Next, the exclusivity of the DBA/2 memory impairment for hippocampus dependent tasks was tested by accessing DBA/2 performance in a visuomotor conditional learning (VMCL) task that is hippocampus-independent and relies predominantly on striatal function. To examine visuomotor learning ability, both strains were trained and tested in the Bussey-Saskida touch screen chamber for rodents [124] by Dr. Anne S. Mallien (Central Institute of Mental Health, Mannheim, Group: Psychiatric animal models). Food-restricted mice were rewarded with milk if they learned to associate a presented symbol with a side-specific touch response. Surprisingly, DBA/2 also showed a severe learning impairment in this task as indicated by lower accuracy and a higher number of correction trials (Figure 7D, left and right, respectively). Thus, the learning impairment of DBA/2 mice seems not to exclusively affect hippocampus-dependent tasks. Since SOR, exploration, nest building, and VMCL all rely on processing and coordination within and between the visual and motor systems, the visuo-spatial function of mice in a water maze task was tested. This task required mice to find a submerged but visible platform over four trials. DBA/2 and C57BL/6 mice performed equally well in this task indicating no visuo-motor impairment (Figure 7E).

All in all, the behavioural analysis corroborates previous studies showing impaired hippocampus dependent memory function in DBA/2 mice and further reveals that these deficits are independent of confounding differences in anxiety or visuo-motor abilities, but are not confined to hippocampus-dependent tasks.

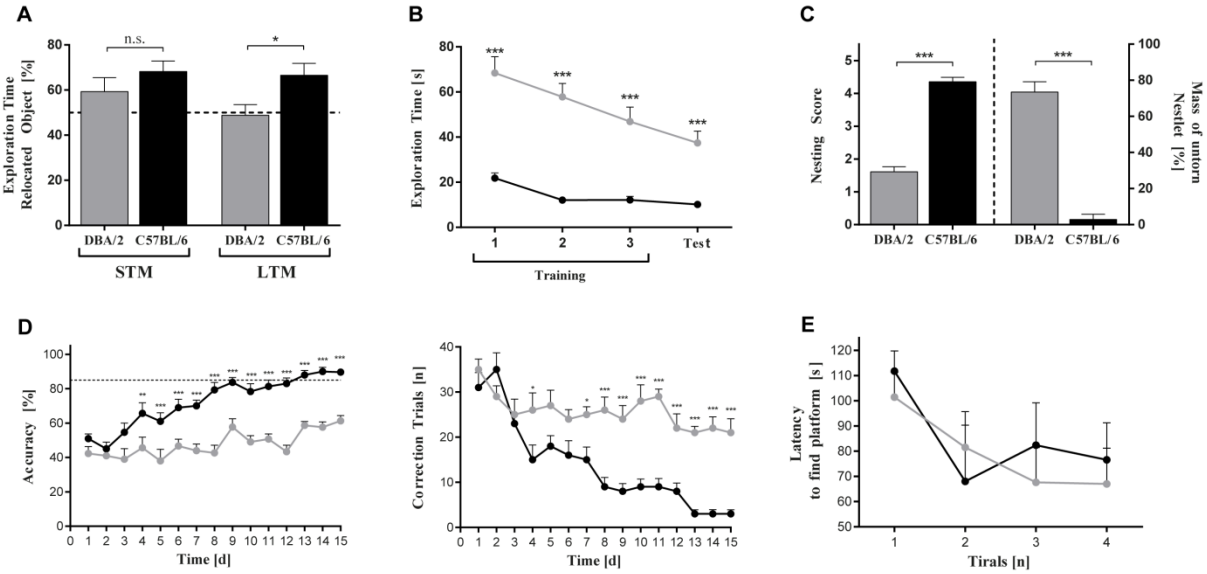

Figure 7: Comparative analysis of DBA/2 and C57BL/6 learning and behaviour. (A) SOR memory performance depicted in exploration time of the relocated object in percent of total exploration time during test session. N (DBA/2, STM) = 11; n (C57BL/6, STM) = 10, n (DBA/2, LTM) = 13; n (C57BL/6, LTM) = 15. For both spatial memory tests STM was tested 1h and LTM 24h after training session. **(B)** Total object exploration time is plotted over the three SOR training sessions and the SOR test session from all STM and LTM experiments. Grey graph = DBA/2, n= 21; black graph = C57BL/6, n= 29. **(C)** Nesting score evaluated according to Deacon (2006) is plotted on the left y axis; mass of untorn cotton nestlet after nesting test in percent of mass of untorn cotton nestlet before test is plotted on right y axis. N (DBA/2) = 12; n (C57BL/6) = 14. **(D)** Left: VMCL learning performance is plotted in accurate responses in percent of total responses. Right: VMCL learning performance is plotted in number of correction trials after an inaccurate response. Grey graph = DBA/2, n = 10; black graph = C57BL/6, n = 10. **(E)** Latency to find the visible platform during four trials of a visible water maze task. Grey graph = DBA/2, n = 11; black graph = C57BL/6, n = 5. All graphs are plotted as mean + SEM. Statistical significance was determined by two-tailed t-test (A, C) and multiple-comparison two-way ANOVA (B, D, E); n.s. = not significant, *p < 0.05, **p < 0.01, ***p < 0.001.

3.1.2. Basic cell properties

To exclude the possibility of DBA/2 hippocampus dysfunction on a general cellular level, the hippocampal structure and basic morphological and electrophysiological parameters of CA1 pyramidal neurons were analysed. Based on the severe learning and memory deficit in DBA/2 a dysfunction on the cellular property level in this strain was expected. First, basic hippocampal morphology was analysed by cresyl violet staining of DBA/2 and C57BL/6 brain slices. The size and morphology of all hippocampal regions (CA1, CA3, DG) appeared normal in DBA/2 compared to C57BL/6 (Figure 8A, example pictures). This finding is consistent with a report from Abusaad and colleagues, who observed in a detailed analysis of hippocampal subregion size and neuronal density no major differences in DBA/2 compared to C57BL/6 [134].

Next, it was aimed to investigate more subtle morphological properties by analysing total dendritic length of basal dendrites of CA1 pyramidal neurons by Golgi staining. CA1 excitatory neurons were chosen because of their well-documented role in spatial memory formation (chapter 1.2.1). Total dendritic length is an indication for neuronal complexity, and

is modulated both during development and by plasticity processes. In DBA/2 a trend towards lower basal dendrite length was observable (Figure 8B). Due to technical limitations with this staining method, it was not feasible to analyse apical dendrites of CA1 pyramidal neurons. However, with the attained data a major impairment in DBA/2 hippocampal morphology can be excluded.

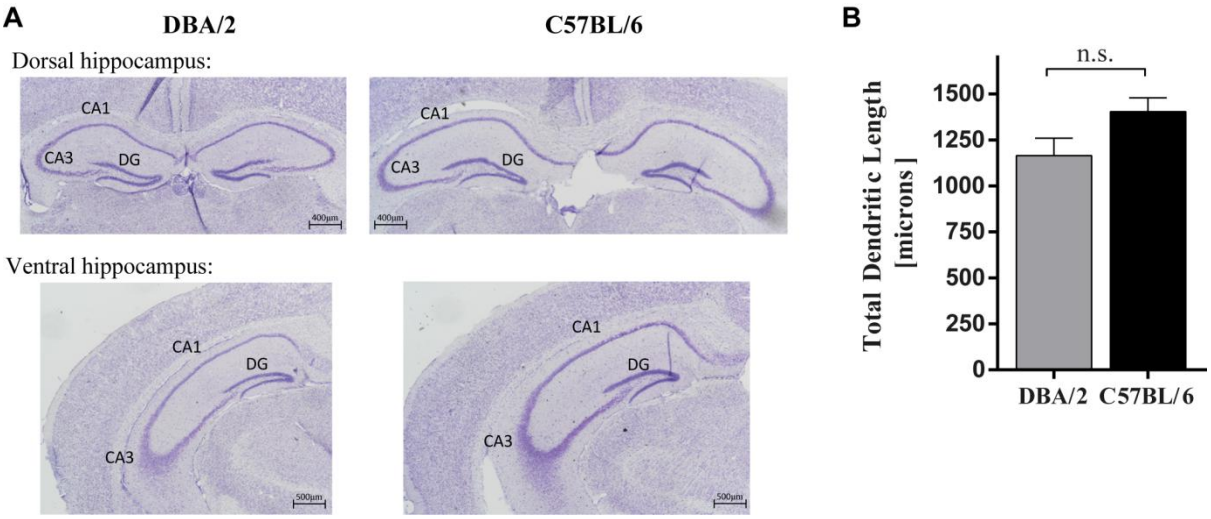

Figure 8: Comparative analysis of DBA/2 and C57BL/6 hippocampal and dendritic morphology. (A) Representative pictures of DBA/2 (left) and C57BL/6 (right) dorsal and ventral hippocampus stained by cresyl violet (Nissl). CA1 = *cornu ammonis* area 1, CA3 = *cornu ammonis* area 3, DG = dentate gyrus. Magnification = 10x. **(B)** Total dendritic length of basal dendrites of CA1 pyramidal neurons. Length was determined after manual tracing of Golgi stained brain slices. N (DBA/2) = 20 cells, 4 animals; n (C57BL/6) = 17 cells, 4 animals. Graph is plotted as mean + SEM. Statistical significance was determined by unpaired, two-tailed t-test, n.s. = not significant, *p < 0.05, **p < 0.01, ***p < 0.001.

Other major factors that influence proper neuronal function are electrophysiological properties. Those properties give clues about basic channel and intracellular signal transmission function. Basic electrophysiological properties of CA1 pyramidal neurons in acute hippocampal slices were measured by Victoria Witte and Dr. Peter C.P. Bengtson (University Heidelberg, Group: Neurobiology). Whole cell patch clamp recordings displayed no differences in whole cell resistance and resting membrane potential although DBA/2 cells showed a larger whole cell capacitance (Table 17). This larger capacitance suggests a larger plasma membrane surface area indicative of a larger dendritic tree in DBA/2 CA1 pyramidal neurons. No difference in action potential threshold, amplitude or half-width were detected, but DBA/2 mice showed an increased amplitude of the afterhyperpolarization potential (AHP) without significant differences in the delay to its peak. The larger AHP amplitude suggests a stronger activation of the big potassium (B) and small potassium (SK) channels, the two calcium-activated potassium channels primarily responsible for the AHP in CA1 pyramidal neurons. Such increased channel activation may arise from a stronger AP-induced calcium influx or a higher channel density. Differences in firing properties were assessed by examination of accommodation in response to 1 s depolarizing current injection steps but no

differences between mouse strains in their accommodation index were observed. Furthermore, no differences in hyperpolarization-activated conductances (hyperpolarization-activated cyclic nucleotide–gated/HCN and inward-rectifier potassium/Kir channels), which are known to regulate dendritic excitability and resting membrane potential, were found. Thus, DBA/2 pyramidal neurons display no changes in passive electrical properties, excitability or hyperpolarization-activated conductances, except a larger whole cell capacitance and AHP amplitude in CA1 pyramidal neurons.
In general no major morphological or electrophysiological cell property differences in CA1 pyramidal neurons were detectable which would be detrimental for DBA/2 neuronal function. This indicates that the severe learning impairment is not caused by a major neuronal dysfunction. Instead, dysfunctional signalling like impaired activity-dependent gene induction is a possible cause of the DBA/2 memory impairment.

Table 17: Comparison of whole-cell patch-clamp electrophysiological properties of DBA/2 and C57BL/6 CA1 pyramidal neurons. Summary statistics (Mean ± SEM (number of cells, number of animals)) obtained from whole-cell patch-clamp recordings of CA1 pyramidal neurons in acute hippocampal slices from 10 week-old C57BL/6 or DBA/2 mice. Resting membrane potential (V_{rest}), action potential (AP), afterhyperpolarization potential (AHP), hyperpolarization-activated cyclic nucleotide regulated (HCN), potassium inward rectifier (Kir). ∗ $p < 0.05$, ∗∗$p < 0.01$ were determined by two-tailed t-tests.

		C57BL/6	***DBA/2***	***p value***
Membrane capacitance	pF	119.69 ± 4.67 (47, 14)	137.38 ± 6.28 (48, 13)	0.027 *
Membrane resistance	MΩ	129.31 ± 6.11 (47, 14)	121.60 ± 5.22 (48, 13)	0.340
V_{rest}	mV	-60.19 ± 0.74 (26, 8)	-58.33 ± 1.20 (28, 8)	0.201
AP threshold	mV	-40.22 ± 1.16 (26, 8)	-37.57 ± 1.35 (28, 8)	0.145
AP amplitude	mV	72.10 ± 2.02 (26, 8)	70.19 ± 2.38 (28, 8)	0.546
AP half width	ms	0.92 ± 0.03 (26, 8)	0.90 ± 0.03 (28, 8)	0.530
AHP amplitude	mV	-15.86 ± 0.90 (26, 8)	-18.71 ± 0.67 (28, 8)	0.014 *
AHP peak delay	ms	4.58 ± 0.54 (26, 8)	4.98 ± 0.62 (28, 8)	0.631
Accommodation index	a.u.	0.40 ± 0.03 (25, 8)	0.44 ± 0.02 (28, 8)	0.187
Kir conductance	nS	2.90 ± 0.41 (25, 8)	3.08 ± 0.42 (28, 8)	0.757
HCN conductance	nS	2.73 ± 0.27 (25, 8)	2.95 ± 0.19 (28, 8)	0.494

3.1.3. *In vitro* IEG expression

Since no strain differences in basic morphology and electrophysiological properties were apparent, it was reasoned that either molecular signalling or hippocampal network activation might be compromised in DBA/2. To differentiate between those two possibilities, IEG induction after synaptic activity in DBA/2 and C57BL/6 primary hippocampal and control cortical neurons was analysed. The well characterized pharmacological induction of action potential (AP) bursting with the $GABA_A$ receptor inhibitor bicuculline (BIC) was applied. BIC treatment results in synaptic NMDA receptor activation, synaptic potentiation and activation of calcium-dependent signalling cascades leading to the induction of a large gene pool including multiple IEGs [135]. Primary neurons were stimulated for 0.5h, 1h, and 2h to

investigate induction quantity as well as induction kinetics of three well characterized NMDA receptor signalling dependent IEGs, *Arc*, *Nr4a1* and *Npas4*. Altered induction in DBA/2 would indicate intrinsic neuronal dysfunction of the signalling and gene induction machinery since primary cultures do not contain complex physiological circuitry and are independent from postnatal developmental signalling. Due to high variability of basal neuronal activity in the cultures, relative gene expression assessed by RT-qPCR was always normalized to the same total brain RNA mix. *Gusb* was used as endogenous control. Basal gene expression and AP bursting-induced IEG induction in both hippocampal and cortical neurons was equivalent in cultures prepared from DBA/2 and C57BL/6 mice with a trend for increased induction in DBA/2 cortical cultures which was even statistically significant for *Npas4* at 1h (Figure 9A:hippocampal cultures, B: cortical cultures). This indicates that NMDA receptor- and calcium-dependent IEG induction pathways are not diminished in DBA/2 neurons. Thus, the machinery for the synaptic activation of transcription relevant to synaptic plasticity and survival programs appears intact in a culture system of isolated hippocampal or cortical DBA/2 neurons.

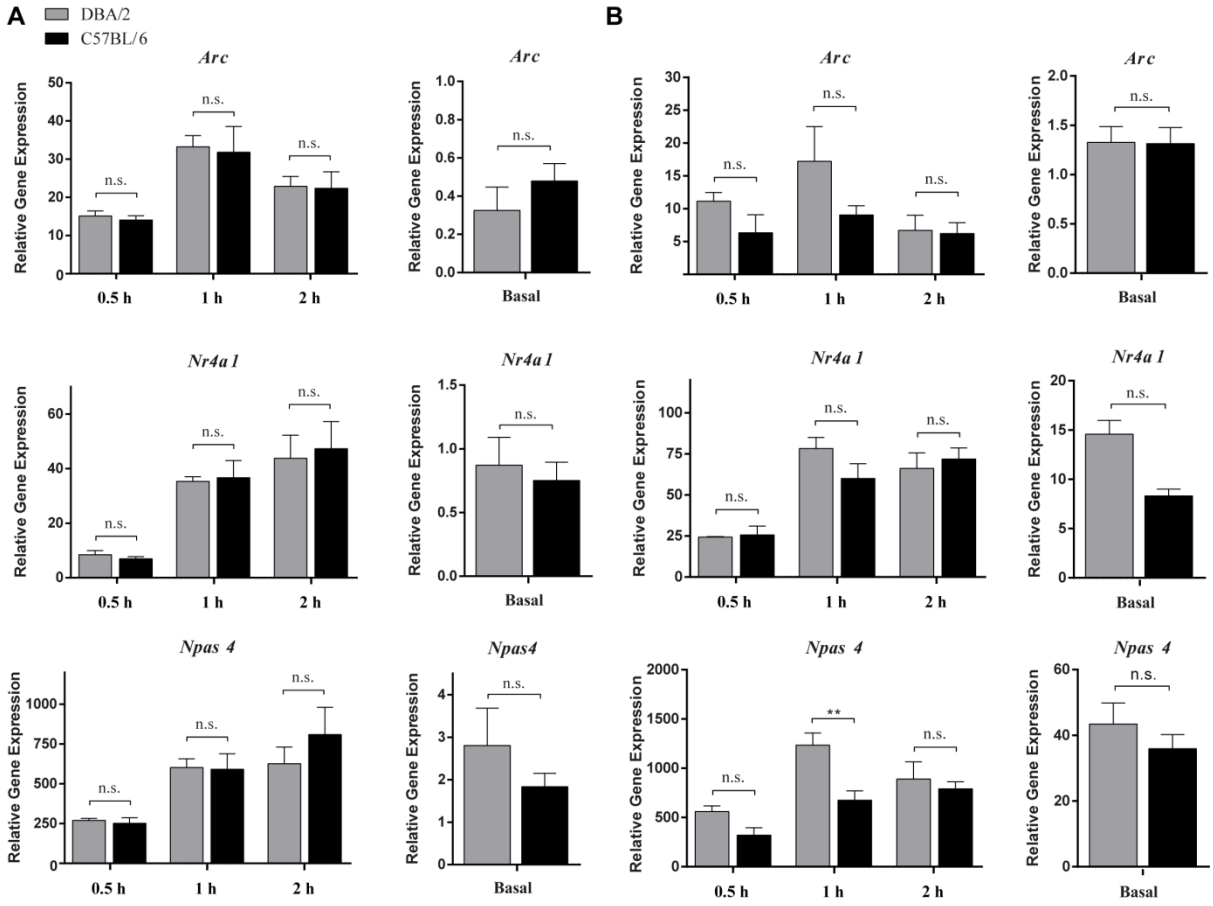

Figure 9: *In vitro* IEG induction of primary hippocampal and cortical cultures. (A, left) Relative gene expression of IEGs *Arc*, *Npas4* and *Nr4a1* after 0.5h, 1h and 2h bicuculline [50µM] treatment of primary hippocampal cultures from DBA/2 (gray columns) and C57BL/6 (black columns) P0 mice. Experiments were conducted on day in vitro (DIV) 10/11 and expression was analyses via RT-qPCR. *Gusb* was used as endogenous control and expression was normalized to a total brain RNA mix from DBA/2 and C57BL/6 adults.

Right of the induction graph, basal gene expression of the respective gene is depicted. N (DBA/2) = 3; n (C57BL/6) = 3. **(B)** Relative gene expression of primary cortical cultures stimulated and analysed in the same manner as hippocampal cultures. N (DBA/2) = 4; n (C57BL/6) = 4. Graphs are plotted as mean + SEM. Statistical significance was determined by ordinary one-way ANOVA with Tukey´s multiple comparison test, n.s. = not significant, *p < 0.05, **p < 0.01, ***p < 0.001.

3.1.4. *In vivo* IEG expression

To analyse DBA/2 transcriptional activation in the intact brain in a live animal it was aimed to induce synaptic activity by kainic acid administered intraperitoneally (i.p.). Kainate receptors are highly expressed in hippocampal regions [136]. Their activation results in excitatory signalling and activity-dependent gene induction, but also convulsant seizures (*status epilepticus*) in a dose dependent manner [137]. Already low kainic acid concentrations of 15 mg/kg body weight, which had little effect on C57BL/6, were lethal for more than 50% of DBA/2 (Figure 10A). In general, DBA/2 reached higher *status epilepticus* scores (Figure 10B). Due to the extreme difference in seizure susceptibility and severity between the strains, gene induction data were not comparable in this experiment and are not shown.

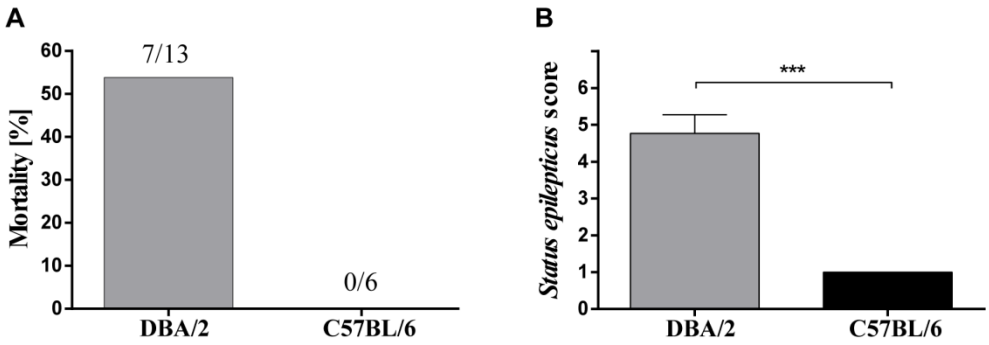

Figure 10: Mortality rate and *status epilepticus* score of DBA/2 and C57BL/6 after kainic acid administration. (A) Number of mice deceased after i.p. administration of 15mg/kg bodyweight kainic acid. **(B)** The *status epilepticus* was scored as follows: 0: no reaction; 1: immobility; 2: sudden shaking, chewing movements; 3: clonus of front extremities; 4: erecting of the body; 5: continuous body erection, seizures; 6: death. Graphs are plotted as mean (A) and mean + SEM (B). N (DBA/2) = 13; n (C57BL/6) = 6. Statistical significance was determined by student´s t-test (B), n.s. = not significant, *p < 0.05, **p < 0.01, ***p < 0.001.

As a result of the failed comparability with the strong kainic acid gene induction protocol, a milder, more behaviourally relevant stimulus was used to induce IEG expression *in vivo*. Expression of several IEGs in several brain regions known for their involvement in spatial memory formation was assessed 30min after the SOR learning paradigm. The aim of this experiment was to analyse IEG induction taking strain differences in whole brain function and brain area activation into account without artificially over-activating neurons as achieved with the kainic acid protocol.

In vivo relative gene induction data was normalized with two different methods; in figure 11, all data was normalized to untrained C57BL/6 home cage (HC) animals and shows basal expression differences as well as quantitative mRNA differences in trained animals; in figure

12 data was normalized to the respective untrained HC animals, and therefore displays strain-dependent differences in gene induction. For most of the analysed classical IEGs, no significant gene induction difference was detected for either normalization in any of the hippocampal CA1, CA3 and DG regions, the retrosplenial cortex (RSC), or the prefrontal cortex (PFC) (Figure 11A, B, C, D, E; Figure 12A, B, C, D, E). Data normalized to C57BL/6 HC show increased expression of *Arc* and *cFos* in the DG of DBA/2 due to a lower basal expression. When normalized to the respective HC animal, however, no induction differences in DG were apparent (Figure 11C, Figure 12C). Likewise the parietal cortex (PC) demonstrates a general lower IEG expression under basal condition in DBA/2 resulting in a lower induction if data is normalized to C57BL/6 home cage animals (Figure 11F). Normalization to the respective HC animals results in no induction difference between the strains (Figure 12F). Due to technical limitations in isolating complexly localized brain areas, dissection and IEG analyses of the entorhinal cortex was not possible.

All in all, IEG induction data indicate normal neuronal NMDA receptor/calcium signalling function and normal hippocampal, RSC and PFC activation *in vivo* after spatial learning in DBA/2. Lower PC basal IEG expression despite normal gene induction was the only difference detected regarding brain region activity.

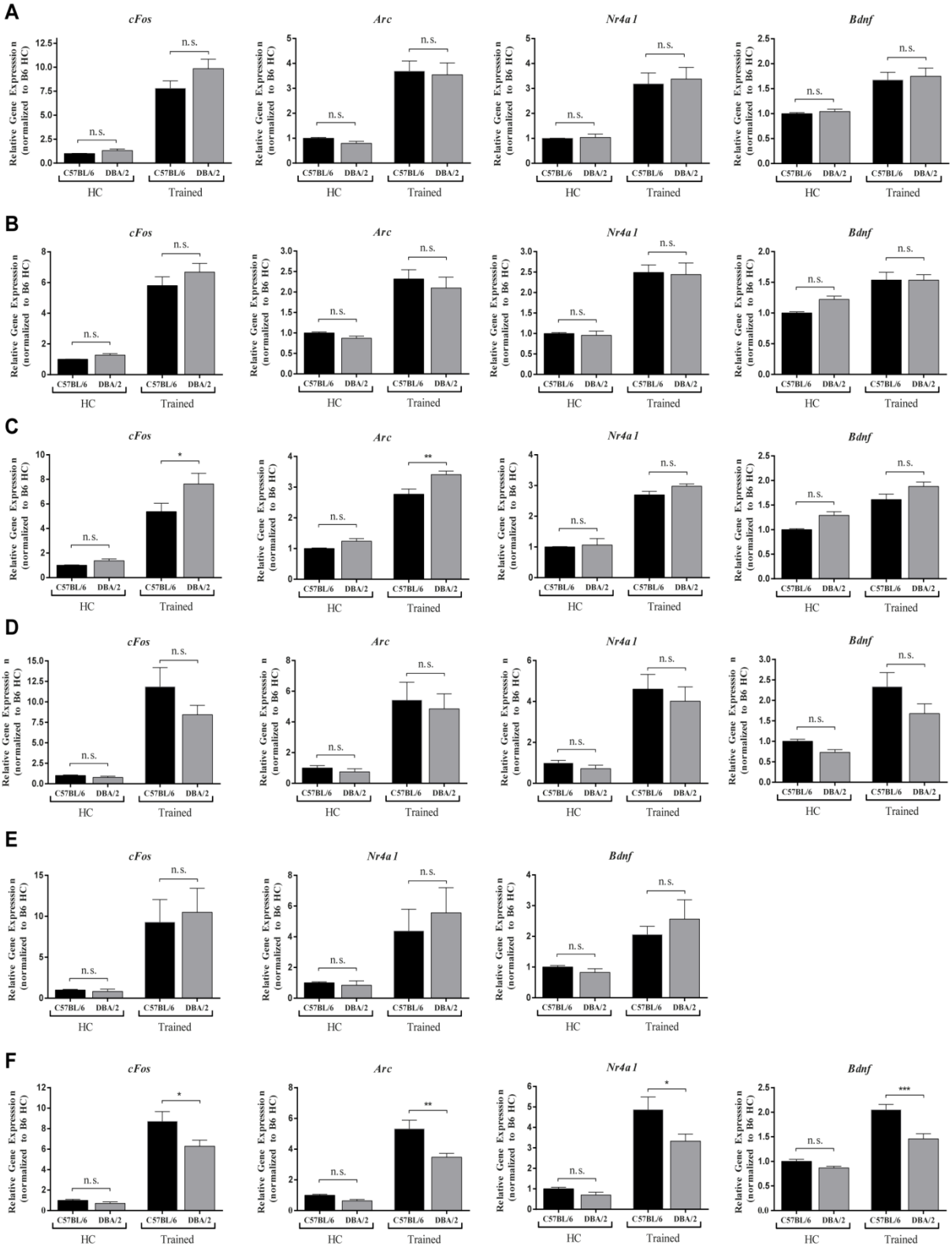

Figure 11: *In vivo* IEG induction after SOR training. RT-qPCR analysis of IEG expression of *cFos*, *Arc*, *Nr4a1* and *Bdnf* 30 min after completion of SOR training in Hippocampal CA1 **(A)**, Hippocampal CA3 **(B)**, Hippocampal dentate gyrus (DG, **C**), retrosplenial cortex (RSC, **D**), prefrontal cortex (PFC, **E**) and parietal cortex (PC, **F**). *Gusb* was used as endogenous control and expression was normalized to C57BL/6 home cage (HC) animals. N DBA/2 = 7; n C57BL/6 = 7. Graphs are plotted as mean + SEM. Statistical significance was determined by ordinary one-way ANOVA with Tukey´s multiple comparison test, n.s. = not significant, *$p < 0.05$, **$p < 0.01$, ***$p < 0.001$.

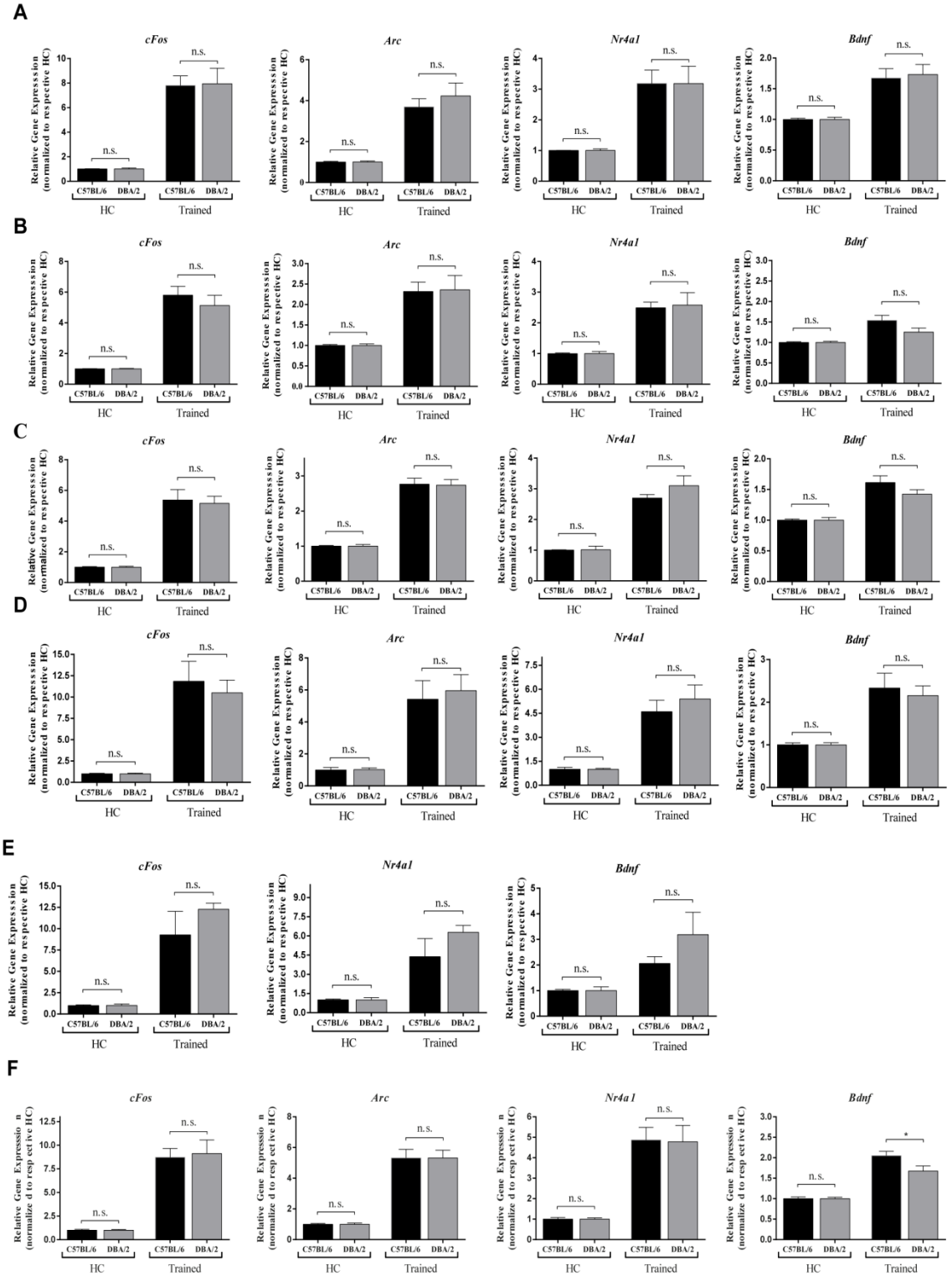

Figure 12: *In vivo* IEG induction after SOR training normalized to respective home cage animals. RT-qPCR analysis of IEG expression of *Fos*, *Arc*, *Nr4a1* and *Bdnf* 30 min after completion of SOR training in Hippocampal CA1 (A), Hippocampal CA3 (B), Hippocampal dentate gyrus (DG, C), retrosplenial cortex (RSC, D), prefrontal cortex (PFC, E) and parietal cortex (PC, F). *Gusb* was used as endogenous control. Expression data from trained C57BL/6 was normalized to C57BL/6 home cage (HC) animals and expression data from trained DBA/2 was normalized to DBA/2 HC animals. N DBA/2 = 7; n C57BL/6 = 7. Graphs are plotted as mean + SEM. Statistical significance was determined by ordinary one-way ANOVA with Tukey´s multiple comparison test, n.s. = not significant, *$p < 0.05$, **$p < 0.01$, ***$p < 0.001$.

Although DBA/2 IEG induction was normal for most classical IEGs (Figure 11 and 12), there was one exception, the transcription factor *Npas4*, which showed higher induction in DBA/2 hippocampal regions after SOR training especially for the C57BL/6 HC animal normalization but also for the respective HC animal normalization (Figure 13A and 14A, respectively). With both normalizations, no difference in PFC and RSC cortical regions was detected. *In vitro* data showed no *Npas4* induction difference in primary hippocampal cultures (Figure 9A), concluding that the elevated hippocampal *in vivo* induction is probably caused by differences in extrinsic hippocampal circuit or network properties and not by functional deficits in intrinsic neuronal synaptic or signalling mechanisms. Although, it should be noted that *Npas4* showed elevated induction at the 1h time point in primary cortical neurons with the *in vitro* protocol (Figure 9B). *Npas4* induction is directly dependent on neuronal activity [138] and calcium signalling [12]. Moreover, activity-induced *Npas4* is, among other functions, known to regulate inhibitory synapse formation on excitatory neurons and is thereby responsible for maintaining the excitatory/inhibitory balance in a circuit [139]. The observed *Npas4* dysregulation pointed to a possible excitatory/inhibitory signalling dysfunction in the DBA/2 hippocampus. *Npas4* overinduction could act either causative or only as indicator for an inhibition/excitation imbalance.

Further indication for disrupted DBA/2 hippocampal inhibitory signalling was the increased basal *Inhba* expression especially in the DBA/2 CA1 subregion (Figure 13B). *Inhba* as described in chapter 1.1.3 encodes one subunit of the neurotrophic factor activin A. It was shown previously that continuous activin A application on developing hippocampal cultures results in suppressed emergence of glutamate-decarboxylase (GAD) 67-positive inhibitory neurons [52]. Additionally, an impaired induction in CA3, DG and PC is also observed (Figure 14B) indicating a broad *Inhba* expression dysregulation in DBA/2.

Altogether, these findings point to dysregulated inhibitory signalling in the DBA/2 hippocampus. Imbalance in excitatory and inhibitory activity could explain the DBA/2 memory impairment as well as other observed aspects of the DBA/2 phenotype like their increased kainic acid-induced seizure susceptibility. Therefore, inhibitory input of CA1 pyramidal neurons was investigated by measuring miniature inhibitory postsynaptic currents (mIPSC) *ex vivo*.

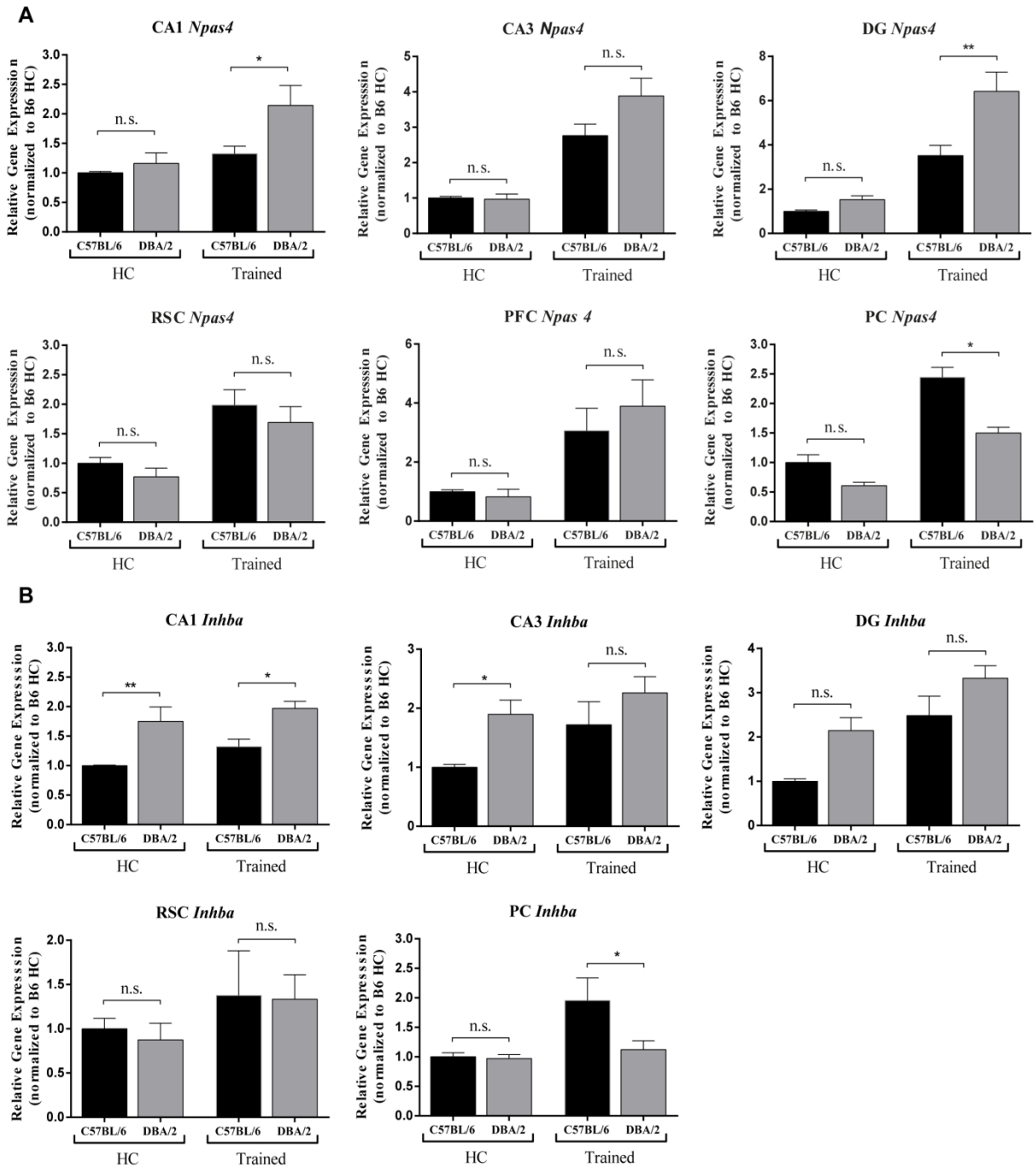

Figure 13: *In vivo Npas4* and *Inhba* induction after SOR training normalized to C57BL/6 home cage animals. *In vivo* gene expression of *Npas4* **(A)** and *Inhba* **(B)** 30 min after completed SOR training in spatial learning associated hippocampal and cortical brain regions. CA1 = *cornu ammonis* area 1, CA3 = *cornu ammonis* area 3, DG = dentate gyrus, RSC = retrosplenial cortex, PFC = prefrontal cortex, PC = parietal cortex. Gene expression was analysed via RT-qPCR. *Gusb* was used as endogenous control. Expression data from trained C57BL/6 was normalized to C57BL/6 home cage (HC) animals and expression data from trained DBA/2 was normalized to C57BL/6 HC animals. N (DBA/2) = 7; n (C57BL/6) = 7. Graphs are plotted as mean + SEM. Statistical significance was determined by ordinary one-way ANOVA with Tukey´s multiple comparison test, n.s. = not significant, *p < 0.05, **p < 0.01, ***p < 0.001.

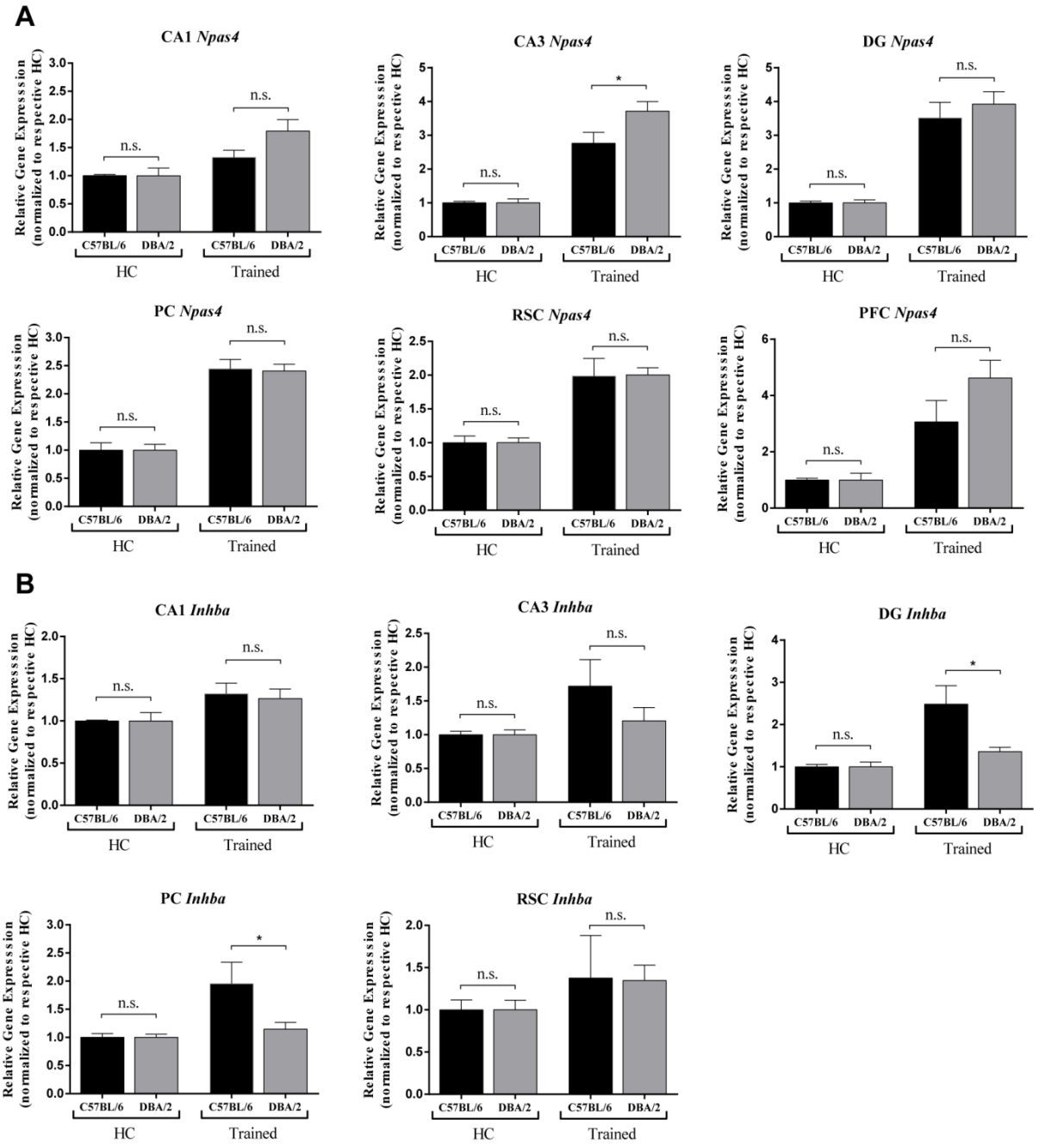

Figure 14: *In vivo Npas4* and *Inhba* induction after SOR training normalized to respective home cage animals. *In vivo* gene expression of *Npas4* **(A)** and *Inhba* **(B)** 30 min after completed SOR training in spatial learning associated hippocampal and cortical brain regions. CA1 = *cornu ammonis* area 1, CA3 = *cornu ammonis* area 3, DG = dentate gyrus, RSC = retrosplenial cortex, PFC = prefrontal cortex, PC = parietal cortex. Gene expression was analysed via RT-qPCR. *Gusb* was used as endogenous control. Expression data from trained C57BL/6 was normalized to C57BL/6 home cage (HC) animals and expression data from trained DBA/2 was normalized to DBA/2 HC animals. N (DBA/2) = 7; n (C57BL/6) = 7. Graphs are plotted as mean + SEM. Statistical significance was determined by ordinary one-way ANOVA with Tukey´s multiple comparison test, n.s. = not significant, *p < 0.05, **p < 0.01, ***p < 0.001.

3.1.5. Attenuated inhibitory signalling in DBA/2

To analyse inhibitory synaptic connectivity mIPSCs were recorded by Victoria Witte and Dr. Peter C.P. Bengtson (University Heidelberg, Group: Neurobiology). A longer inter-event interval (IEI, the inverse of frequency) in CA1 pyramidal neurons of DBA/2 mice was found (Figure 15A right, 15B: example traces). This difference was not accompanied by a reduction in mIPSC amplitude (Figure 15A left). The increased mIPSC IEI in DBA/2 in the absence of any change in amplitude suggests that the difference in IEI reflects either a reduced number of functional inhibitory synapses or a reduction in presynaptic GABA signals due to decreased release probability or reduced number of GABAergic neurons. However, independent from the cause of increased mIPSC IEI, the measured data suggests lower inhibitory input onto DBA/2 CA1 pyramidal neurons.

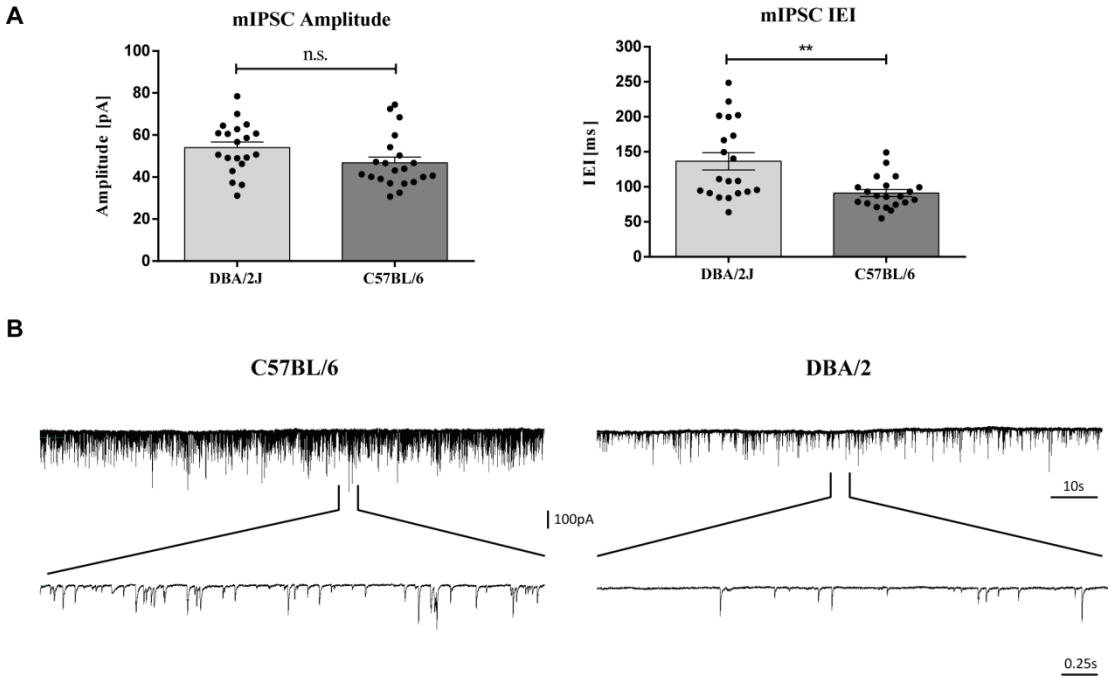

Figure 15: DBA/2 and C57BL/6 mIPSC data of CA1 pyramidal neurons. (A) Amplitude [pA] (left) and inter event interval [ms] (IEI, right) of DBA/2 and C57BL/6 miniature inhibitory post synaptic currents (mIPSC). **(B)** Sample traces of mIPSC of C57BL/6 (left) and DBA/2 (right). mIPSC were mediated by $GABA_A$ receptors, since gabazine, a $GABA_A$ blocker, was able to block all inward currents after recording (data not shown). Currents were recorded *ex vivo* in CA1 pyramidal neurons in current clamp during blockage of AMPA receptors with NBQX and action potentials (voltage-gated sodium channels) by TTX. Graphs are plotted as dot plot and mean + SEM. Statistical significance was determined by unpaired two-tailed Student´s t-test, n.s. = not significant, *p < 0.05, **p < 0.01, ***p < 0.001.

Altogether, the gathered data suggests that one factor underlying the DBA/2 memory impairment is an excitation/inhibition imbalance with increased hippocampal activity rather than general intrinsic morphological or molecular signalling dysfunction. Further indications and its implication for inter-individual memory differences will be discussed in section 4.1.2.

Although, the DBA/2 learning impairment is probably not caused by a general activity-induced gene dysregulation, the observed alteration of IEGs associated with particular function in inhibition/excitation signalling pointed to the inhibition signalling impairment in DBA/2. This demonstrated that memory impairments which are not caused by general gene activation disruption can still display expression changes of particular genes. Those genes can be indicators as well as potentiators of the impairment cause (see 4.1.2). Changes in activity-dependent gene expression are a hub for neuronal plasticity and memory function and slight expression and induction changes can disturb neuronal function. For that reason the following section aimed to investigate activity-dependent gene expression during excitotoxicity which is a common phenomenon in several neurodegenerative pathologies.

3.2. Activity-dependent gene regulation during excitotoxicity

As previously reported (chapter 1.3.2) dephosphorylation and degradation of CREB follow toxic glutamate application in primary hippocampal neurons. This process is called CREB shut-off. As a result of this shut-off, expression of the neurotrophic factor *Bdnf* is decreased after excitotoxic stimuli. Effects on other activity-induced genes are not reported. Among upstream pathways of activity-dependent gene induction only ERK1/2 was analysed during excitotoxicity. ERK1/2 displayed a similar dephosphorylation as CREB. However, sustained expression and phosphorylation also depends on the continuation of synaptic activity. To differentiate between an active shut-off by phosphatase and proteinase activation from a passive shut-off where deactivation/dephosphorylation occurs due to the loss of synaptic activity, a specific gene expression assay in primary hippocampal neurons was established (Figure 16A, chapter 2.2.3). This assay allows the differentiation between the active and the passive excitotoxicity-induced shut-off of gene expression and protein phosphorylation. The proportion of the active shut-off was especially in focus for this thesis since it is a direct effect of excitotoxicity/eNMDAR activation.

3.2.1. Differential transcription shut-off

First, expression of several well characterized IEGs was analysed with the *in vitro* shut-off assay, depicted in figure 16A. Three different protocols were established (short, intermediate, long protocol) to analyse genes with different expression maxima/kinetics (Figure 16B). In the upper left corner of every graph a short timeline of all applied drugs is depicted to clarify the experiment procedure. Cultures were stimulated with BIC for 0.5h, 1h or 2h (short, intermediate, long protocol, respectively), after which the sodium channel blocker tetrodotoxin (TTX) and/or NMDA (30µM) was applied for the same duration as BIC (detailed description in chapter 2.2.3 and Figure 16B). TTX inhibits voltage-gated sodium channels, thereby preventing action potential firing, resulting in a loss of synaptic activity. TTX models the passive excitotoxicity-induced shut-off in this assay (1h BIC + 1h TTX on

top = TTX control) by blocking synaptic activity, which occurs during excitotoxicity due to massive neuronal depolarization. On top of TTX, NMDA is applied in one sample, therefore, active NMDA-induced dephosphorylation events should arise in addition to the passive events. Another sample was treated with NMDA only after BIC to see the total excitotoxic shut-off. As control, instead of TTX and/or NMDA the transcriptional inhibitor actinomycin D (Act. D) was used to compare the shut-off effect with total transcription halt. Since it is difficult to quantify the gene shut-off when expression already decays naturally, it was tested whether IEG expression was still in rise at the time of shut-off induction. Therefore, cells were treated with BIC only for different durations (0.5h, 1h, 2h).

Figure 16C shows as example the expression profile of the short protocol for the IEG *Arc* and its passive and active transcription shut-off. *Arc*, *cFos* and *Egr1* are rapid IEGs, therefore transcription is only still on the rise after 0.5h (Appendix 1). All three genes show a mild, not significant active shut-off (Figure 16D) of around -20% to -7% compared to the passive shut-off (TTX only control). The intermediate protocol gives information for most of the analysed IEGs like *Bdnf* (Figure 16E) and *Npas4* (Figure 16F). *Bdnf* displays no passive shut off, but a strong active one (-49.1% of TTX control). Even stronger is the active shut-off for *Inhba* with -76.2% of TTX control (Figure 16G). Surprisingly, not all genes showed an active shut-off, some of them (*Npas4*, *Nr4a1*) displayed enhanced transcription during excitotoxicity/eNMDAR activation (Figure 16G). This indicates that the transcriptional shut-off is not a global event and affects IEGs differentially.

The long protocol was not suitable for most analysed IEGs since it detects the active shut-off for genes with induction maxima later than 2h. For broad shut-off analysis the intermediate protocol is the most suitable, because it detects a strong active shut-off and adequate gene induction for most analysed IEGs (Table 18, Appendix 1). Therefore, the intermediate protocol was used for all following expression shut-off experiments.

Table 18: Overview of active transcriptional shut-off of different assay protocols in percent of respective TTX control. Assays were conducted according to Figure 17A. Short protocol = 0.5h Bic + 0.5h TTX and/or NMDA; intermediate protocol = 1h BIC + 1h TTX and/or NMDA; long protocol = 2h BIC + 2h TTX and/or NMDA. Expression was analysed by RT-qPCR with *Gusb* as endogenous control. Induction data was normalized to untreated control and active shut-off is displayed as percent of TTX control (= passive shut-off). Mean percentage is shown; n=3.

Gene	Short protocol		Intermediate protocol		Long protocol	
	TTX/NMDA	NMDA	TTX/NMDA	NMDA	TTX/NMDA	NMDA
Inhba	53,06	52,94	22,68	22,93	43,75	39,39
Bdnf	61,19	37,97	49,67	44,25	70,15	64,99
Arc	79,96	71,48	198,25	184,80	146,93	146,95
Npas4	83,15	76,63	153,11	143,84	1893,84	1961,59
Atf3	62,20	54,44	60,45	54,93	110,52	76,07

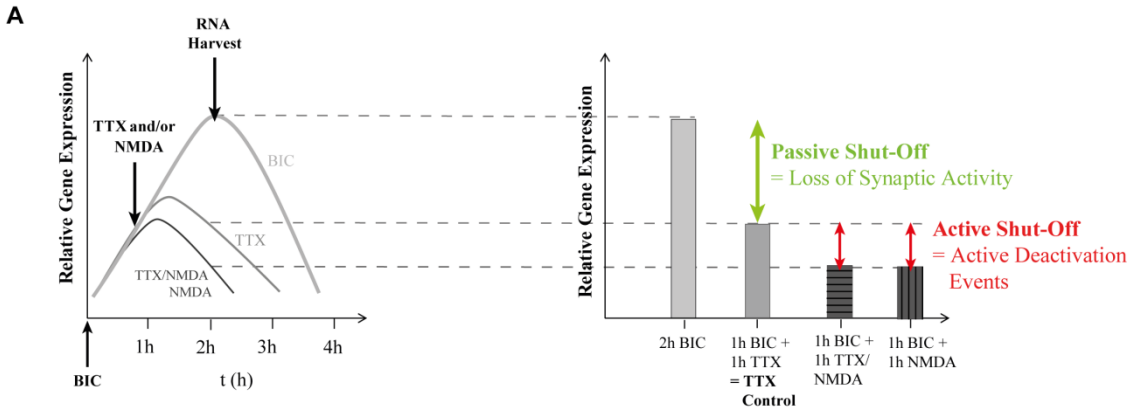
A
RNA Harvest
TTX and/or NMDA
BIC
TTX
TTX/NMDA
NMDA
Relative Gene Expression
1h
2h
3h
4h
BIC
t (h)
Passive Shut-Off
= Loss of Synaptic Activity
Active Shut-Off
= Active Deactivation Events
2h BIC
1h BIC + 1h TTX = TTX Control
1h BIC + 1h TTX/ NMDA
1h BIC + 1h NMDA

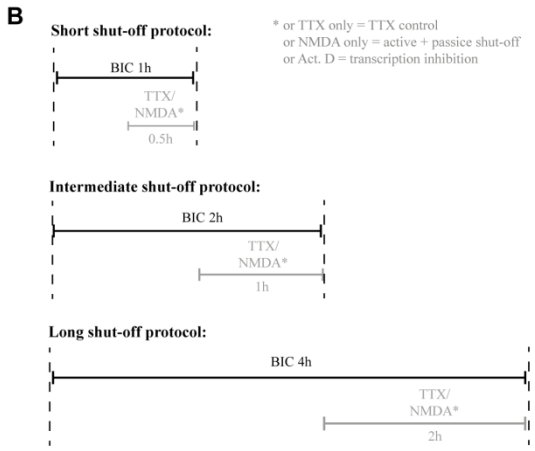
B
Short shut-off protocol:
BIC 1h
TTX/ NMDA*
0.5h
* or TTX only = TTX control
or NMDA only = active + passice shut-off
or Act. D = transcription inhibition
Intermediate shut-off protocol:
BIC 2h
TTX/ NMDA*
1h
Long shut-off protocol:
BIC 4h
TTX/ NMDA*
2h

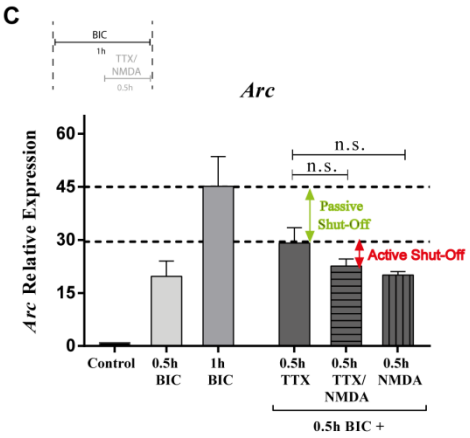
C
Arc
Arc Relative Expression
n.s.
n.s.
Passive Shut-Off
Active Shut-Off
Control
0.5h BIC
1h BIC
0.5h TTX
0.5h TTX/ NMDA
0.5h NMDA
0.5h BIC +

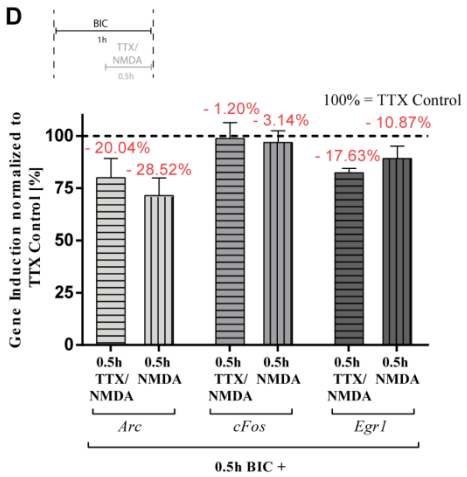
D
Gene Induction normalized to TTX Control [%]
100% = TTX Control
- 20.04%
- 28.52%
- 1.20%
- 3.14%
- 17.63%
- 10.87%
0.5h TTX/ NMDA
0.5h NMDA
Arc
cFos
Egr1
0.5h BIC +

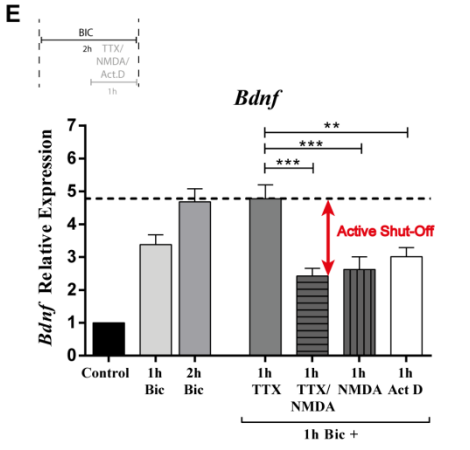
E
Bdnf
Bdnf Relative Expression
Active Shut-Off
Control
1h Bic
2h Bic
1h TTX
1h TTX/ NMDA
1h NMDA
1h Act D
1h Bic +

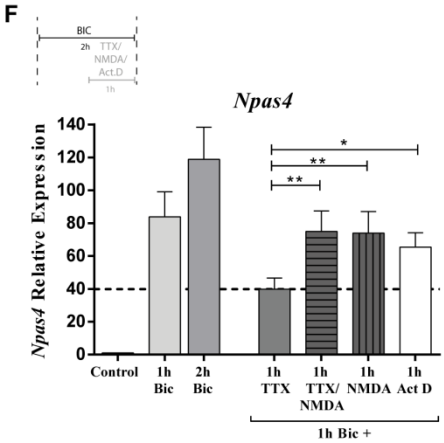
F
Npas4
Npas4 Relative Expression
Control
1h Bic
2h Bic
1h TTX
1h TTX/ NMDA
1h NMDA
1h Act D
1h Bic +

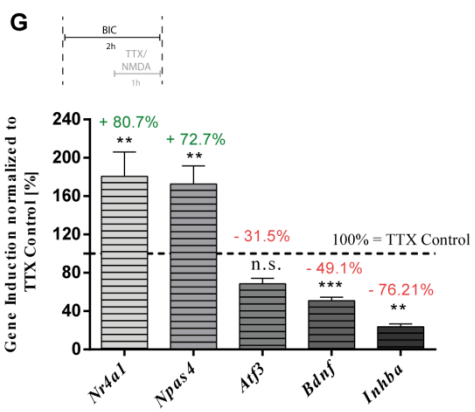
G
Gene Induction normalized to TTX Control [%]
+ 80.7%
+ 72.7%
- 31.5%
n.s.
- 49.1%
- 76.21%
100% = TTX Control
Nr4a1
Npas4
Atf3
Bdnf
Inhba

Figure 16: Transcription shut-off during excitotoxicity. (A) Schematic illustration of transcriptional downregulation induced by passive (tetrodotoxin = TTX) and active (excitotoxicity = NMDA, NMDA/TTX; transcription inhibition = actinymycin D) events. Intermediate shut-off protocol is shown as example. **(B)** Graphical diagrams depicting the stimulation procedure of the short, intermediate and long transcriptional shut-off protocols. The short protocol is designed for rapid early genes, the intermediate protocol for delayed early response genes, and the long protocol for delayed response genes. Duration of TTX/NMDA stimulation was identical for pure TTX (= TTX control), pure NMDA, and actinomycin D (Act.D) stimulated samples (gray). **(C)** Transcription profile of the rapid IEG *Arc* during the short shut-off protocol. N = 3. **(D)** Overview of the active shut-off for TTX/NMDA samples of rapid IEGs (*Arc*, *cFos*, *Homer1*) acquired by the short protocol. N = 3. Transcription profile of IEGs *Bdnf* **(E)** and *Npas4* **(F)** during the intermediate shut-off protocol. N = 8. **(G)** Overview of the active shut-off for TTX/NMDA samples of delayed IEGs (*Npas4, Nr4a1, Atf3, Bdnf, Inhba*) acquired by the intermediate protocol. N = 8. Primary hippocampal neurons were always treated with 50 µM bicuculline (BIC), 30 µM TTX, 30 µM NMDA and 10 µM Act.D according to the respective protocol. Expression was analysed by RT-qPCR with *Gusb* as endogenous control. Induction data was normalized to untreated control (C, E, F). Active shut-off is displayed as percentage of TTX control (= passive shut-off; D, G). All graphs are plotted as mean + SEM. Statistical significance in comparison to TTX control was determined by repeated measures one-way ANOVA with Tukey´s multiple comparison test, n.s. = not significant, *$p < 0.05$, **$p < 0.01$, ***$p < 0.001$.

3.2.2. Rescue of transcription shut-off with NMDA receptor inhibitors

In order to analyse whether the shut-off extent correlates with NMDA concentration, different NMDA concentrations were used in the intermediate protocol. The active *Inhba* and *Bdnf* shut-off showed an NMDA concentration dependency (Figure 17A). It was concluded that the transcriptional shut-off of those genes also depends on the levels of eNMDAR activation. Gene expression rescue should be accomplishable by NMDA receptor inhibition. Since sNMDAR activation is crucial for normal brain function (see chapter 1.2.2), inhibitors suitable for human medication should not block sNMDARs, only eNMDARs specifically. The described shut-off analysis combined with normal gene induction analysis can serve as an NMDA receptor inhibition assay, indicating specific eNMDAR inhibition. Suitable inhibitors should display normal gene induction, rescue of the transcriptional shut-off, and attenuated or blocked excitotoxicity induced necrosis.

For this assay diverse NMDA receptor inhibitors were tested: the allosteric NR2B inhibitor Ifenprodil, a combination of MK801 and APV to block NMDA receptors unspecifically, as well as Memantine, an open-channel blocker, and ConG, a competitive inhibitor specific for NR2B containing receptors. A detailed description of their mode of action is shown in Figure 4 (chapter 1.3.1). Since *Inhba* and *Bdnf* show the most severe active shut-off, expression rescue was only analysed for those two genes (Figure 17D). In parallel, gene induction by BIC stimulation was compared between inhibitor-treated and untreated neurons (Figure 17C). The attenuation of NMDA toxicity by NMDA receptor inhibition in comparison with sole NMDA treatment was also analysed (Figure 17B). For all experiments inhibitors were pre-incubated for one hour upon BIC treatment.

All tested inhibitors successfully attenuated excitotoxicity-induced cell death (Figure 17B). However, inhibitors accomplished gene induction and shut-off rescue differentially. MK801/APV, 100 µM Memantine and 1 µM ConG showed attenuated gene induction indicating that they were blocking sNMDARs (Figure 17C). MK801/APV and 1 µM ConG however showed complete rescue of the active *Inhba* and *Bdnf* shut-off (Figure 17D). Highly-concentrated memantine showed no rescue effect since it blocked *Inhba* and *Bdnf* induction/sNMDARs too massively (Figure 17C, D). Low concentrated Memantine and ConG did not inhibit *Inhba* and *Bdnf* induction, but could not rescue the active shut-off completely. However, an attenuated active shut-off was observed for both inhibitors. Ifenprodil-treated cells showed the highest induction (Figure 17C). Ifenprodil was also the most successful inhibitor in rescuing the active shut-off (Figure 17D).
In general, the established assay was suitable to detect NMDA receptor inhibitor differences in sNMDAR/eNMDAR block specificity which could be very useful for drug research aiming against excitotoxicity in neurodegeneration. Ifenprodil might be a promising candidate since it did not inhibit *Inhba*/*Bdnf* induction but did block the active shut-off. The implemented assay with its high NMDA concentration of 30 µM, however, uses a strong and rapid excitotoxic insult. In neurodegeneration toxicity is probably initiated by sustained and weaker eNMDAR activation.

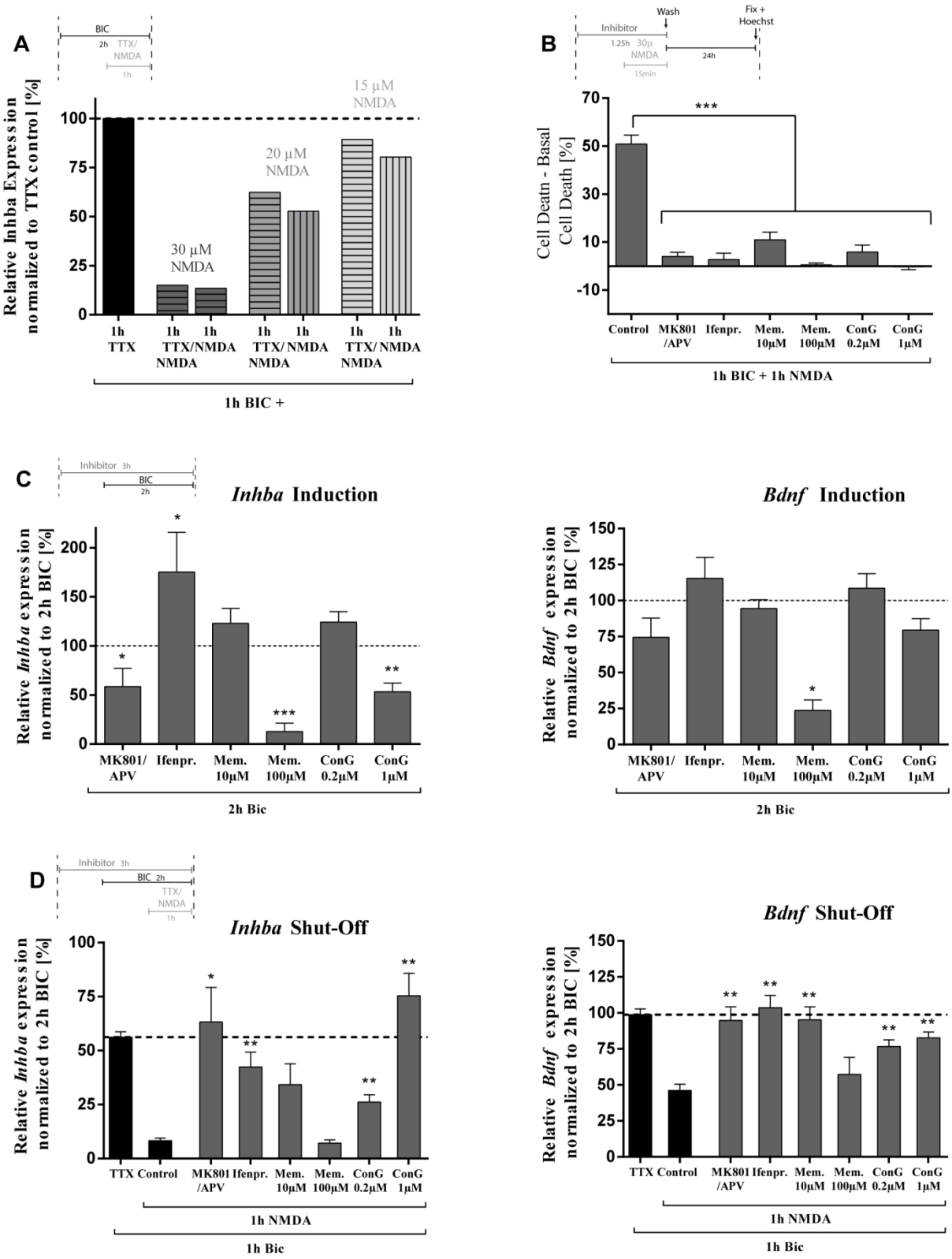

Figure 17: NMDA receptor inhibitor assay containing *Inhba* and *Bdnf* shut-off and induction as well as cell death analysis. (A) NMDA concentration dependency of active *Inhba* transcription shut-off shown for the TTX/NMDA sample during the intermediate protocol. Data was normalized to TTX control. N = 1. **(B)** Increase of cell death in inhibitor untreated (control) and treated cultures. For cell death analysis cells were treated according to NMDA shut-off protocol, washed with medium, fixed and stained with Hoechst 24h later. Cell

death was determined by counting dense nuclei. Basal cell death of untreated cells was subtracted from data. N = 4. **(C)** *Inhba* (left) and *Bdnf* (right) gene expression after 2h BIC treatment and NMDA receptor inhibitor application. N = 4. **(D)** Rescue of *Inhba* (left) and *Bdnf* (right) shut-off by NMDA receptor inhibitors. N = 3. Expression data of (C) and (D) was normalized to 2h BIC expression of inhibitor untreated cells. Primary hippocampal neurons were pre-treated for 1h with 10 µM MK801/50 µM APV, 3 µM Ifenprodil (Ifenpr.), 10 µM or 100 µM Memantine (Mem.), 0.2 µM or 1 µM Conantokin G (ConG). Shut-off was performed as previously described with the intermediate protocol. Expression was analysed by RT-qPCR with *Gusb* as endogenous control. All graphs are plotted as mean + SEM. Statistical significance was determined by ordinary one-way ANOVA with Tukey´s multiple comparison test (B) and unpaired t-test in comparison to relative 2h BIC expression (C) and shut-off control data (D; control = 1h BIC + 1h TTX/NMDA without inhibitor); n.s. = not significant, *p < 0.05, **p < 0.01, ***p < 0.001.

3.2.3. Transcription shut-off induced by mild excitotoxicity

To establish a protocol with weak eNMDAR activation, first, a low NMDA concentration of 10 µM was tested that does not result in necrotic cell death. However, 10 µM NMDA did not initiate active shut-off events for *Bdnf* and *Inhba* (Figure 18A). Therefore, another means of inducing excitotoxicity was established. Threo-β-benzyloxyaspartic acid (TBOA), an inhibitor of excitatory amino acid transporters (EAAT) 1 and 2, was used after BIC treatment to force neurons to synaptic glutamate spill-over (Figure 18B) [140]. First BIC induced synaptic activity fills the synaptic cleft with glutamate. By inhibiting EAAT 1/2, which are predominantly located in glia cells [141], glutamate uptake is impaired; glutamate spills over the synaptic cleft and activates eNMDARs in close proximity to the synapse. This model recapitulates neurodegenerative conditions where elevated synaptic glutamate concentration and impaired glutamate uptake are observed [116, 142].

One hour TBOA (50µM) application compared to one hour NMDA (30µM) resulted in much lower cell death increase (Figure 18E). For most genes, no active shut-off was observed (Figure 18C, Appendix 2). *Npas4* and *Nr4a1* displayed normal gene induction without a passive shut-off (Figure 18D, Appendix 2). *Inhba* on the other hand still displayed an active shut-off of around -50% compared to TTX control (Figure 18C). It appears that *Inhba* expression is especially sensitive to eNMDAR activation and even mild insults result in *Inhba* transcriptional downregulation.

Additionally, it was tested whether memantine at the eNMDAR specific concentration of 10 µM [143] is able to rescue TBOA-induced *Inhba* downregulation. A significant rescue of the active *Inhba* shut-off was observed (Figure 18F), more substantial than the rescue of the 30 µM NMDA-induced downregulation. Comparison of BIC-induced gene expression in the presence of 10 µM memantine also revealed interesting trends. Genes that show high active shut-off susceptibility like *Inhba* and *Bdnf* tended to have upregulated expression during memantine-induced eNMDAR inhibition. Genes that displayed elevated expression upon bath NMDA application like *Npas4* and *Nr4a1* had a trend for reduced expression during eNMDAR inhibition (Figure 18G). The differential aspect of this eNMDAR dependency and transcriptional shut-off is possibly caused by differential activation/deactivation of upstream kinases and transcription factors. Dephosphorylation events during excitotoxicity are only reported for CREB and ERK1/2 deactivation thus far.

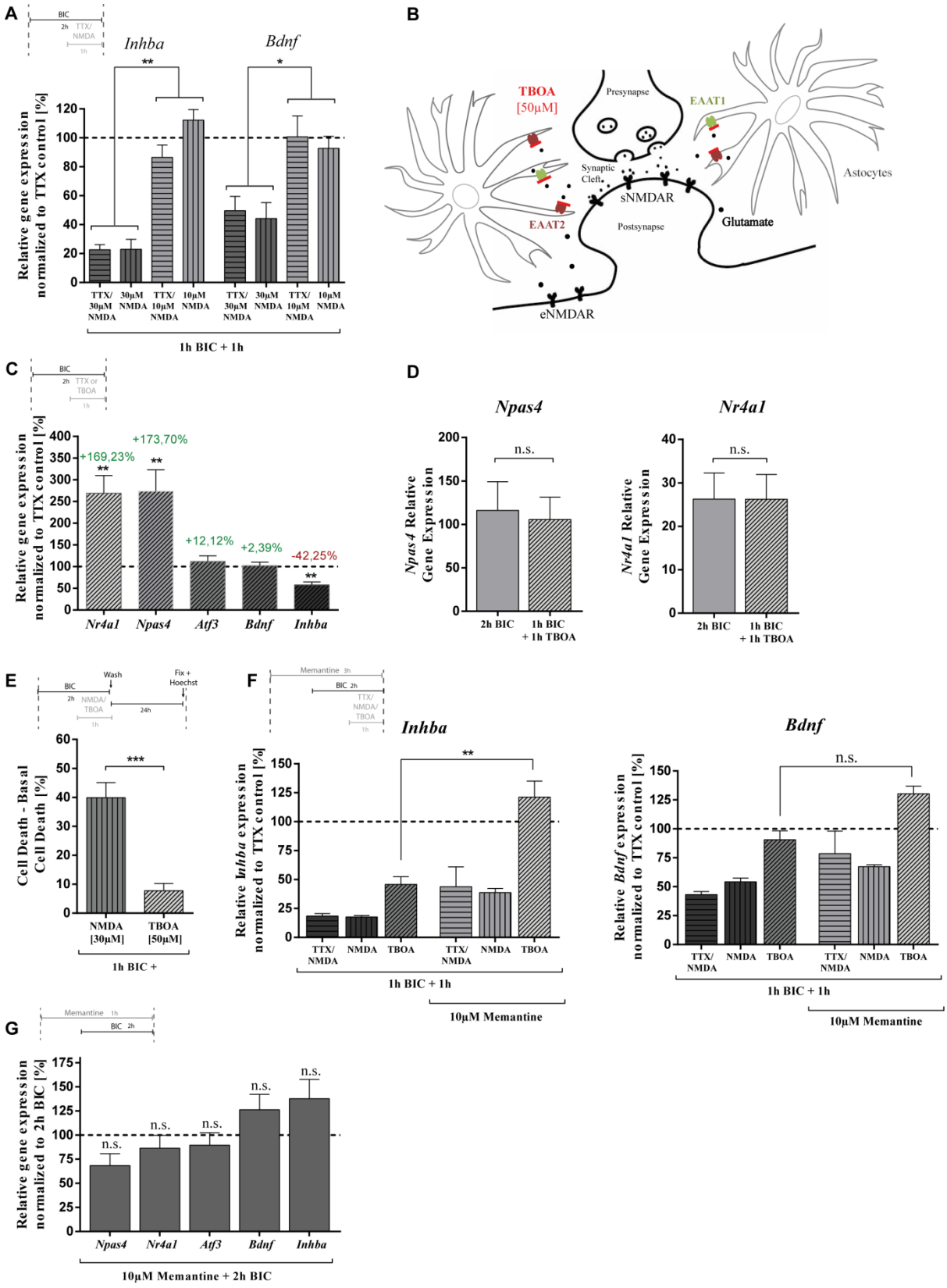

Figure 18: Transcription shut-off induced by mild excitotoxic insults. (A) Active transcription shut-off of *Inhba* and *Bdnf* induced by 10 µM NMDA. Data is normalized to TTX control. N = 3. **(B)** Schematic figure of Threo-β-benzyloxyaspartic acid (TBOA) protocol resulting in synaptic glutamate spill and mild eNMDAR activation. EAAT = excitatory amino acid transporter. **(C)** Overview of the active shut-off extent induced by the

TBOA protocol of *Npas4*, *Nr4a1*, *Atf3*, *Inhba* and *Bdnf* normalized to TTX control. N = 5. **(D)** *Npas4* (left) and *Nr4a1* (right) relative gene expression normalized to untreated cells. N = 3. **(E)** Percent of dead cells 24h after 1h 30 µM bath NMDA and 1h bath TBOA application. Cell death was determined by counting Hoechst stained dense nuclei. Basal cell death of untreated cells was subtracted from presented data. N = 6. **(F)** Active shut-off (intermediate and TBOA protocol) and memantine (10µM) rescue of *Inhba* (left) and *Bdnf* (right) expression. N = 3. **(G)** Overview of 2h BIC induced gene expression (*Npas4*, *Nr4a1*, *Atf3*, *Inhba*, *Bdnf*) with pre-incubation of memantine (1h, 10µM). N = 3. Data is normalized to respective 2h BIC expression without memantine. Expression was analysed by RT-qPCR with *Gusb* as endogenous control. All graphs are plotted as mean + SEM. Statistical significance was determined by repeated measures one-way ANOVA with Tukey´s multiple comparison (A, F), paired ordinary t-test against TTX control (C) and 2h BIC (G) and unpaired ordinary t-test (D, E), n.s. = not significant, *p < 0.05, **p < 0.01, ***p < 0.001.

3.2.4. Differential kinase and transcription factor deactivation

To determine the mechanism behind the differential transcription shut-off, activity of several kinases and transcription factors involved in activity-dependent gene induction was investigated. Protein activity was determined by Western blot analysis with antibodies specific for activity-related phosphorylation sites. Due to short-lived protein activity, the stimulation protocol was shortened to 20 min maximum BIC stimulation. TTX and/or NMDA were introduced after 10 min for another 10 min.

For ERK1/2 activity, phosphorylation of Thr^{202}/Tyr^{204} was analysed due to its association with ERK1/2 activation [144]. Surprisingly, ERK1/2 did not show an active dephosphorylation after NMDA application (Figure 19A). ERK1/2 activity is already downregulated massively by TTX. This indicates that ERK1/2 deactivation is predominantly involved in the passive transcription shut-off, but not the active shut-off. In contrast, activity of the transcriptional co-regulator ELK-1 (phosphorylation of Ser^{383}), which is involved in SRF activation, is not diminished by TTX, but shows active dephosphorylation after NMDA application (Figure 19B). Therefore, ELK-1 is a candidate for active shut-off transmission. CREB the central hub for activity-dependent gene induction shows passive and active dephosphorylation at Ser^{133} (Figure 19C) and is therefore probably involved in passive and active shut-off processes.

Excitotoxicity-induced dephosphorylation is not the only shut-off mechanism, however. Also degradation of CREB 20 min after NMDA application has been reported [92]. Protein degradation was analysed by using total protein antibodies and applying the intermediate protocol with 1h BIC and 1h TTX and/or NMDA treatment for Western blot analysis. With this protocol, degradation of CREB was confirmed (Figure 19D). Furthermore, phosphorylation (Ser^{408}) and total protein of MEF2A was analysed with the longer protocol. MEF2A showed no degradation, but similar to CREB both passive and active dephosphorylation at the analysed site (Figure 20 E).

All in all, excitotoxicity-induced dephosphorylation appears to be a global phenomenon since all analysed proteins showed dephosphorylation after NMDA application at the investigated sites. Broad dephosphorylation can be achieved by activation of unspecific phosphatases like protein phosphatise 1 (PP1).

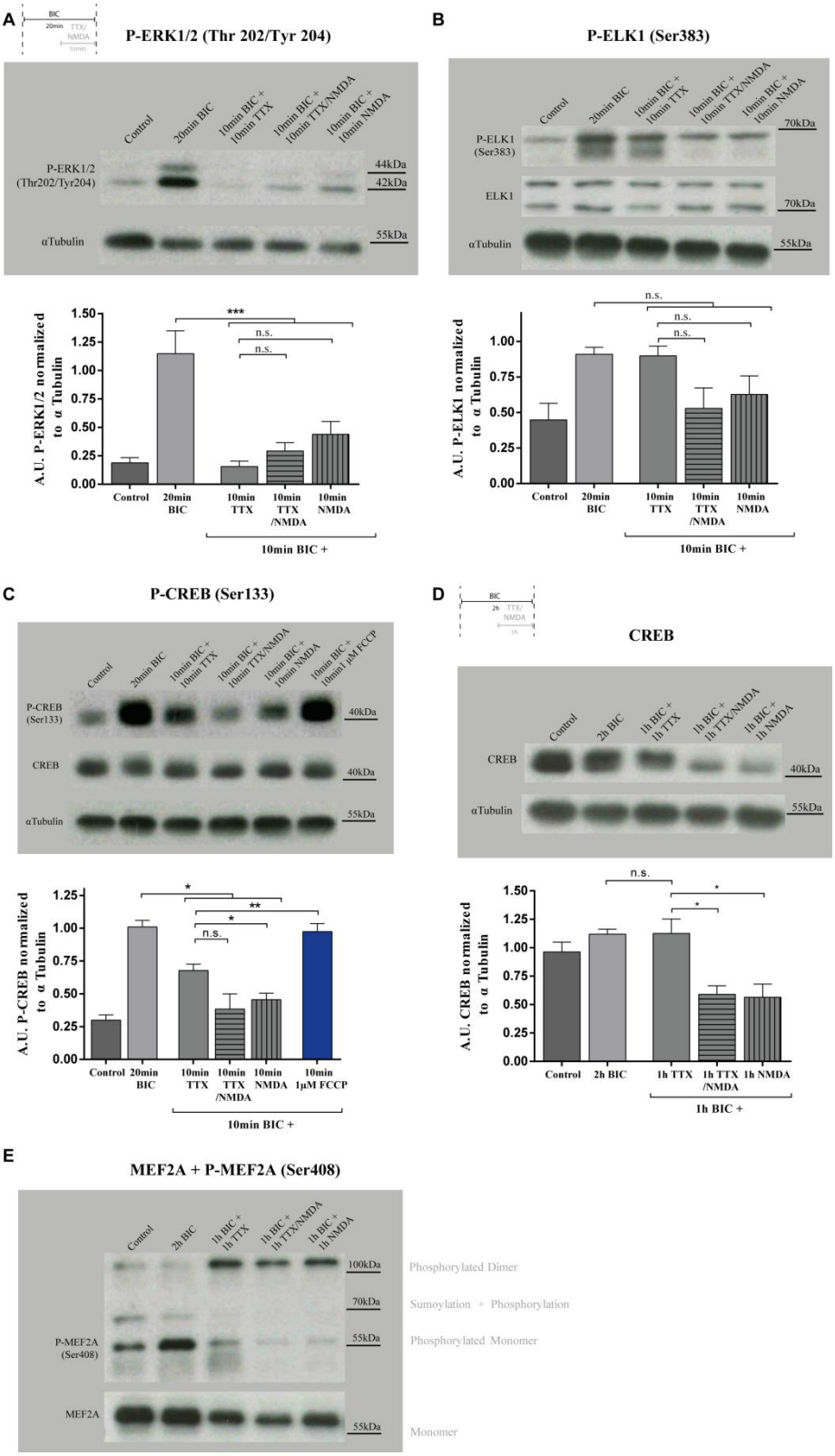

Figure 19: Activity shut-off induced by 30 µM NMDA. (A) Example blot of ERK1/2 phosphorylation at Thr^{202}/Tyr^{204} after 10min/10min shut-off protocol application. Below: Quantification of ERK1/2 phosphorylation. N = 3. **(B)** Example blot of ELK1 phosphorylation at Ser^{383} after 10min/10min shut-off protocol application. Below: Quantification of ELK1 phosphorylation. N = 3. **(C)** Example blot of CREB phosphorylation at Ser^{133} after 10min/10min shut-off protocol application. Below: Quantification of CREB

phosphorylation. N = 4. **(D)** Example blot of total CREB after 1h/1h (intermediate) shut-off protocol application. Below: Quantification of CREB expression. N = 3. **(E)** Example blots of MEF2A expression (top) and MEF2A phosphorylation at Ser^{408} (below) after 1h/1h (intermediate) shut-off protocol application. Right: Possible protein modifications explaining additional P-MEF2A bands. Quantified intensities in arbitrary units (A.U.) were always normalized to respective alpha tubulin band intensity as loading control. All graphs are plotted as mean + SEM. Statistical significance was determined by repeated measures one-way ANOVA with Tukey´s multiple comparison test, n.s. = not significant, *p < 0.05, **p < 0.01, ***p < 0.001.

3.2.5. Mechanism of shut-off induction: Phosphatases

CREB dephosphorylation at Ser^{133} depends on PP1 activity [96]. Whether PP1 is also responsible for the observed CREB dephosphorylation during the established shut-off protocol was tested by applying the PP1 inhibitor okadaic acid (OA) during the intermediate transcription shut-off together with BIC. Successful inhibition of CREB dephosphorylation should result in attenuated active shut-off intensity. Unexpectedly, OA application with the previously reported PP1-specific concentration of 2 µM resulted in immense *Inhba* and *Bdnf* downregulation and no attenuation of the transcriptional shut-off (Figure 20A).

Another candidate phosphatase possibly involved in CREB dephosphorylation and transcription downregulation is calcineurin (PP-2B). Calcineurin can be inhibited by application of a cyclosporinA/FK506 mixture (250 µM/1 µM, respectively) [96]. Similar to OA, this inhibitor combination reduced transcription immensely, but did not prevent transcription shut-off (Figure 20A). It appears that those phosphatase inhibitors are reducing basal gene expression at the applied concentrations.

Next to CREB, also upstream ERK1/2 dephosphorylation might be involved in transcription downregulation. Therefore, preventing ERK1/2 dephosphorylation by inhibiting the ERK1/2 phosphatase striatal-enriched protein tyrosine phosphatase (STEP) with TC-2153 (1 µM) was tested next [145]. TC-2153 application did not rescue *Inhba* and *Bdnf* shut-off, although it did not downregulate transcription further like OA and cyclosporinA/FK506 (Figure 20A).

The involvement of another unreported potential phosphatase was tested, the phosphatase and tensin homolog (PTEN). PTEN is able to dephosphorylate CREB, and dominant negative as well as nuclear-shuttling-impaired PTEN prevent excitotoxic neuronal cell death [100, 101]. For PTEN inhibition three drugs were tested; SF1670 (30 µM), bbV(phen) (100µM) and VO-Ohpic trihydrate (30µM) [146]. Again, none of the inhibitors was able to attenuate *Inhba* and *Bdnf* transcription shut-off (Figure 20B). SF1670 and bbV(phen) even downregulated BIC-mediated induction of *Inhba* and *Bdnf* (Figure 20C).

In conclusion, phosphatase inhibition showed no effect on active excitotoxicity-induced transcription downregulation. However, independency of the transcriptional shut-off from these phosphatases cannot be concluded, since another possible explanation might be unspecific side effects of the used drugs, interfering with general gene expression. Knockout/knockdown of phosphatase expression or overexpression of dominant negative forms in combination with the shut-off protocol could clarify this question. Since phosphatase inhibition did not uncover information about shut-off initiation mechanism, another possible initiator was investigated: mitochondrial depolarization.

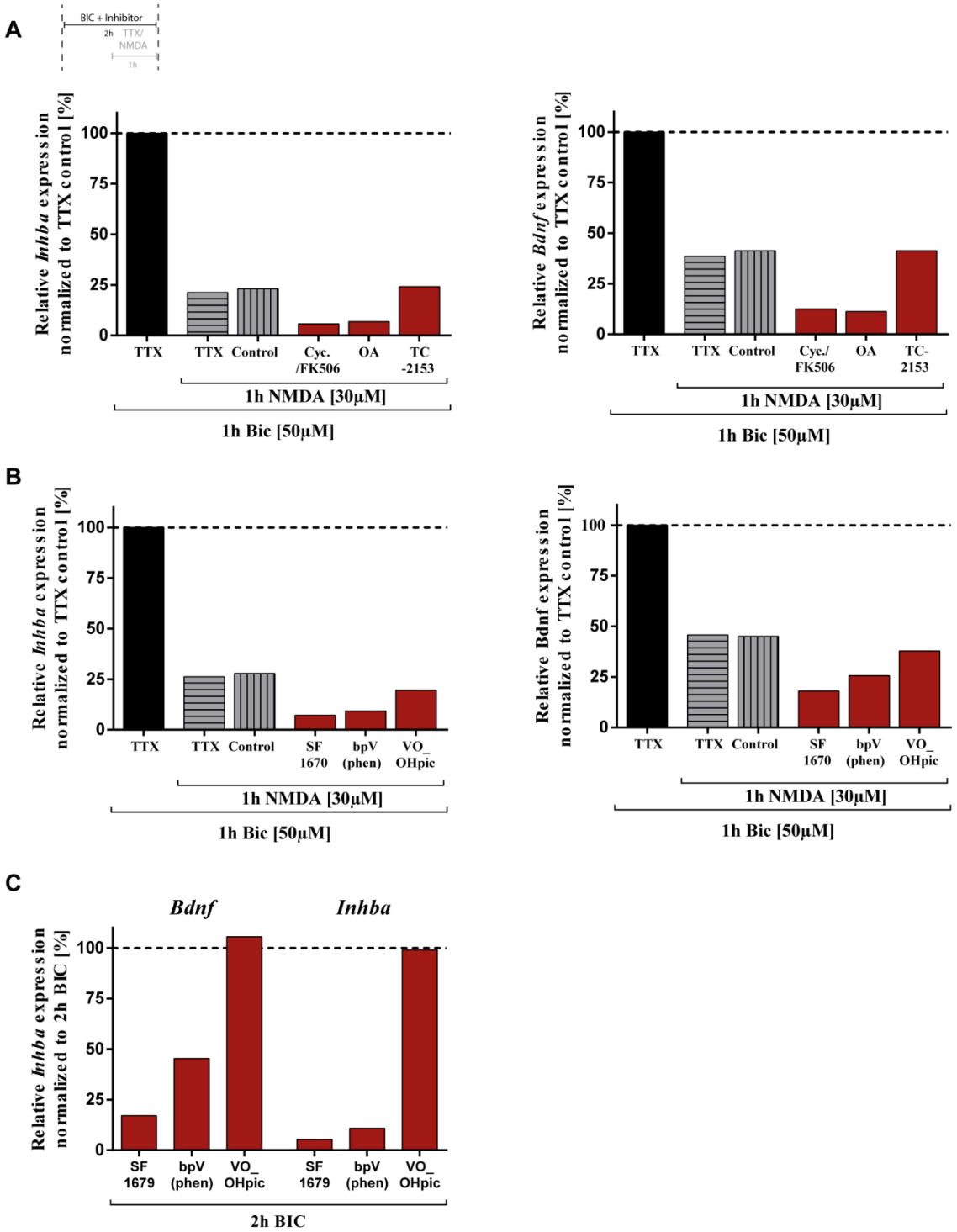

Figure 20: Rescue of excitotoxicity induced *Inhba* and *Bdnf* transcription shut-off by phosphatase inhibitors. (A) *Inhba* (left) and *Bdnf* (right) transcription shut-off during the intermediate shut-off protocol and phopsphatase inhibition. Inhibitors were applied together with BIC. Okadaic acid (1 µM) = PP1 inhibition, CyclosporinA/FK506 (250 µM/1 µM) = PP-2B inhibition, TC-2153 (1 µM) = STEP inhibition. **(B)** *Inhba* (left) and *Bdnf* (right) shut-off during PTEN inhibition. Data is depicted as percentage of respective TTX control expression (100% = TTX control gene expression). **(C)** 2h BIC induced expression of *Inhba* and *Bdnf* during PTEN inhibitor treatment normalized to respective 2h BIC samples without inhibitors. Inhibitors were applied together with BIC. PTEN inhibitors: SF1670 (30 µM), bbV(phen) (100 µM) and VO-Ohpic trihydrate (30 µM). Expression of primary hippocampal neurons was analysed by RT-qPCR with *Gusb* as endogenous control. N = 1.

3.2.6. Mechanism of shut-off induction: Mitochondrial Depolarization

Mitochondrial depolarization is one major hallmark of excitotoxicity-induced cell death (see chapter 1.3.1). It occurs seconds after bath NMDA application and massive depolarization represents a point of no return for cell death induction. Once mitochondria depolarize several death promoting signal cascades are activated reaching the cytoplasm and nucleus like ROS, Cyclosporin A and Bcl-2 signalling [147]. Therefore, it was hypothesized that death signalling caused by mitochondrial depolarization is one possible initiator for the observed dephosphorylation and transcriptional downregulation events.

To test this theory, mitochondria were depolarized directly without NMDA receptor activation using the ionophore and uncoupling reagent carbonyl cyanide-4-(trifluoromethoxy) phenylhydrazone (FCCP) [148], and the transcription of *Bdnf* and *Inhba* was analysed. Instead of immense calcium influx initiated by eNMDAR activation, FCCP results in hydrogen ion influx in the mitochondrial matrix. Nonetheless, both mechanisms uncouple mitochondria, lead to loss of mitochondrial membrane potential (Ψ_m) and initiate death signalling. In the case of mitochondrial depolarization as central shut-off initiator, FCCP-induced mitochondrial depolarization should cause similar transcriptional downregulation effects as NMDA application. However, the extent of membrane potential loss depends on FCCP concentration directly. Moreover, when administered at high concentrations, FCCP can also damage the plasma membrane [149].

Therefore, the first task was to determine what FCCP concentration causes a similar mitochondrial depolarization as 30 µM NMDA. Only similar depolarization events would allow for the comparison of gene expression with results obtained by the intermediate shut-off protocol. Depolarization was determined by measuring the loss of mitochondrial membrane potential via rhodamine-123 (Rh-123) imaging [150]. In comparison with 30 µM bath NMDA application, 0.5 µM FCCP showed the most similar depolarization performance in terms of kinetics (Figure 21A) and magnitude (Figure 21B) of membrane potential loss. Next, 0.5 µM FCCP was used in the intermediate transcription shut-off protocol instead of NMDA. However, with this concentration no NMDA-comparable shut-off was observed for *Inhba* and *Bdnf* transcription (Figure 21C). Unsuccessful shut-off initiation by FCCP was also observed in terms of CREB dephosphorylation even with 1 µM FCCP (Figure 19C, right lane, blue column).

Since mitochondrial depolarization/loss of mitochondrial membrane potential does not cause an active transcription shut-off of *Inhba* and *Bdnf*, it can be concluded that the shut-off occurs in parallel with mitochondrial depolarization events downstream of eNMDAR activation.

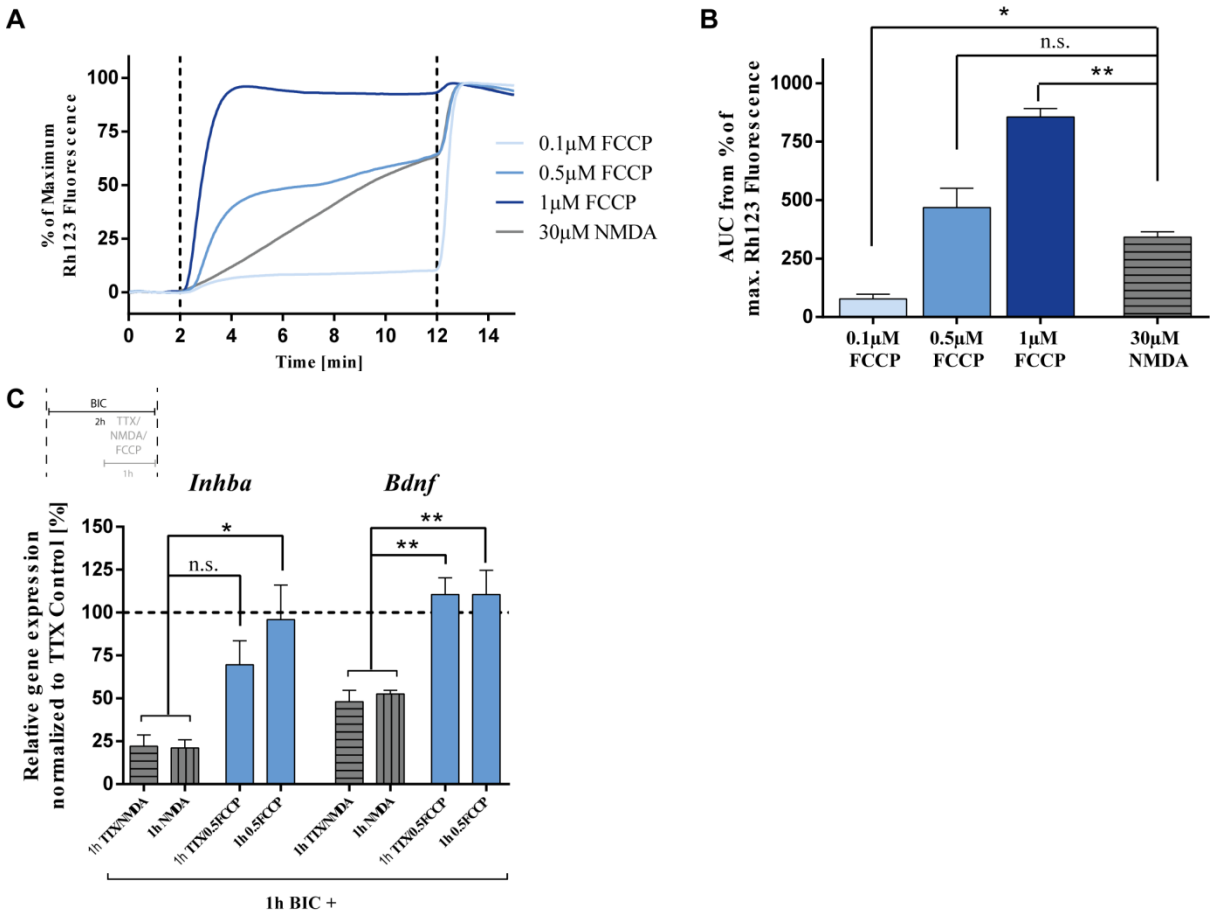

Figure 21: Mitochondrial depolarization as possible initiator of excitotoxicity induced transcription shut-off. (A) Loss of mitochondrial membrane potential (Ψm) over time (min) by different concentrations of the uncoupling reagent FCCP (bright blue = 0.1 µM, blue = 0.5 µM, dark blue = 1 µM) and NMDA (30µM, gray). Mean of 5-9 different experiments (cover slips) is plotted stemming from 3 different culture preparations. Ψm loss was determined by rhodamine-123 (Rho-123) imaging. Decreasing Ψm results in increasing Rho-123 fluorescence in non-mitochondria containing cell compartments like the nucleus. Rho-123 fluorescence of the nuclear compartment was measured and normalized to maximal Ψm loss/fluorescence induced by 5 µM FCCP (at t = 12min). **(B)** Area under the curve (AUC) of figure 21A. **(C)** Transcriptional *Inhba* and *Bdnf* shut-off after intermediate protocol with 0.5 µM FCCP (blue) and 30µM NMDA (gray). Expression was analysed by RT-qPCR with *Gusb* as endogenous control. Data is depicted as percentage of respective TTX control expression (100% = TTX control gene expression). Graphs are plotted as mean (A) or mean + SEM (B, C). Statistical significance was determined by ordinary one-way ANOVA with Tukey´s multiple comparison; n.s. = not significant, $p > 0.05$; *$p < 0.05$; ** $p < 0.01$.

Chapter 4

Discussion

4.1. Relevance of activity-dependent gene expression for spatial memory performance in DBA/2

The first aim of this study was to investigate the DBA/2 spatial memory impairment and its cellular and molecular causes with a focus on a potential activity-dependent gene induction impairment since disturbed NMDA receptor signalling and IEG expression are responsible for a variety of learning deficits. First, the spatial memory impairment of DBA/2 was confirmed with the hippocampus dependent tasks CFC and SOR (3.1.1). Also behaviour indicative of a hippocampal dysfunction like impaired nest building and increased activity in a novel environment was observed (3.1.1). However, it was also discovered that the DBA/2 impairment partially affects short-term memory and that it is not exclusive for spatial memory performance since DBA/2 also showed a significant impairment in the striatum-dependent VMCL task. By analysing DBA/2 hippocampal and dendritic morphology as well as passive electrophysiological properties of CA1 pyramidal neurons, no significant strain differences in those basic learning-relevant features were observed (3.1.2). Also IEG expression *in vitro* and for most of the analysed genes *in vivo* revealed no general brain activation and IEG induction dysfunction in DBA/2 (3.1.3). Attenuated *in vivo* IEG expression in DBA/2 PC was detected as well as increased hippocampal induction of the transcription factor *Npas4* after SOR training and increased basal *Inhba* expression in hippocampal and cortical regions (3.1.3). *Npas4* and *Inhba* are linked with inhibition/excitation balance and inhibitory neuron development, respectively. In accordance, attenuated inhibitory input signals in DBA/2 pyramidal neurons via mIPSC recordings were discovered (3.1.4). Altogether, this study indicates that the DBA/2 memory impairment is not caused by general intrinsic morphological or molecular signalling dysfunction but rather by an excitation/inhibition imbalance with increased hippocampal activity. Additional indications for such an imbalance are listed in 4.1.2. To confirm the imbalanced signalling in DBA/2 further experiments are suggested (4.1.4).

4.1.1. Broad DBA/2 learning impairment – indication for memory acquisition deficits

The DBA/2 learning impairment, which was observed in this study, is not restricted to hippocampus-specific tasks (CFC, SOR), but includes tasks which are not predominantly

dependent on hippocampal function (VMCL). It is difficult to find confirmation of this discovery in literature, since mainly hippocampus-mediated learning or addiction behaviour is reported for DBA/2 in comparison to C57BL/6. However, some of the reported DBA/2 learning impairments are not strictly hippocampus-dependent such as novel-object recognition learning. Furthermore, it was discovered that DBA/2 performance in conditioned taste aversion learning, which depends on amygdala and thalamus function, does not differ from C57BL/6 performance [151] and in passive avoidance learning tasks DBA/2 even outperform C57BL/6 [152]. To confirm the observed hippocampus-unspecific DBA/2 learning impairment it is necessary to access DBA/2 performance in other hippocampus-independent tasks under different experimental conditions.
Besides the non-exclusive spatial LTM impairment in DBA/2, a tendency for impaired spatial STM was discovered in this study (1h post-training; CFC significant impairment, SOR only trend). Unfortunately, no other spatial memory performance with this short post-training time span is reported for DBA/2. However, DBA/2 display elevated impulsivity and attention deficits as accessed by 5-choice serial reaction time task [153]. An attention deficit might explain the DBA/2 learning impairment for several diverse tasks and for STM. One special form of STM which is closely intertwined with attention is working memory. A comparative study from 1990 also indicates impaired DBA/2 performance in a radial maze spatial working memory task [154]. It is suggested to investigate DBA/2 performance for further working memory tasks such as the spontaneous and forced Y-maze alternation tasks or the working memory version of the Morris water maze task [155]. The broad memory impairment of DBA/2 affecting several regions and forms of memory could be explained by a DBA/2 memory acquisition dysfunction. However, it would be difficult to differentiate between acquisition, attention and working memory problems in behavioural tasks.

4.1.2. Imbalanced excitation/inhibition signalling

In recent years the significance of balanced excitation/ inhibition signalling became the focus of research in a broad range of learning tasks and in neurodevelopmental disorders. The molecular cause of the balance disruption can be diverse [156, 157] and reduced (depression, autism) [158, 159] as well as elevated (Rett syndrome, intellectual disability, Down syndrome) [160-162] inhibitory signalling was found to underlie LTP and memory impairments in mouse disease models. The relevance of balanced excitation/inhibition signalling also becomes increasingly apparent for human age-dependent memory decline [60, 163, 164]. Similar to DBA/2, the neurodevelopmental disorders autism and epilepsy, which often show comorbidity, display elevated neuronal excitation in hippocampal regions [159].
In epilepsy, GABAergic receptors are altered and the number of GABAergic neurons, especially parvalbumin-containing neurons, is decreased [165]. DBA/2 display increased seizure susceptibility and severity as well [166, 167] which is in line with the data of kainic acid application in this thesis. Kainic acid resulted in significantly greater seizure severity in DBA/2 than in C57BL/6 (3.1.2). Reduced hippocampal network inhibition in DBA/2 could explain the kainic acid results and the reported occurrence of sound-induced seizures in

DBA/2 [166]. Furthermore, a kainic acid induced rat model of epilepsy displayed encoding deficits during spatial memory formation. This model showed fewer neurons with place field activity and the remaining neurons with place field activity carried less spatial information and were less precise and less stable [168]. Such an encoding impairment could also underlie the DBA/2 spatial memory impairment. Therefore, place cell measurement by *in vivo* electrophysiological recordings in an open field task would be very informative. DBA/2 encoding dysfunction would be in line with the epileptic phenotype of DBA/2.

Another neurological disease with a strong indication for excitation/inhibition imbalance is schizophrenia. This psychological disorder displays hippocampal and in particular CA1 hyperactivity [169]. Hypermetabolism, which occurs first in the CA1 subregion in schizophrenic models, is related to enhanced glutamate release, and correlates with CA1 tissue loss and elevated excitation [170]. Schizophrenic patients also display a broad learning and memory impairment with a dysfunctional working memory [171], whereas other higher brain functions like abstraction are normal [172]. Working memory which might be impaired in DBA/2, too, depends on persistent cell activity and inhibition is especially critical for providing a corrective negative feedback that stabilizes this persistent activity and thereby working memory [173]. Furthermore, abnormal PC function is reported in schizophrenia and is proposed to explain attention deficits [174, 175]. In DBA/2 a non-involvement of the PC in spatial learning as well as attention deficits are reported as well [153, 176] and are coherent with the obtained PC gene expression data indicating reduced DBA/2 basal PC activity (3.1.4). In line with these findings, it has been reported that DBA/2 also display schizophrenia-like behaviour [177].

All in all, it is intriguing that the DBA/2 learning impairment is possibly caused by imbalanced excitation/inhibition signalling, since DBA/2 are not produced by artificial genetic modifications but rather emerged naturally by inbreeding. Compared to C57BL/6, DBA/2 carry genetic variants in a physiological unartificial extent, comparable to two individuals. Although, DBA/2 display an extreme phenotype it would be interesting to investigate if cases of inter-individual differences in human learning performance can be traced back to a difference in the relative levels of excitation and inhibition. Balanced signalling determined by development or altered during aging could gradually undermine memory performance. A slight shift could impair memory ability moderately and a strong shift could result in neurological diseases (Figure 22).

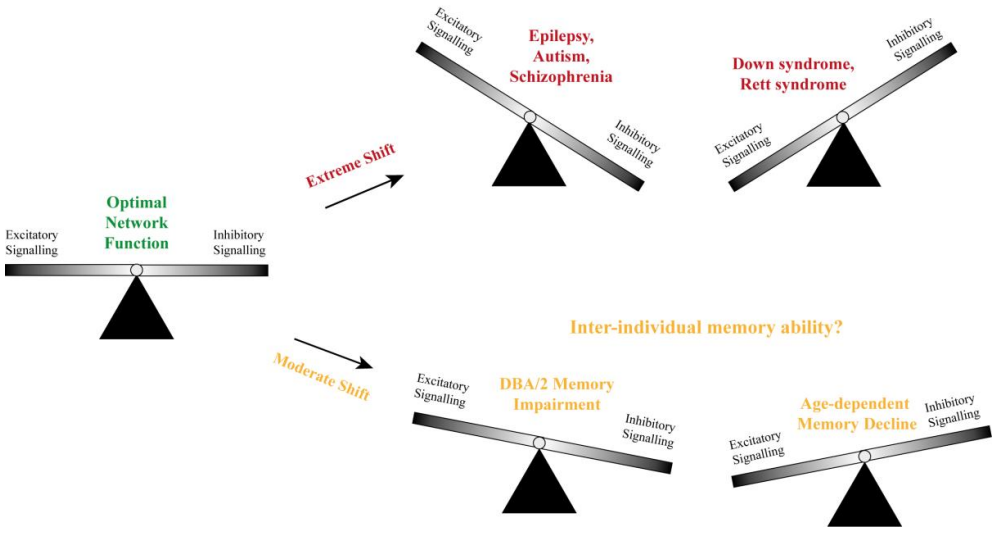

Figure 22: Graphical model of imbalanced excitatory/inhibitory signalling. It is proposed that balanced excitatory and inhibitory signalling is optimal for network function and thereby memory formation (left, green). In neurodevelopmental diseases the balance is shifted to dominating excitatory or dominating inhibitory signals; either way, network performance is diminished and memory impairment occurs (upper right, red). During aging a shift towards increased inhibition was observed in prefrontal cortex regions, correlating with mild memory impairment (lower right, yellow). In course of degenerative and aging processes the shift might become stronger in parallel to memory decline. Inter-individual differences in memory ability could be a neurodevelopment preposition towards slightly off balanced signalling.

4.1.3. Expression and induction alteration of specific IEGs as indicators for learning deficits and signalling imbalance

Basic cellular and electrophysiological properties (3.1.2) as well as intrinsic gene-induction ability (3.1.3) was normal in DBA/2 hippocampal neurons. Since also i*n vivo* gene induction was not significantly different between the strains for most of the analysed IEGs and regions (3.1.4), it can be concluded that neither diminished hippocampal activation nor *in vivo* gene induction processes cause the DBA/2 memory impairment. Instead, an indication for imbalanced hippocampal inhibitory/excitatory signalling as potent cause was found (3.1.5). Although altered general IEG induction mechanisms are probably not causative in the case of the DBA/2 memory impairment, altered expression and induction of particular genes did provide a link to the likely origin of the impairment. Among the analysed IEGs after SOR, only *Npas4* and *Inhba* showed abnormal hippocampal expression in DBA/2 suggesting a special relevance of those two genes for spatial learning ability. Intriguingly, both genes are related to inhibitory processes and inhibitory cell development [52, 138], implying the necessity of balanced excitation/inhibition signalling for memory performance.

However, no *Npas4* basal expression difference in home cage (HC) animals was apparent, suggesting that attenuated DBA/2 CA1 inhibition is not caused by abnormal *Npas4* expression, but rather that elevated DBA/2 *Npas4* induction is a symptom of reduced inhibition in DBA/2 since *Npas4* transcription activation is highly dependent on neuronal activity. Although one function of *Npas4* signalling is the increase of inhibitory synapses on excitatory neurons, it appears that increased *Npas4* induction in DBA/2 is not sufficient to

counteract the decreased DBA/2 CA1 inhibition, which is probably caused by another neurodevelopmental mechanism.
On the other hand, the observed elevated *Inhba* expression could be one of these causative dysregulations in DBA/2 development resulting in reduced inhibition, since *Inhba* expression is altered under basal conditions in DBA/2. Activin A, which is coded by *Inhba*, reduces the number of inhibitory neurons in hippocampal cultures. Unfortunately, details about *Inhba* and Activin A function in GABAergic development and their relevance for excitation inhibition signalling in learning processes are not known. Therefore, it is proposed to investigate the influence of *Inhba*/Activin A on inhibitory and excitatory circuit development and learning since the presented data indicates great relevance of *Inhba* with regards to learning abilities.

4.1.4. Outlook – Investigating DBA/2 inhibitory signalling

Besides the already proposed experiments, it would be necessary to measure miniature excitatory postsynaptic currents (mEPSCs) in DBA/2 and C57BL/6 *ex vivo* to determine the excitatory/inhibitory signal ratio. Also recordings of electrophysiological signals *in vivo* during spatial navigation in a novel environment are suggested. In case a shift in DBA/2 towards increased excitation/decreased inhibition is confirmed with this experiments, it would be interesting to investigate whether a rescue of this hippocampal imbalance would also result in a rescue of the diverse aspects of DBA/2 behaviour, in particular spatial memory ability. However, such rescue would be very challenging since genetic manipulations like *Npas4* overexpression or *Inhba* knockdown can easily tilt the excitation/inhibition balance to the other extreme, causing a signalling imbalance again. Therefore, investigating the molecular cause of the DBA/2 imbalance during development seems to carry more promise. Candidate pathways other than *Inhba*/Activin A signalling would be GABAergic and cholinergic signalling since a reduction in high affinity GABA receptors and lower alpha7 nicotinic receptor expression especially in CA1 region are reported for DBA/2 [178, 179].
Data gathered in part one of this thesis lead to the overall conclusion that - under physiological conditions - a general activity-dependent gene induction dysregulation might not be the cause of memory ability differences. However, specific genes can serve as indicator of the underlying molecular dysregulation that causes memory deficits. Dysregulation of such particular genes might contribute to and exacerbate already existing impairments (elevated *Inhba*). Dysregulation of other genes might be a compensatory mechanism trying to counteract the original impairment (Elevated excitation upregulates *Npas4* which increased inhibitory synapse formation). Thus, even with intact gene induction machinery at the cellular and molecular levels, dysregulation of single neuronal activity-dependent genes might be enough to strongly contribute to functional impairments and consequently lead to phenotypic disabilities like memory impairment. Since such functional disabilities are also characteristic of neurological diseases, the second part of this thesis aimed to investigate expression of particular important IEGs during pathological conditions, in particular during excitotoxicity.

4.2. Dysregulation of activity-dependent genes during excitotoxicity

Increased synaptic glutamate levels followed by excitotoxicity often occur in several neurodegenerative diseases such as HD, ALS and AD alongside other pathological signals [105]. Those diseases are not initially caused by excitotoxic processes, but excitotoxicity-induced mechanisms might aggravate the disease progress. The first part of this thesis highlighted the potential relevance of single activity-dependent genes for learning and memory processes. The goal of the second part of the thesis was to investigate such particular important IEGs and their regulation during excitotoxicity. It has been shown previously that CREB is dephosphorylated and *Bdnf* downregulated upon glutamate toxicity *in vitro* [86]. Whether the expression of other IEGs or the activation status of important upstream kinases and transcription factors changes during excitotoxicity, has not yet been investigated.

In 3.2.1 it was shown that IEGs are dysregulated differentially in hippocampal cultures during excitototoxic stimuli. Furthermore, the established shut-off protocol offered the opportunity to differentiate between passive downregulation caused by decay of synaptic activity and active downregulation caused by excitotoxicity-dependent deactivation processes. Interestingly, upstream kinases and transcription factors/cofactors displayed differential deactivation during passive shut-off while excitotoxic NMDA application always caused dephorsphorylation of the analysed proteins (3.2.4). This indicates that a broadly acting dephosphorylation mechanism is induced during excitotoxicity. Therefore, rescue of IEG downregulation by inhibition of broadly acting phosphatases (PP1, PP2B, PTEN, STEP) was tested (3.2.5). Unfortunately, none of the inhibitors was able to rescue IEG downregulation; in contrast, gene expression was further downregulated by inhibitor application, possibly due to nonspecific drug side effects. Mitochondrial depolarization was also investigated as another possible shut-off initiation mechanism. However, the FCCP concentration which caused a similar depolarization as NMDA did not result in a similar transcription downregulation (3.2.6).

4.2.1. Relevance of differential excitotoxicity-induced gene downregulation

The major finding of this part of the thesis is the differential effect of excitotoxicity on activity-dependent gene expression. However, a much broader analysis via transcriptome sequencing of activity-dependent gene expression is needed to confirm the presented findings and interpretations. Nonetheless, primary conclusions can be drawn about general IEG regulation during excitotoxicity.

First of all, the transcription of rapid IEGs like *cFos*, *Arc* and *Egr1* depends strongly on neuronal activity and appears to be unaffected by active shut-off mechanisms (3.2.1; Appendix 1, Figure 24A: *cFos*-like genes). *Npas4* and *Nr4a*, which also belong to the more rapid IEGs, similarly do not experience active transcription shut-off. For all of these genes, the involvement of poised polymerases during activity-dependent induction is reported [180]. Therefore, it is unlikely that excitotoxicity affects poised polymerase-dependent gene induction actively. Interestingly – when compared with cultures in which synaptic activity

was merely silenced via TTX - *Npas4* and *Nr4a1* transcription was even observed to increase upon bath NMDA application. Taking the gene induction data during eNMDAR inhibition by memantine into account (Figure 18G), it appears that some IEGs depend predominantly on sNMDAR activation (*Inhba*, *Bdnf*) and others like *Npas4* and *Nr4a1* more on general NMDA receptor activation and calcium influx, independent of the influx route. Expression of those *Npas4*-type genes might be saturated only at very high calcium concentrations, whereas *Inhba*-type genes need lower calcium concentrations for induction of expression, while high calcium concentrations might inhibit transcription (Figure 23A).

Furthermore, the severe *Inhba* and *Bdnf* active shut-off is an interesting finding since both genes are very important for neuronal survival and viability [181, 182]. This is especially meaningful for diseases with excitotoxic co-incidence. Downregulation of important pro-survival factors renders neurons more vulnerable, accelerating degeneration and disease progress. Transcriptome sequencing would reveal whether pro-survival genes are especially sensitive towards excitotoxicity. In the case of *Inhba*, which was the most sensitive analysed gene, even mild excitotoxic signals resulted in expression downregulation (3.2.3). Since it is reported that *Inhba*/Activin A downregulates eNMDAR signals [51], excitotoxicity-induced *Inhba* downregulation might activate a toxic feed-forward cycle with continued eNMDAR signal elevation, *Inhba* reduction and progressive toxicity (Figure 23B).

Since *Inhba* transcription is highly sensitive to eNMDAR activation and is sNMDAR signal dependent, it is proposed to use *Inhba* expression as marker for healthy NMDA receptor activation (3.2.2). Reduced *Inhba* expression could indicate excitotoxic signalling in diseases. In combination with basic induction analysis, eNMDAR inhibitors or drugs against excitotoxicity could be evaluated as was shown in 3.3.2, which would be beneficial for drug development.

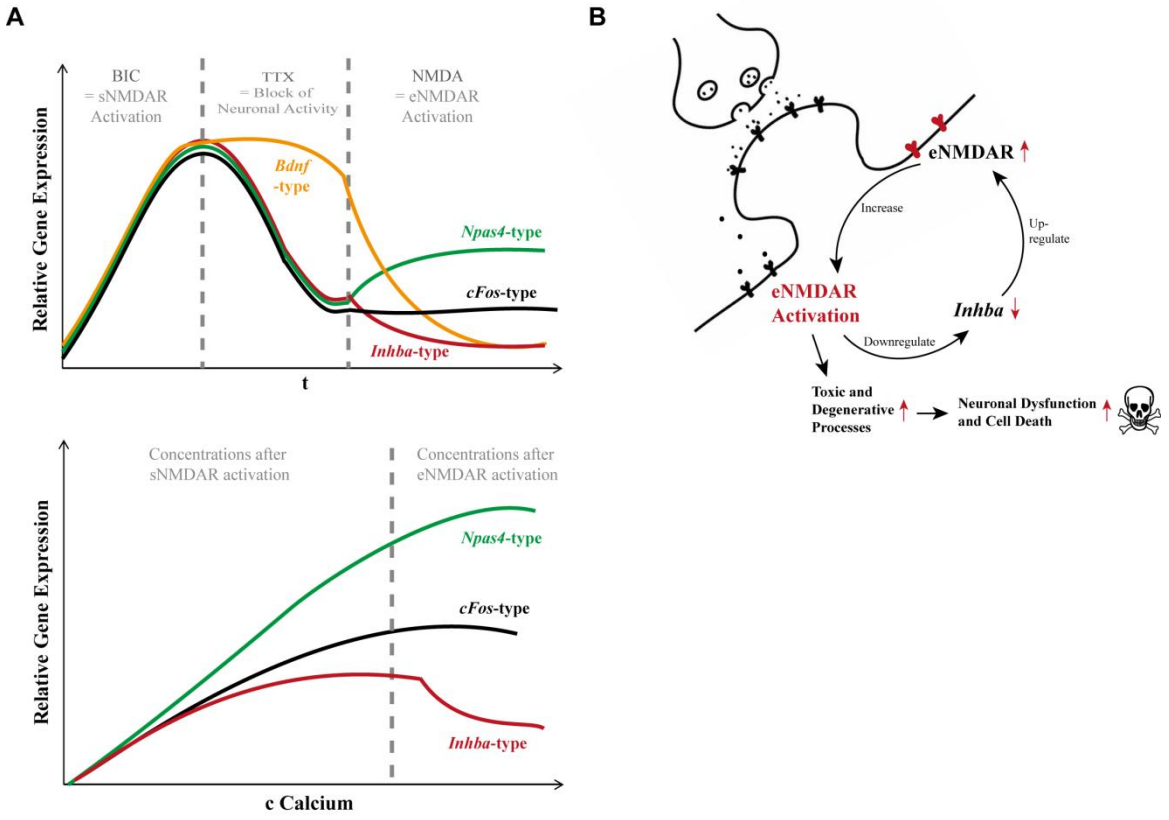

Figure 23: Proposed differential IEG classification and *Inhba*-dependent toxic cycle development during excitotoxicity. (A) Hypothetical course of gene expression of neuronal activity-dependent genes similar to *Inhba* (*Inhba*-type, red line), *Bdnf* (*Bdnf*-type, orange line), *Npas4* (*Npas4*-type, green line) and *cFos* (*cFos*-like, black line) during BIC, TTX and NMDA treatment is depicted over time (top). Theoretical dependency of gene expression level to calcium concentration is plotted (bottom). In this hypothesis *cFos*-like genes display expression saturation at high/toxic calcium concentrations (c, dotted line), *Inhba*-like genes are downregulated at high calcium concentrations and saturation for *Npas4*-like genes occurs only at very high calcium levels. The mechanistic cause behind calcium-dependent expression saturation can be diverse for every particular gene (specific transcription factor deactivation, repressor activation etc.). **(B)** Activation of eNMDARs downregulate *Inhba* expression severely. Thus, less Activin A might result in upregulated eNMDARs, whereby eNMDAR signalling is elevated, *Inhba* is downregulated even more et cetera. In parallel, *Inhba* downregulation and elevated eNMDAR signalling also increases excitotoxicity-induced cell death processes.

4.2.2. Cause of differential excitotoxicity-induced gene expression

The observed differential effect of NMDA on IEG expression leads to the obvious question about the underlying mechanisms, particularly since several important kinases and transcription factors involved in activity-dependent gene induction displayed dephosphorylation upon NMDA application (Figure 19). It cannot be excluded that not-well characterized transcription factors, which are resistant against this dephosphorylation event, might still be involved in the differential transcription shut-off. However, this possibility seems unlikely since broad dephosphorylation during excitotoxiciy is indicated by the presented data. Analysis of total protein (Ser, Tyr and Thr) phosphorylation, either by

Western blotting with antibodies against total phosphorylation or more sophisticated proteomic methods would clarify the extent of excitotoxicity-induced dephosphorylation.

Another possible explanation for the differential shut-off of IEGs in response to excitotoxic NMDA might be the activation of second-messengers and transcription factors by dephosphorylation. For example, MEF2, which also showed dephosphorylation after NMDA application (Figure 19E), is reported to exhibit increased DNA binding in a calcineurin (PP2B)-dependent hypophosphorylated state [35, 183, 184]. Chromatin immunoprecipitation (ChIP) followed by DNA sequencing (ChIP-Seq) after the shut-off protocol could reveal whether MEF2-DNA binding is increased upon NMDA application and whether MEF2 binds the DNA promotor regions of genes with *Npas4*-like shut-off expression such as *Npas4* itself and *Nr4a1*.

Strong eNMDAR activation induces very strong and sustained cytoplasmic and nuclear calcium influx [86]. The transcription repressor downstream regulatory element antagonistic modulator (DREAM) directly binds calcium, and as a result DNA-binding and transcription repression is stopped [37]. It might be possible that excitotoxic high sustained calcium concentrations deactivate DREAM repression and activate DREAM-regulated transcription. Thus, DREAM DNA binding during excitotoxicity should be analysed via ChIP-Seq and promoter analysis to reveal its relevance for the differential shut-off. Interestingly, it is reported that especially *Npas4*, *Nr4a1* and other rapid IEGs are DREAM target genes, and are massively downregulated by a dominant active DREAM mutant [185]. It would be informative to determine how *Npas4* and *Nr4a1* expression is affected in neurons expressing the described dominant active DREAM mutant after the shut-off protocol. If DREAM does indeed participate in the differential shut-off, then *Npas4* and *Nr4a1* would not be expected to display increased expression upon NMDA addition in comparison to the TTX control.

Another intriguing question, raised by the differential shut-off aspect is why the extent to which different CREB-dependent genes actively shut-off is so variable. *cFos*, for example, displayed no significant active shut-off, while *Bdnf* on the other hand was immensely downregulated. The combination of transcription-factor binding sites might determine the effect of excitotoxicity. One possibility is that not all factors are dephosphorylated to the same extent, and sites where MEF2, CREB and SRF binding occurs simultaneously are not as susceptible as sites with only one active element. Transcriptome sequencing and promotor analysis of shut-off affected and unaffected genes could reveal whether some elements or element combinations are typical for *Npas4*-like, *cFos*-like or *Inhba*-like genes.

4.2.3. Excitotoxicity-induced gene downregulation in neurodegeneration

The excitotoxic stimulus-induced differential transcription shut-off and its underlying mechanisms might be especially relevant for our understanding of neurodegenerative diseases. As previously mentioned, excitotoxicity is implicated alongside other pathologic mechanisms in several neurodegenerative diseases [105]. Shut-off-sensitive genes (*Inhba*-type, *Bdnf*-type) might be specifically downregulated in patients. Therefore, supplementing those

genes/proteins might attenuate the disease phenotype and slow down disease progress. The mechanistic cause behind the shut-off sensitivity could also serve as a target for disease drug development, especially since complete eNMDAR inhibition without affecting sNMDARs is difficult to accomplish.

Bdnf is one of the best characterized IEGs. As a neurotrophic pro-survival factor, its expression in several neurological diseases has been investigated. In patient samples, *Bdnf* transcription and protein downregulation was observed in AD, HD and Parkinsons´s disease [108, 186-188]. Since *Inhba* displays an even stronger active shut-off than *Bdnf* it would be very interesting to analyse its expression in those diseases, too.

The occurrence of excitotoxicity is best described in HD. HD model mice (YAC128) show lower levels of phosphorylated CREB compared to healthy control mice (YAC72). Furthermore, supplementing memantine at low doses (1 mg/kg) rescues P-CREB levels and the behavioural phenotype of YAC128 [106]. Analysing the expression of other shut-off sensitive genes like *Inhba* in HD models and rescuing the possible *in vivo* shut-off with memantine would verify the occurrence and relevance of the transcription shut-off in neurodegeneration, in particular for HD. The proposed toxic cycle of *Inhba* shut-off (Figure 23B) could be especially relevant for HD progression.

4.3. Activity-induced genes during physiological and pathological signalling

The overall aim of this thesis was to investigate the regulation of neuronal activity-dependent genes during physiological and pathological conditions. The first part demonstrated that in learning-impaired DBA/2 mice, which were used as model for inter-individual differences in memory ability, gene induction and expression of most analysed IEGs was not impaired. However, altered expression/induction was observed for two genes, *Inhba* and *Npas4*. Since functional studies of those genes indicated an involvement in excitation/inhibition regulation [52, 139], mIPSCs were recorded. DBA/2 displayed a dysregulation which could be the probable primary cause of the DBA/2 learning impairment, decreased inhibitory signal input in CA1 pyramidal neurons. Certainly, this inhibitory dysregulation in DBA/2 needs to be investigated further, for example by *in vivo* electrophysiological recordings. Nonetheless, the expression and induction analysis of just a few IEGs and knowing about their function was sufficient to guide to further mechanistic dysregulations in DBA/2.

In the second part of the thesis it was found that during pathological excitotoxic signals, activity-regulated genes are affected differentially. Expression of some IEGs like *Inhba* was particularly affected. Downregulation of those specific excitotoxicity-susceptible genes might enhance neurodegenerative disease progress, since excitotoxic signals are found in several of those age-dependent diseases [105]. Since learning is a highly optimized process, even small changes result in reduced function [189, 190]. Therefore, slight dysregulation of single activity-dependent genes could be enough to disturb optimized functionality and thereby learning ability. Such slight changes may arise via genetic disposition (DBA/2), pathological disease

signals (excitotoxicity), and also during the normal aging process. This is especially problematic since worldwide the portion of the older population increases and healthy learning ability, as one of the central adaptation processes for all living beings, is essential for life quality and society. Understanding the function and regulation of neuronal activity-controlled genes is crucial in order to develop strategies against neurodevelopmental, neurodegenerative and aging-dependent memory decline.

Appendix

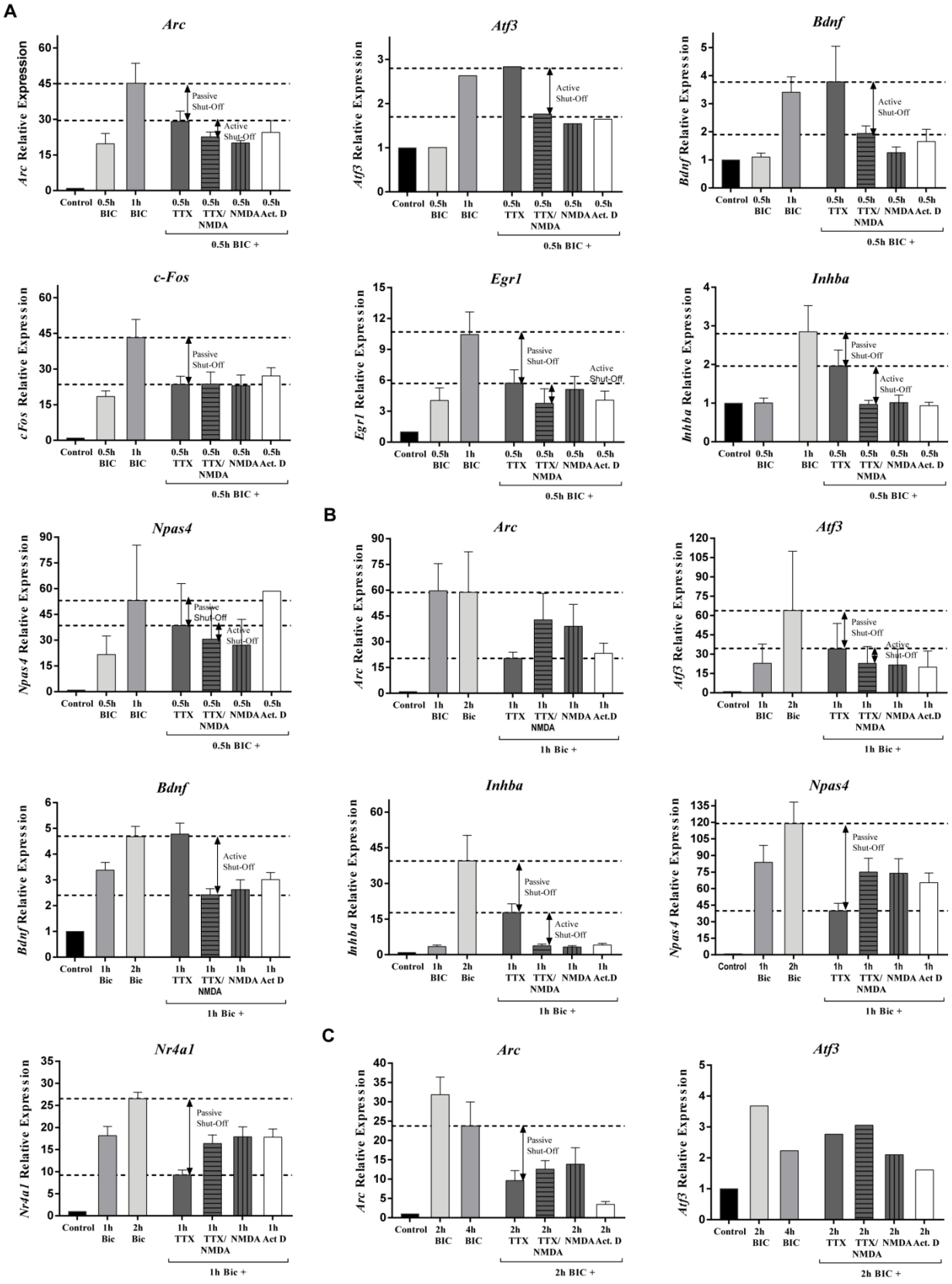
A
Arc
Arc Relative Expression
Passive Shut-Off
Active Shut-Off
Control 0.5h BIC 1h BIC 0.5h TTX 0.5h TTX/ NMDA 0.5h NMDA 0.5h Act. D
0.5h BIC +
Atf3
Atf3 Relative Expression
Bdnf
Bdnf Relative Expression
c-Fos
cFos Relative Expression
Egr1
Egr1 Relative Expression
Inhba
Inhba Relative Expression
Npas4
Npas4 Relative Expression
B
Arc
Control 1h BIC 2h Bic 1h TTX 1h TTX/ NMDA 1h NMDA 1h Act.D
1h Bic +
Atf3
Bdnf
Bdnf Relative Expression
Inhba
Inhba Relative Expression
Npas4
Npas4 Relative Expression
C
Nr4a1
Nr4a1 Relative Expression
Arc
Control 2h BIC 4h BIC 2h TTX 2h TTX/ NMDA 2h NMDA 2h Act. D
2h BIC +
Atf3

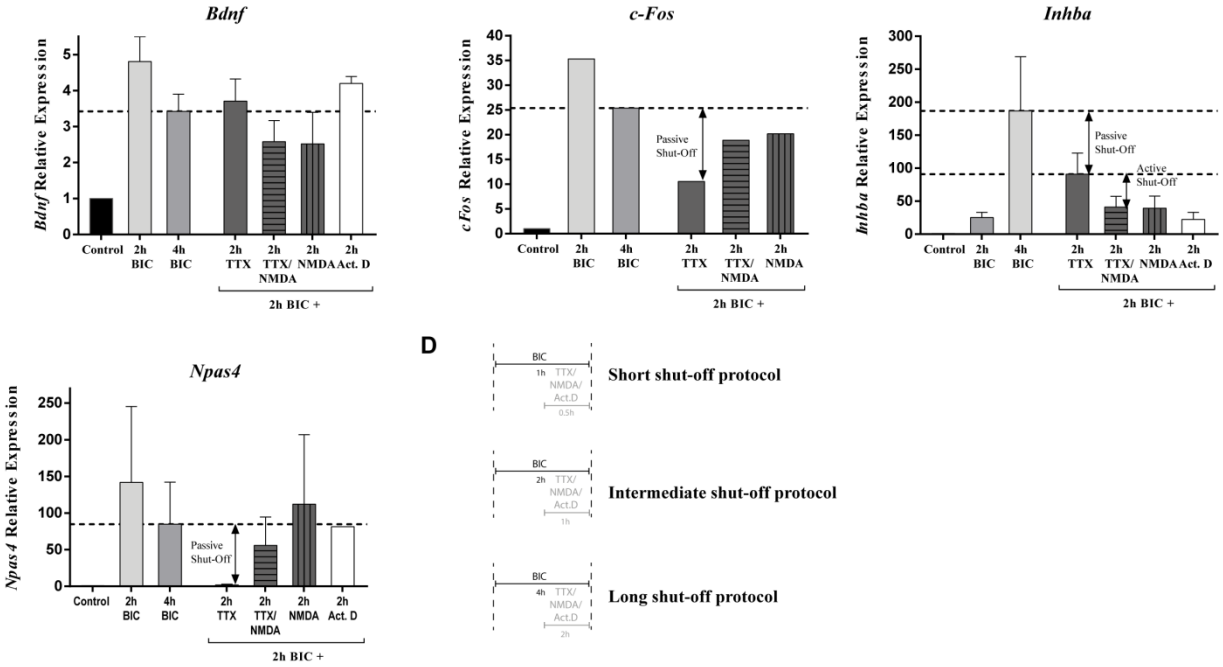

Appendix 1: Overview of passive and active shut-off of several IEGs for all three NMDA shut-off protocols. Transcription of *Arc*, *Atf3*, *Bdnf*, *cFos*, *Inhba*, *Npas4* and *Nr4a1 during* the short **(A)**, intermediate **(B)** and long **(C)** shut-off protocol. Primary hippocampal neurons were treated with BIC [50µM], TTX [1µM], NMDA [30µM] and actinomycin D [10µg/µl] according to shut-off protocols described in chapter 2.2.3 and depicted in **(D)**. Dotted line shows gene expression level of TTX control. Expression was analysed by RT-qPCR with *Gusb* as endogenous control. Data was normalized to the respective unstimulated sample. All graphs are plotted as mean + SEM. N=1-8.

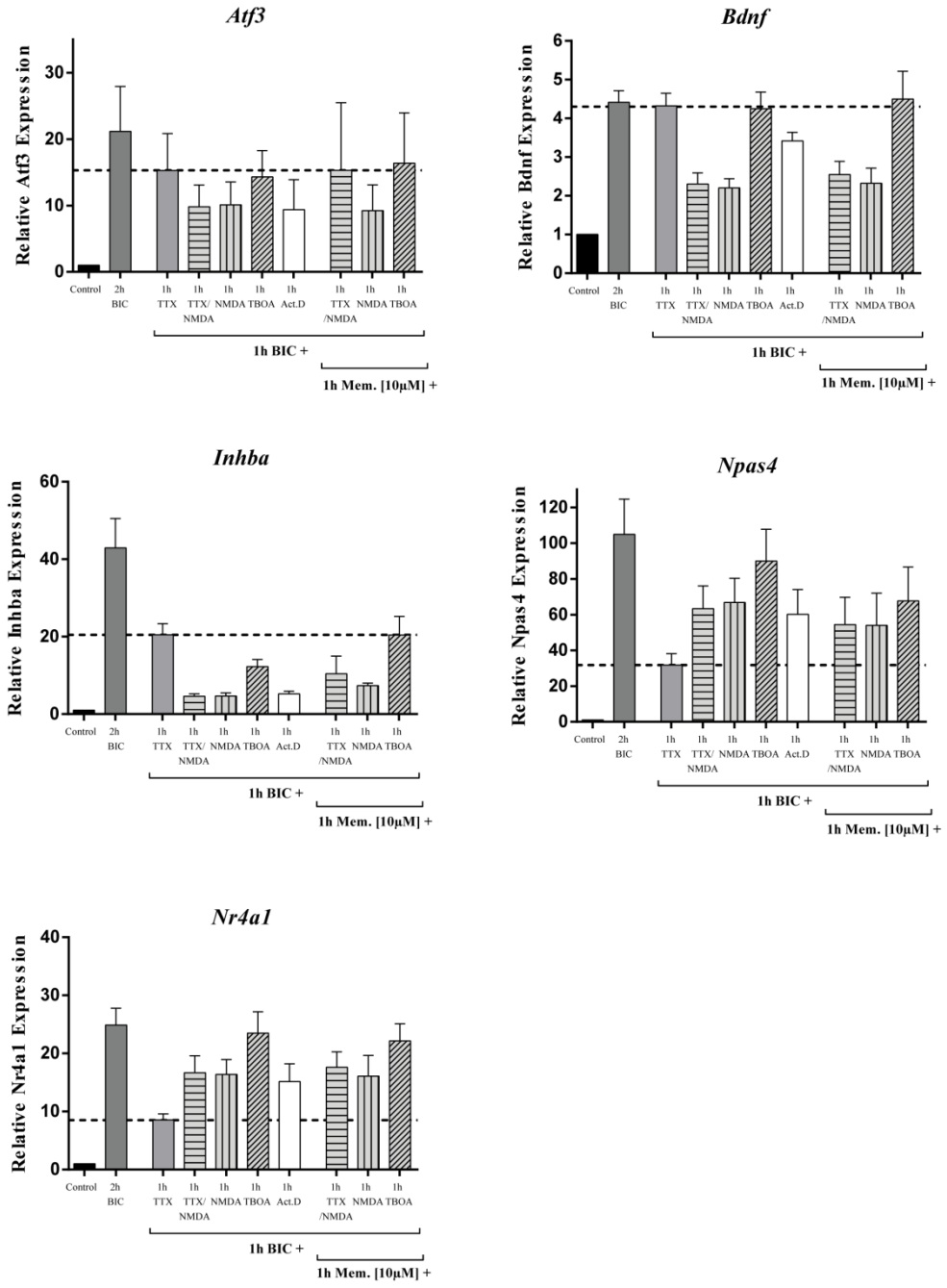

Appendix 2: Overview of passive and active shut-off of several IEGs during the TBOA shut-off protocol. Transcription of *Atf3*, *Bdnf*, *Inhba*, *Npas4* and *Nr4a1* during the TBOA shut-off protocol. Primary hippocampal neurons were treated with BIC [50µM], TTX [1µM] and NMDA [30µM] according to intermediate shut-off protocol. Instead of NMDA, TBOA [50µM] was applied for 1h to induce mild excitotoxicity. The left part of each graph shows the expression shut-off and the right part the same shut-off condition during memantine [10µM] incubation (1h before BIC, protocol described in chapter 2.2.3). Dotted line shows gene expression level of TTX control. Expression was analysed by RT-qPCR with *Gusb* as endogenous control. Data was normalized to the respective unstimulated sample. All graphs are plotted as mean + SEM. N=3-8.

References

1. Zucker, R.S. and W.G. Regehr, *Short-term synaptic plasticity.* Annu Rev Physiol, 2002. **64**: p. 355-405.
2. George, J., et al., *Palmitoylation of LIM Kinase-1 ensures spine-specific actin polymerization and morphological plasticity.* Elife, 2015. **4**: p. e06327.
3. Henley, J.M. and K.A. Wilkinson, *Synaptic AMPA receptor composition in development, plasticity and disease.* Nat Rev Neurosci, 2016. **17**(6): p. 337-50.
4. Martin, K.C., et al., *Synapse-specific, long-term facilitation of aplysia sensory to motor synapses: a function for local protein synthesis in memory storage.* Cell, 1997. **91**(7): p. 927-38.
5. Martin, K.C., M. Barad, and E.R. Kandel, *Local protein synthesis and its role in synapse-specific plasticity.* Curr Opin Neurobiol, 2000. **10**(5): p. 587-92.
6. Xia, Z., et al., *Calcium influx via the NMDA receptor induces immediate early gene transcription by a MAP kinase/ERK-dependent mechanism.* J Neurosci, 1996. **16**(17): p. 5425-36.
7. Lerea, L.S., L.S. Butler, and J.O. McNamara, *NMDA and non-NMDA receptor-mediated increase of c-fos mRNA in dentate gyrus neurons involves calcium influx via different routes.* J Neurosci, 1992. **12**(8): p. 2973-81.
8. Tyssowski, K.M., et al., *Different Neuronal Activity Patterns Induce Different Gene Expression Programs.* Neuron, 2018. **98**(3): p. 530-546 e11.
9. Douglas, R.M., M. Dragunow, and H.A. Robertson, *High-frequency discharge of dentate granule cells, but not long-term potentiation, induces c-fos protein.* Brain Res, 1988. **464**(3): p. 259-62.
10. Sheng, H.Z., R.D. Fields, and P.G. Nelson, *Specific regulation of immediate early genes by patterned neuronal activity.* J Neurosci Res, 1993. **35**(5): p. 459-67.
11. Gallin, W.J. and M.E. Greenberg, *Calcium regulation of gene expression in neurons: the mode of entry matters.* Curr Opin Neurobiol, 1995. **5**(3): p. 367-74.
12. Zhang, S.J., et al., *Nuclear calcium signaling controls expression of a large gene pool: identification of a gene program for acquired neuroprotection induced by synaptic activity.* PLoS Genet, 2009. **5**(8): p. e1000604.
13. Fowler, T., R. Sen, and A.L. Roy, *Regulation of primary response genes.* Mol Cell, 2011. **44**(3): p. 348-60.
14. Tullai, J.W., et al., *Immediate-early and delayed primary response genes are distinct in function and genomic architecture.* J Biol Chem, 2007. **282**(33): p. 23981-95.
15. Herschman, H.R., *Primary response genes induced by growth factors and tumor promoters.* Annu Rev Biochem, 1991. **60**: p. 281-319.

16. Lerea, L.S. and J.O. McNamara, *Ionotropic glutamate receptor subtypes activate c-fos transcription by distinct calcium-requiring intracellular signaling pathways.* Neuron, 1993. **10**(1): p. 31-41.

17. Bading, H., et al., *N-methyl-D-aspartate receptors are critical for mediating the effects of glutamate on intracellular calcium concentration and immediate early gene expression in cultured hippocampal neurons.* Neuroscience, 1995. **64**(3): p. 653-64.

18. Hardingham, G.E., et al., *Control of recruitment and transcription-activating function of CBP determines gene regulation by NMDA receptors and L-type calcium channels.* Neuron, 1999. **22**(4): p. 789-98.

19. Flavell, S.W. and M.E. Greenberg, *Signaling mechanisms linking neuronal activity to gene expression and plasticity of the nervous system.* Annu Rev Neurosci, 2008. **31**: p. 563-90.

20. Lyons, M.R. and A.E. West, *Mechanisms of specificity in neuronal activity-regulated gene transcription.* Prog Neurobiol, 2011. **94**(3): p. 259-95.

21. Thomas, G.M. and R.L. Huganir, *MAPK cascade signalling and synaptic plasticity.* Nat Rev Neurosci, 2004. **5**(3): p. 173-83.

22. Wayman, G.A., et al., *Calmodulin-kinases: modulators of neuronal development and plasticity.* Neuron, 2008. **59**(6): p. 914-31.

23. Hill, C.S. and R. Treisman, *Transcriptional regulation by extracellular signals: mechanisms and specificity.* Cell, 1995. **80**(2): p. 199-211.

24. Muller, U. and T.J. Carew, *Serotonin induces temporally and mechanistically distinct phases of persistent PKA activity in Aplysia sensory neurons.* Neuron, 1998. **21**(6): p. 1423-34.

25. Impey, S., et al., *Cross talk between ERK and PKA is required for Ca2+ stimulation of CREB-dependent transcription and ERK nuclear translocation.* Neuron, 1998. **21**(4): p. 869-83.

26. Nonaka, M., et al., *Towards a better understanding of cognitive behaviors regulated by gene expression downstream of activity-dependent transcription factors.* Neurobiol Learn Mem, 2014. **115**: p. 21-9.

27. Impey, S., et al., *Induction of CRE-mediated gene expression by stimuli that generate long-lasting LTP in area CA1 of the hippocampus.* Neuron, 1996. **16**(5): p. 973-82.

28. Rouillard, A.D., et al., *The harmonizome: a collection of processed datasets gathered to serve and mine knowledge about genes and proteins.* Database (Oxford), 2016. **2016**.

29. Inoue, M., et al., *Synaptic activity-responsive element (SARE): A unique genomic structure with an unusual sensitivity to neuronal activity.* Commun Integr Biol, 2010. **3**(5): p. 443-6.

30. Lonze, B.E. and D.D. Ginty, *Function and regulation of CREB family transcription factors in the nervous system.* Neuron, 2002. **35**(4): p. 605-23.

31. Posern, G. and R. Treisman, *Actin' together: serum response factor, its cofactors and the link to signal transduction.* Trends Cell Biol, 2006. **16**(11): p. 588-96.

32. McKinsey, T.A., C.L. Zhang, and E.N. Olson, *MEF2: a calcium-dependent regulator of cell division, differentiation and death.* Trends Biochem Sci, 2002. **27**(1): p. 40-7.

33. Cole, C.J., et al., *MEF2 negatively regulates learning-induced structural plasticity and memory formation.* Nat Neurosci, 2012. **15**(9): p. 1255-64.

34. Flavell, S.W., et al., *Activity-dependent regulation of MEF2 transcription factors suppresses excitatory synapse number.* Science, 2006. **311**(5763): p. 1008-12.

35. Mao, Z. and M. Wiedmann, *Calcineurin enhances MEF2 DNA binding activity in calcium-dependent survival of cerebellar granule neurons.* J Biol Chem, 1999. **274**(43): p. 31102-7.

36. Andreasson, K. and P.F. Worley, *Induction of beta-A activin expression by synaptic activity and during neocortical development.* Neuroscience, 1995. **69**(3): p. 781-96.

37. Carrion, A.M., et al., *DREAM is a Ca2+-regulated transcriptional repressor.* Nature, 1999. **398**(6722): p. 80-4.

38. Okuno, H., et al., *Inverse synaptic tagging of inactive synapses via dynamic interaction of Arc/Arg3.1 with CaMKIIbeta.* Cell, 2012. **149**(4): p. 886-98.

39. Shepherd, J.D., et al., *Arc/Arg3.1 mediates homeostatic synaptic scaling of AMPA receptors.* Neuron, 2006. **52**(3): p. 475-84.

40. Tu, J.C., et al., *Coupling of mGluR/Homer and PSD-95 complexes by the Shank family of postsynaptic density proteins.* Neuron, 1999. **23**(3): p. 583-92.

41. Sheng, M. and M.E. Greenberg, *The regulation and function of c-fos and other immediate early genes in the nervous system.* Neuron, 1990. **4**(4): p. 477-85.

42. Minatohara, K., M. Akiyoshi, and H. Okuno, *Role of Immediate-Early Genes in Synaptic Plasticity and Neuronal Ensembles Underlying the Memory Trace.* Front Mol Neurosci, 2015. **8**: p. 78.

43. Jones, M.W., et al., *A requirement for the immediate early gene Zif268 in the expression of late LTP and long-term memories.* Nat Neurosci, 2001. **4**(3): p. 289-96.

44. McNulty, S.E., et al., *Differential roles for Nr4a1 and Nr4a2 in object location vs. object recognition long-term memory.* Learn Mem, 2012. **19**(12): p. 588-92.

45. Sun, X. and Y. Lin, *Npas4: Linking Neuronal Activity to Memory.* Trends Neurosci, 2016. **39**(4): p. 264-275.

46. Ramamoorthi, K., et al., *Npas4 regulates a transcriptional program in CA3 required for contextual memory formation.* Science, 2011. **334**(6063): p. 1669-75.

47. Lu, Y., K. Christian, and B. Lu, *BDNF: a key regulator for protein synthesis-dependent LTP and long-term memory?* Neurobiol Learn Mem, 2008. **89**(3): p. 312-23.

48. Cattaneo, A., et al., *The human BDNF gene: peripheral gene expression and protein levels as biomarkers for psychiatric disorders.* Transl Psychiatry, 2016. **6**(11): p. e958.

49. Xia, Y. and A.L. Schneyer, *The biology of activin: recent advances in structure, regulation and function.* J Endocrinol, 2009. **202**(1): p. 1-12.

50. Link, A.S., F. Zheng, and C. Alzheimer, *Activin Signaling in the Pathogenesis and Therapy of Neuropsychiatric Diseases.* Front Mol Neurosci, 2016. **9**: p. 32.

51. Lau, D., et al., *BDNF Reduces Toxic Extrasynaptic NMDA Receptor Signaling via Synaptic NMDA Receptors and Nuclear-Calcium-Induced Transcription of inhba/Activin A.* Cell Rep, 2015. **12**(8): p. 1353-66.

52. Sekiguchi, M., et al., *Neuron type-selective effects of activin on development of the hippocampus.* Neurosci Lett, 2009. **452**(3): p. 232-7.

53. Meighan, S.E., et al., *Effects of extracellular matrix-degrading proteases matrix metalloproteinases 3 and 9 on spatial learning and synaptic plasticity.* J Neurochem, 2006. **96**(5): p. 1227-41.

54. Tulving, E. and H.J. Markowitsch, *Episodic and declarative memory: role of the hippocampus.* Hippocampus, 1998. **8**(3): p. 198-204.

55. Cowan, N., *What are the differences between long-term, short-term, and working memory?* Prog Brain Res, 2008. **169**: p. 323-38.

56. Eichenbaum, H., *Hippocampus: cognitive processes and neural representations that underlie declarative memory.* Neuron, 2004. **44**(1): p. 109-20.

57. Squire, L.R., *The legacy of patient H.M. for neuroscience.* Neuron, 2009. **61**(1): p. 6-9.

58. Bird, C.M. and N. Burgess, *The hippocampus and memory: insights from spatial processing.* Nat Rev Neurosci, 2008. **9**(3): p. 182-94.

59. Aimone, J.B., W. Deng, and F.H. Gage, *Resolving new memories: a critical look at the dentate gyrus, adult neurogenesis, and pattern separation.* Neuron, 2011. **70**(4): p. 589-96.

60. Lee, I., et al., *Comparison of population coherence of place cells in hippocampal subfields CA1 and CA3.* Nature, 2004. **430**(6998): p. 456-9.

61. Morellini, F., *Spatial memory tasks in rodents: what do they model?* Cell Tissue Res, 2013. **354**(1): p. 273-86.

62. Morris, R., *Developments of a water-maze procedure for studying spatial learning in the rat.* J Neurosci Methods, 1984. **11**(1): p. 47-60.

63. Laroche, S., S. Davis, and T.M. Jay, *Plasticity at hippocampal to prefrontal cortex synapses: dual roles in working memory and consolidation.* Hippocampus, 2000. **10**(4): p. 438-46.

64. Colby, C.L. and M.E. Goldberg, *Space and attention in parietal cortex.* Annu Rev Neurosci, 1999. **22**: p. 319-49.

65. Auger, S.D., S.L. Mullally, and E.A. Maguire, *Retrosplenial cortex codes for permanent landmarks.* PLoS One, 2012. **7**(8): p. e43620.

66. Malinow, R. and R.C. Malenka, *AMPA receptor trafficking and synaptic plasticity.* Annu Rev Neurosci, 2002. **25**: p. 103-26.

67. Cummings, J.A., et al., *Ca2+ signaling requirements for long-term depression in the hippocampus.* Neuron, 1996. **16**(4): p. 825-33.

68. Bridi, M.S. and T. Abel, *The NR4A orphan nuclear receptors mediate transcription-dependent hippocampal synaptic plasticity.* Neurobiol Learn Mem, 2013. **105**: p. 151-8.

69. Weng, F.J., et al., *Npas4 Is a Critical Regulator of Learning-Induced Plasticity at Mossy Fiber-CA3 Synapses during Contextual Memory Formation.* Neuron, 2018. **97**(5): p. 1137-1152 e5.

70. Kranz, T.M., et al., *De novo mutations from sporadic schizophrenia cases highlight important signaling genes in an independent sample.* Schizophr Res, 2015. **166**(1-3): p. 119-24.

71. Ebert, D.H. and M.E. Greenberg, *Activity-dependent neuronal signalling and autism spectrum disorder.* Nature, 2013. **493**(7432): p. 327-37.

72. Kanai, R. and G. Rees, *The structural basis of inter-individual differences in human behaviour and cognition.* Nat Rev Neurosci, 2011. **12**(4): p. 231-42.

73. Paylor, R., et al., *DBA/2 and C57BL/6 mice differ in contextual fear but not auditory fear conditioning.* Behav Neurosci, 1994. **108**(4): p. 810-7.

74. Owen, E.H., et al., *Assessment of learning by the Morris water task and fear conditioning in inbred mouse strains and F1 hybrids: implications of genetic background for single gene mutations and quantitative trait loci analyses.* Neuroscience, 1997. **80**(4): p. 1087-99.

75. Paylor, R., L. Baskall, and J.M. Wehner, *Behavioral dissociations between C57BL/6 and DBA/2 mice on learning and memory tasks: A hippocampal-dysfunction hypothesis.* Psychobiology, 1993. **21**(1): p. 11-26.

76. Jones, M.W., et al., *Synaptic plasticity in the hippocampus of awake C57BL/6 and DBA/2 mice: interstrain differences and parallels with behavior.* Hippocampus, 2001. **11**(4): p. 391-6.

77. Volpe, B.T., et al., *Loss of hippocampal CA1 pyramidal neurons correlates with memory impairment in rats with ischemic or neurotoxin lesions.* Behav Neurosci, 1992. **106**(3): p. 457-64.

78. Lenselink, A.M., et al., *Strain Differences in Presynaptic Function: PROTEOMICS, ULTRASTRUCTURE, AND PHYSIOLOGY OF HIPPOCAMPAL SYNAPSES IN DBA/2J AND C57Bl/6J MICE.* J Biol Chem, 2015. **290**(25): p. 15635-45.

79. Crusio, W.E. and H. Schwegler, *Hippocampal mossy fiber distribution covaries with open-field habituation in the mouse.* Behav Brain Res, 1987. **26**(2-3): p. 153-8.

80. Wehner, J.M., S. Sleight, and M. Upchurch, *Hippocampal protein kinase C activity is reduced in poor spatial learners.* Brain Res, 1990. **523**(2): p. 181-7.

81. Young, E.A., et al., *Alterations in hippocampal GAP-43 phosphorylation and protein level following contextual fear conditioning.* Brain Res, 2000. **860**(1-2): p. 95-103.

82. Fordyce, D.E., et al., *Genetic and activity-dependent regulation of zif268 expression: association with spatial learning.* Hippocampus, 1994. **4**(5): p. 559-68.

83. Hardingham, G.E. and H. Bading, *The Yin and Yang of NMDA receptor signalling.* Trends Neurosci, 2003. **26**(2): p. 81-9.

84. Arundine, M. and M. Tymianski, *Molecular mechanisms of calcium-dependent neurodegeneration in excitotoxicity.* Cell Calcium, 2003. **34**(4-5): p. 325-37.

85. Sattler, R., et al., *Distinct influx pathways, not calcium load, determine neuronal vulnerability to calcium neurotoxicity.* J Neurochem, 1998. **71**(6): p. 2349-64.

86. Hardingham, G.E., Y. Fukunaga, and H. Bading, *Extrasynaptic NMDARs oppose synaptic NMDARs by triggering CREB shut-off and cell death pathways.* Nat Neurosci, 2002. **5**(5): p. 405-14.

87. Li, J.H., et al., *Developmental changes in localization of NMDA receptor subunits in primary cultures of cortical neurons.* Eur J Neurosci, 1998. **10**(5): p. 1704-15.

88. Stocca, G. and S. Vicini, *Increased contribution of NR2A subunit to synaptic NMDA receptors in developing rat cortical neurons.* J Physiol, 1998. **507 (Pt 1)**: p. 13-24.

89. Chen, H.S., et al., *Open-channel block of N-methyl-D-aspartate (NMDA) responses by memantine: therapeutic advantage against NMDA receptor-mediated neurotoxicity.* J Neurosci, 1992. **12**(11): p. 4427-36.

90. Sattler, R. and M. Tymianski, *Molecular mechanisms of glutamate receptor-mediated excitotoxic neuronal cell death.* Mol Neurobiol, 2001. **24**(1-3): p. 107-29.

91. White, R.J. and I.J. Reynolds, *Mitochondrial depolarization in glutamate-stimulated neurons: an early signal specific to excitotoxin exposure.* J Neurosci, 1996. **16**(18): p. 5688-97.

92. Tan, Y.W., et al., *Increasing levels of wild-type CREB up-regulates several activity-regulated inhibitor of death (AID) genes and promotes neuronal survival.* BMC Neurosci, 2012. **13**: p. 48.

93. Qiu, J., et al., *Mitochondrial calcium uniporter Mcu controls excitotoxicity and is transcriptionally repressed by neuroprotective nuclear calcium signals.* Nat Commun, 2013. **4**: p. 2034.

94. Ivanov, A., et al., *Opposing role of synaptic and extrasynaptic NMDA receptors in regulation of the extracellular signal-regulated kinases (ERK) activity in cultured rat hippocampal neurons.* J Physiol, 2006. **572**(Pt 3): p. 789-98.

95. Paul, S., et al., *NMDA-mediated activation of the tyrosine phosphatase STEP regulates the duration of ERK signaling.* Nat Neurosci, 2003. **6**(1): p. 34-42.

96. Bito, H., K. Deisseroth, and R.W. Tsien, *CREB phosphorylation and dephosphorylation: a Ca(2+)- and stimulus duration-dependent switch for hippocampal gene expression.* Cell, 1996. **87**(7): p. 1203-14.

97. Lankiewicz, S., et al., *Activation of calpain I converts excitotoxic neuron death into a caspase-independent cell death.* J Biol Chem, 2000. **275**(22): p. 17064-71.

98. Wu, H.Y., et al., *Critical role of calpain-mediated cleavage of calcineurin in excitotoxic neurodegeneration.* J Biol Chem, 2004. **279**(6): p. 4929-40.

99. Faddis, B.T., M.J. Hasbani, and M.P. Goldberg, *Calpain activation contributes to dendritic remodeling after brief excitotoxic injury in vitro.* J Neurosci, 1997. **17**(3): p. 951-9.

100. Gu, T., et al., *CREB is a novel nuclear target of PTEN phosphatase.* Cancer Res, 2011. **71**(8): p. 2821-5.

101. Zhang, S., et al., *Critical role of increased PTEN nuclear translocation in excitotoxic and ischemic neuronal injuries.* J Neurosci, 2013. **33**(18): p. 7997-8008.

102. Dieterich, D.C., et al., *Caldendrin-Jacob: a protein liaison that couples NMDA receptor signalling to the nucleus.* PLoS Biol, 2008. **6**(2): p. e34.

103. Melgarejo da Rosa, M., et al., *Synaptic GluN2B/CaMKII-alpha Signaling Induces Synapto-Nuclear Transport of ERK and Jacob.* Front Mol Neurosci, 2016. **9**: p. 66.

104. Zhou, X., et al., *NMDA receptor-mediated excitotoxicity depends on the coactivation of synaptic and extrasynaptic receptors.* Cell Death Dis, 2013. **4**: p. e560.

105. Bading, H., *Therapeutic targeting of the pathological triad of extrasynaptic NMDA receptor signaling in neurodegenerations.* J Exp Med, 2017. **214**(3): p. 569-578.

106. Milnerwood, A.J., et al., *Early increase in extrasynaptic NMDA receptor signaling and expression contributes to phenotype onset in Huntington's disease mice.* Neuron, 2010. **65**(2): p. 178-90.

107. Dau, A., et al., *Chronic blockade of extrasynaptic NMDA receptors ameliorates synaptic dysfunction and pro-death signaling in Huntington disease transgenic mice.* Neurobiol Dis, 2014. **62**: p. 533-42.

108. Zuccato, C., et al., *Loss of huntingtin-mediated BDNF gene transcription in Huntington's disease.* Science, 2001. **293**(5529): p. 493-8.

109. West, M.J., et al., *Differences in the pattern of hippocampal neuronal loss in normal ageing and Alzheimer's disease.* Lancet, 1994. **344**(8925): p. 769-72.

110. Selkoe, D.J., *Alzheimer's disease results from the cerebral accumulation and cytotoxicity of amyloid beta-protein.* J Alzheimers Dis, 2001. **3**(1): p. 75-80.

111. Hardy, J. and D. Allsop, *Amyloid deposition as the central event in the aetiology of Alzheimer's disease.* Trends Pharmacol Sci, 1991. **12**(10): p. 383-8.

112. Li, S., et al., *Soluble Abeta oligomers inhibit long-term potentiation through a mechanism involving excessive activation of extrasynaptic NR2B-containing NMDA receptors.* J Neurosci, 2011. **31**(18): p. 6627-38.

113. Holsinger, R.M., et al., *Quantitation of BDNF mRNA in human parietal cortex by competitive reverse transcription-polymerase chain reaction: decreased levels in Alzheimer's disease.* Brain Res Mol Brain Res, 2000. **76**(2): p. 347-54.

114. Peng, S., et al., *Precursor form of brain-derived neurotrophic factor and mature brain-derived neurotrophic factor are decreased in the pre-clinical stages of Alzheimer's disease.* J Neurochem, 2005. **93**(6): p. 1412-21.

115. Kitiyanant, N., et al., *BDNF-, IGF-1- and GDNF-secreting human neural progenitor cells rescue amyloid beta-induced toxicity in cultured rat septal neurons.* Neurochem Res, 2012. **37**(1): p. 143-52.

116. Rothstein, J.D., L.J. Martin, and R.W. Kuncl, *Decreased glutamate transport by the brain and spinal cord in amyotrophic lateral sclerosis.* N Engl J Med, 1992. **326**(22): p. 1464-8.

117. Meredith, G.E., et al., *Impaired glutamate homeostasis and programmed cell death in a chronic MPTP mouse model of Parkinson's disease.* Exp Neurol, 2009. **219**(1): p. 334-40.

118. Frigo, M., et al., *Glutamate and multiple sclerosis.* Curr Med Chem, 2012. **19**(9): p. 1295-9.

119. Yi, J.H. and A.S. Hazell, *Excitotoxic mechanisms and the role of astrocytic glutamate transporters in traumatic brain injury.* Neurochem Int, 2006. **48**(5): p. 394-403.

120. Mallien, A.S., et al., *Daily exposure to a touchscreen-paradigm and associated food restriction evokes an increase in adrenocortical and neural activity in mice.* Horm Behav, 2016. **81**: p. 97-105.

121. Richter, S.H., et al., *Touchscreen-paradigm for mice reveals cross-species evidence for an antagonistic relationship of cognitive flexibility and stability.* Front Behav Neurosci, 2014. **8**: p. 154.

122. Koppe, G., et al., *CACNA1C gene regulates behavioral strategies in operant rule learning.* PLoS Biol, 2017. **15**(6): p. e2000936.

123. Talpos, J.C., et al., *A novel touchscreen-automated paired-associate learning (PAL) task sensitive to pharmacological manipulation of the hippocampus: a translational rodent model of cognitive impairments in neurodegenerative disease.* Psychopharmacology (Berl), 2009. **205**(1): p. 157-68.

124. Horner, A.E., et al., *The touchscreen operant platform for testing learning and memory in rats and mice.* Nat Protoc, 2013. **8**(10): p. 1961-84.

125. Delotterie, D.F., et al., *Touchscreen tasks in mice to demonstrate differences between hippocampal and striatal functions.* Neurobiol Learn Mem, 2015. **120**: p. 16-27.

126. Deacon, R.M.J., *Assessing nest building in mice.* Nature Protocols, 2006. **1**: p. 1117.

127. Belz, T., et al., *Inactivation of the gene for the nuclear receptor tailless in the brain preserving its function in the eye.* Eur J Neurosci, 2007. **26**(8): p. 2222-7.

128. Mulisch, M. and U. Welsch, *Romeis-Mikroskopische Technik*. 18 ed. 2010: Springer Spektrum.

129. Tipps, M.E., et al., *Delay and trace fear conditioning in C57BL/6 and DBA/2 mice: issues of measurement and performance.* Learn Mem, 2014. **21**(8): p. 380-93.

130. Gerlai, R., *Contextual learning and cue association in fear conditioning in mice: a strain comparison and a lesion study.* Behav Brain Res, 1998. **95**(2): p. 191-203.

131. Kochli, D.E., et al., *The amygdala is critical for trace, delay, and contextual fear conditioning.* Learn Mem, 2015. **22**(2): p. 92-100.

132. Deacon, R.M., A. Croucher, and J.N. Rawlins, *Hippocampal cytotoxic lesion effects on species-typical behaviours in mice.* Behav Brain Res, 2002. **132**(2): p. 203-13.

133. Nadel, L., *Dorsal and ventral hippocampal lesions and behavior.* Physiology & Behavior, 1968. **3**(6): p. 891-900.

134. Abusaad, I., et al., *Stereological estimation of the total number of neurons in the murine hippocampus using the optical disector.* J Comp Neurol, 1999. **408**(4): p. 560-6.

135. Hardingham, G.E., F.J. Arnold, and H. Bading, *Nuclear calcium signaling controls CREB-mediated gene expression triggered by synaptic activity.* Nat Neurosci, 2001. **4**(3): p. 261-7.

136. Wisden, W. and P.H. Seeburg, *A complex mosaic of high-affinity kainate receptors in rat brain.* J Neurosci, 1993. **13**(8): p. 3582-98.

137. Gall, C., K. Murray, and P.J. Isackson, *Kainic acid-induced seizures stimulate increased expression of nerve growth factor mRNA in rat hippocampus.* Brain Res Mol Brain Res, 1991. **9**(1-2): p. 113-23.

138. Lin, Y., et al., *Activity-dependent regulation of inhibitory synapse development by Npas4.* Nature, 2008. **455**(7217): p. 1198-204.

139. Spiegel, I., et al., *Npas4 regulates excitatory-inhibitory balance within neural circuits through cell-type-specific gene programs.* Cell, 2014. **157**(5): p. 1216-29.

140. Tsukada, S., et al., *Effects of a novel glutamate transporter blocker, (2S, 3S)-3-[3-[4-(trifluoromethyl)benzoylamino]benzyloxy]aspartate (TFB-TBOA), on activities of hippocampal neurons.* Neuropharmacology, 2005. **48**(4): p. 479-91.

141. Danbolt, N.C., *Glutamate uptake.* Prog Neurobiol, 2001. **65**(1): p. 1-105.

142. Masliah, E., et al., *Deficient glutamate transport is associated with neurodegeneration in Alzheimer's disease.* Ann Neurol, 1996. **40**(5): p. 759-66.

143. Volbracht, C., et al., *Neuroprotective properties of memantine in different in vitro and in vivo models of excitotoxicity.* Eur J Neurosci, 2006. **23**(10): p. 2611-22.

144. Roskoski, R., Jr., *ERK1/2 MAP kinases: structure, function, and regulation.* Pharmacol Res, 2012. **66**(2): p. 105-43.

145. Xu, J., et al., *Inhibitor of the tyrosine phosphatase STEP reverses cognitive deficits in a mouse model of Alzheimer's disease.* PLoS Biol, 2014. **12**(8): p. e1001923.

146. Spinelli, L., Y.E. Lindsay, and N.R. Leslie, *PTEN inhibitors: an evaluation of current compounds.* Adv Biol Regul, 2015. **57**: p. 102-11.

147. Smaili, S.S., et al., *Mitochondria in Ca2+ signaling and apoptosis.* J Bioenerg Biomembr, 2000. **32**(1): p. 35-46.

148. Dispersyn, G., et al., *Bcl-2 protects against FCCP-induced apoptosis and mitochondrial membrane potential depolarization in PC12 cells.* Biochim Biophys Acta, 1999. **1428**(2-3): p. 357-71.

149. Nicholls, D.G., *Simultaneous monitoring of ionophore- and inhibitor-mediated plasma and mitochondrial membrane potential changes in cultured neurons.* J Biol Chem, 2006. **281**(21): p. 14864-74.

150. Toescu, E.C. and A. Verkhratsky, *Assessment of mitochondrial polarization status in living cells based on analysis of the spatial heterogeneity of rhodamine 123 fluorescence staining.* Pflugers Arch, 2000. **440**(6): p. 941-7.

151. Rebecca Glatt, A., et al., *Temporal and qualitative dynamics of conditioned taste aversions in C57BL/6J and DBA/2J mice self-administering LiCl.* Physiol Behav, 2016. **153**: p. 97-108.

152. Baarendse, P.J., et al., *Differential involvement of the dorsal hippocampus in passive avoidance in C57bl/6J and DBA/2J mice.* Hippocampus, 2008. **18**(1): p. 11-9.

153. Patel, S., et al., *Attentional performance of C57BL/6 and DBA/2 mice in the 5-choice serial reaction time task.* Behav Brain Res, 2006. **170**(2): p. 197-203.

154. Schwegler, H., W.E. Crusio, and I. Brust, *Hippocampal mossy fibers and radial-maze learning in the mouse: a correlation with spatial working memory but not with non-spatial reference memory.* Neuroscience, 1990. **34**(2): p. 293-8.

155. Dudchenko, P.A., *An overview of the tasks used to test working memory in rodents.* Neurosci Biobehav Rev, 2004. **28**(7): p. 699-709.

156. Foss-Feig, J.H., et al., *Searching for Cross-Diagnostic Convergence: Neural Mechanisms Governing Excitation and Inhibition Balance in Schizophrenia and Autism Spectrum Disorders.* Biol Psychiatry, 2017. **81**(10): p. 848-861.

157. Del Pino, I., B. Rico, and O. Marin, *Neural circuit dysfunction in mouse models of neurodevelopmental disorders.* Curr Opin Neurobiol, 2018. **48**: p. 174-182.

158. Brambilla, P., et al., *GABAergic dysfunction in mood disorders.* Mol Psychiatry, 2003. **8**(8): p. 721-37, 715.

159. Bozzi, Y., G. Provenzano, and S. Casarosa, *Neurobiological bases of autism-epilepsy comorbidity: a focus on excitation/inhibition imbalance.* Eur J Neurosci, 2018. **47**(6): p. 534-548.

160. Dani, V.S., et al., *Reduced cortical activity due to a shift in the balance between excitation and inhibition in a mouse model of Rett syndrome.* Proc Natl Acad Sci U S A, 2005. **102**(35): p. 12560-5.

161. Houbaert, X., et al., *Target-specific vulnerability of excitatory synapses leads to deficits in associative memory in a model of intellectual disorder.* J Neurosci, 2013. **33**(34): p. 13805-19.

162. Kleschevnikov, A.M., et al., *Hippocampal long-term potentiation suppressed by increased inhibition in the Ts65Dn mouse, a genetic model of Down syndrome.* J Neurosci, 2004. **24**(37): p. 8153-60.

163. Barron, H.C., et al., *Unmasking Latent Inhibitory Connections in Human Cortex to Reveal Dormant Cortical Memories.* Neuron, 2016. **90**(1): p. 191-203.

164. Legon, W., et al., *Altered Prefrontal Excitation/Inhibition Balance and Prefrontal Output: Markers of Aging in Human Memory Networks.* Cereb Cortex, 2016. **26**(11): p. 4315-4326.

165. Cossart, R., C. Bernard, and Y. Ben-Ari, *Multiple facets of GABAergic neurons and synapses: multiple fates of GABA signalling in epilepsies.* Trends Neurosci, 2005. **28**(2): p. 108-15.

166. Le Gal La Salle, G. and R. Naquet, *Audiogenic seizures evoked in DBA/2 mice inducec-fos oncogene expression into subcortical auditory nuclei.* Brain Research, 1990. **518**(1-2): p. 308-312.

167. McLin, J.P. and O. Steward, *Comparison of seizure phenotype and neurodegeneration induced by systemic kainic acid in inbred, outbred, and hybrid mouse strains.* Eur J Neurosci, 2006. **24**(8): p. 2191-202.

168. Ewell, L.A., *The Stuff of Memories: Sharp Wave Ripple Memory Consolidation in Epilepsy.* Epilepsy Curr, 2018. **18**(4): p. 253-254.

169. Heckers, S. and C. Konradi, *GABAergic mechanisms of hippocampal hyperactivity in schizophrenia.* Schizophr Res, 2015. **167**(1-3): p. 4-11.

170. Schobel, S.A., et al., *Differential targeting of the CA1 subfield of the hippocampal formation by schizophrenia and related psychotic disorders.* Arch Gen Psychiatry, 2009. **66**(9): p. 938-46.

171. Van Snellenberg, J.X., et al., *Mechanisms of Working Memory Impairment in Schizophrenia.* Biol Psychiatry, 2016. **80**(8): p. 617-26.

172. Saykin, A.J., et al., *Neuropsychological function in schizophrenia. Selective impairment in memory and learning.* Arch Gen Psychiatry, 1991. **48**(7): p. 618-24.

173. Lim, S. and M.S. Goldman, *Balanced cortical microcircuitry for maintaining information in working memory.* Nat Neurosci, 2013. **16**(9): p. 1306-14.

174. Nuechterlein, K.H., et al., *Attention/vigilance in schizophrenia: performance results from a large multi-site study of the Consortium on the Genetics of Schizophrenia (COGS).* Schizophr Res, 2015. **163**(1-3): p. 38-46.

175. Danckert, J., M. Saoud, and P. Maruff, *Attention, motor control and motor imagery in schizophrenia: implications for the role of the parietal cortex.* Schizophr Res, 2004. **70**(2-3): p. 241-61.

176. Thinus-Blanc, C., et al., *The differences shown by C57BL/6 and DBA/2 inbred mice in detecting spatial novelty are subserved by a different hippocampal and parietal cortex interplay.* Behav Brain Res, 1996. **80**(1-2): p. 33-40.

177. Singer, P., J. Feldon, and B.K. Yee, *Are DBA/2 mice associated with schizophrenia-like endophenotypes? A behavioural contrast with C57BL/6 mice.* Psychopharmacology (Berl), 2009. **206**(4): p. 677-98.

178. Horton, R.W., S.A. Prestwich, and B.S. Meldrum, *gamma-Aminobutyric acid and benzodiazepine binding sites in audiogenic seizure-susceptible mice.* J Neurochem, 1982. **39**(3): p. 864-70.

179. Stevens, K.E., et al., *Genetic correlation of inhibitory gating of hippocampal auditory evoked response and alpha-bungarotoxin-binding nicotinic cholinergic receptors in inbred mouse strains.* Neuropsychopharmacology, 1996. **15**(2): p. 152-62.

180. Saha, R.N., et al., *Rapid activity-induced transcription of Arc and other IEGs relies on poised RNA polymerase II.* Nat Neurosci, 2011. **14**(7): p. 848-56.

181. Nagahara, A.H. and M.H. Tuszynski, *Potential therapeutic uses of BDNF in neurological and psychiatric disorders.* Nat Rev Drug Discov, 2011. **10**(3): p. 209-19.

182. Buchthal, B., U. Weiss, and H. Bading, *Post-injury Nose-to-Brain Delivery of Activin A and SerpinB2 Reduces Brain Damage in a Mouse Stroke Model.* Mol Ther, 2018. **26**(10): p. 2357-2365.

183. Heidenreich, K.A. and D.A. Linseman, *Myocyte enhancer factor-2 transcription factors in neuronal differentiation and survival.* Mol Neurobiol, 2004. **29**(2): p. 155-66.

184. Wu, H., et al., *Activation of MEF2 by muscle activity is mediated through a calcineurin-dependent pathway.* EMBO J, 2001. **20**(22): p. 6414-23.

185. Mellstrom, B., et al., *DREAM controls the on/off switch of specific activity-dependent transcription pathways.* Mol Cell Biol, 2014. **34**(5): p. 877-87.

186. Howells, D.W., et al., *Reduced BDNF mRNA expression in the Parkinson's disease substantia nigra.* Exp Neurol, 2000. **166**(1): p. 127-35.

187. Mogi, M., et al., *Brain-derived growth factor and nerve growth factor concentrations are decreased in the substantia nigra in Parkinson's disease.* Neurosci Lett, 1999. **270**(1): p. 45-8.

188. Phillips, H.S., et al., *BDNF mRNA is decreased in the hippocampus of individuals with Alzheimer's disease.* Neuron, 1991. **7**(5): p. 695-702.

189. Deneve, S. and C.K. Machens, *Efficient codes and balanced networks.* Nat Neurosci, 2016. **19**(3): p. 375-82.

190. Bishop, N.A., T. Lu, and B.A. Yankner, *Neural mechanisms of ageing and cognitive decline.* Nature, 2010. **464**(7288): p. 529-35.